

Electronic Thesis and Dissertation Repository

---

9-9-2020 11:30 AM

## Hydrostatic Performance Of Reinforced Concrete Pipe For Infiltration

Lui Sammy Wong, *The University of Western Ontario*

Supervisor: Nehdi, Moncef L., *The University of Western Ontario*

A thesis submitted in partial fulfillment of the requirements for the Doctor of Philosophy degree in Civil and Environmental Engineering

© Lui Sammy Wong 2020

Follow this and additional works at: <https://ir.lib.uwo.ca/etd>



Part of the [Civil Engineering Commons](#)

---

### Recommended Citation

Wong, Lui Sammy, "Hydrostatic Performance Of Reinforced Concrete Pipe For Infiltration" (2020). *Electronic Thesis and Dissertation Repository*. 7397.  
<https://ir.lib.uwo.ca/etd/7397>

This Dissertation/Thesis is brought to you for free and open access by Scholarship@Western. It has been accepted for inclusion in Electronic Thesis and Dissertation Repository by an authorized administrator of Scholarship@Western. For more information, please contact [wlsadmin@uwo.ca](mailto:wlsadmin@uwo.ca).

## **ABSTRACT**

Groundwater infiltration into underground sewer systems has long been a costly issue for municipalities. With reinforced concrete pipe (RCP) being a primary option for sewer systems, existing hydrostatic testing methods conducted by manufacturers to measure internal pipe pressure, as required by specifications, do not reflect in-situ external hydrostatic conditions. This thesis records the development of a novel testing method to evaluate the RCP joint performance for infiltration. The test is safe and easy to conduct by RCP producers at the factory. The test method mimics field conditions of possible RCP joint gap and joint offset. Over 100 tests were conducted, including 600 mm, 900 mm and 1200 mm RCP with conventional single offset self-lubricated gaskets. This study also evaluates the gasket performance for infiltration. Pipe joint performance curves were developed based on the test results. Comparison to laboratory load-deformation tests on gaskets was conducted, indicating that predictions of the sealing potential derived using gasket geometry agreed well with the results of infiltration tests. The study shows that the joint gap plays an important role in the sealing potential. The developed apparatus allows the observation of gasket movement under infiltration pressure against the gasket leading to failure. The performance curves also allow the prediction of an infiltration potential leading to a practical applicational procedure to guide RCP installation. A case study of deep RCP pipe subjected to groundwater pressure illustrated the usefulness of the performance curves to derive maximum allowable joint gaps, which contractors could rely on during RCP installation. The findings should allow deducing technical guidance on how water tightness of RCP can be achieved at installation below the prevailing groundwater level. Two oversampling methods: Synthetic Minority Over-sampling Technique (SMOTE) and Density-Based SMOTE, were employed to address the unbalanced dataset. Accordingly, applying advanced machine learning techniques, the scale of variation in the test data can be analyzed and accurately predicted using tree-based supervised classification methods: random forest, extra trees and gradient boosting.

## Keywords

Concrete pipe; Infiltration; Joint; Performance; Hydrostatic Pressure; Test; Machine Learning; Supervised Learning; Gradient Boosting; SMOTE, DBSMOTE.

## **SUMMARY FOR THE LAY AUDIENCE**

Groundwater infiltration into sewer systems is a costly problem for many municipalities. With reinforced concrete pipe (RCP) being one of the most commonly used pipe options for sewer systems, existing hydrostatic testing methods conducted by manufacturers measuring internal pressure do not reflect in-situ external hydrostatic conditions. This thesis presents the development of a novel testing method to evaluate the RCP joint performance for infiltration. The test is safe and easy to conduct by RCP producers at the factory. The test also mimics the field conditions of possible joint gaps and joint offsets. The test procedure was repeated many times for 600 mm, 900 mm and 1200 mm RCP. The performance of commonly used single offset self-lubricated gaskets and various alignments were evaluated. Performance curves were developed based on the testing results. Comparisons to the laboratory load-deformation tests on gaskets were also conducted, indicating that predictions of the sealing potential derived using gasket geometry agreed with the results of the infiltration tests. The study shows that the joint gap plays an important role in the sealing potential. The apparatus developed allows the observation of gasket movements under infiltration pressures against the gasket leading to failure. The performance curves also allow the prediction of an infiltration potential leading to a practical applicational procedure to guide the installation of the pipe. A case study of deep RCP pipe subjected to groundwater pressure illustrated the usefulness of the performance curves to derive maximum allowable joint gap, which contractors could rely on during RCP installation. The findings should allow deducing technical guidance on how water tightness of RCP can be achieved at installations below the prevailing groundwater level. Lastly, with the application of advanced machine learning techniques, the scale of the variation in the test data can be analyzed and predicted using classification methods. The modeling technique, procedure and accuracy evaluation are presented.

## CO-AUTHORSHIP STATEMENT

This thesis was prepared according to the integrated-article layout designated by the Faculty of Graduate Studies at Western University, London, Ontario, Canada. All the work stated in this thesis, including experimental testing, data analysis, machine learning models, and writing of draft manuscripts for publication, was carried out by the candidate under the supervision and guidance of Professor M.L. Nehdi. Any other co-authors assisted in conducting the experimental program and/or revision of the initial draft of the manuscript. The following publications have been either published, accepted or submitted to peer-reviewed technical journals and international conferences:

Wong, L. and Nehdi, M.L. (2018) Critical Analysis of Precast Concrete Pipe Standards, *Infrastructures*, 3(3), 18 p. ; <https://doi.org/10.3390/infrastructures3030018>

Wong, L. and Nehdi, M.L. (2018) New Test Method for RCP Joint Hydrostatic Infiltration, CSCE Conference 2018, Fredericton, New Brunswick, Canada.

Wong, L. and Nehdi, M.L. (2020, In Press) Quantifying Resistance of Reinforced Concrete Pipe Joints to Water Infiltration, *ASCE Journal of Pipeline Systems - Engineering and Practice*.

Wong, L. and Nehdi, M.L. (2020, Submitted) Predicting Hydrostatic Infiltration in Reinforced Concrete Sewer Pipes Considering Joint Gap and Joint Offset, *ASCE Journal of Pipeline Systems - Engineering and Practice*.

Wong, L., Marani, A. and Nehdi, M.L. (2020, Submitted) Coupled Gradient Boosting – Ensemble Oversampling Hybrid Model for Prediction of Concrete Pipe Joint Infiltration, *ASCE Journal of Pipeline Systems - Engineering and Practice*.

## **DEDICATION**

To:            My Wife:     Grace Tsoi

                 My Children: Kalos Wong and Charis Wong

                 My Parents:    Wa Chan, Kan Chuen Wong

## **ACKNOWLEDGMENTS**

Professor M. L. Nehdi – supervisor and mentor, his encouragement, vision and guidance, allowed me to open doors to the new field of machine learning in Con Civil Engineering.

Brian Wood – President at Con Cast Pipe, my former employer, for his financial support and his vision in the industry and pursuing innovation.

Con Cast Pipe – Support in the space and technical staff (Andrew Cleland, James Cameron, Tien Nguyen) at different stages of the experimental program.

Press Seal Corporation and Hamilton Kent – supplies of gasket samples, and their technical inputs, laboratory for material testing.

James Malpass, P.Eng. – technical mentor, his practical experience and guidance provided great help. Being a distant student, he welcomed me to stay at his place for certain occasions such as inclement weather or examinations.

# TABLE OF CONTENTS

<b>ABSTRACT</b> .....	ii
<b>CO-AUTHORSHIP STATEMENT</b> .....	v
<b>ACKNOWLEDGMENTS</b> .....	vii
<b>TABLE OF CONTENTS</b> .....	viii
<b>LIST OF TABLES</b> .....	xiii
<b>LIST OF FIGURES</b> .....	xv
<b>LIST OF NOMENCLATURE</b> .....	xix
<b>LIST OF ABBREVIATION</b> .....	xxi
<b>LIST OF APPENDICES</b> .....	xxiii
<b>PREFACE</b> .....	xxiv
<b>CHAPTER 1</b> .....	1
1 Introduction .....	1
1.1 Research Needs and Motivation .....	2
1.2 Research Objectives.....	2
1.3 Thesis Outline and Format.....	2
1.4 Original Contribution.....	4
1.5 References.....	5
<b>CHAPTER 2</b> .....	6
2 Literature Review.....	6
2.1 Inflow and Infiltration.....	6
2.2 Reinforced Concrete Pipe Development.....	9
2.2.1 History of RCP.....	9
2.2.2 Industry Challenges .....	10
2.3 Specification Review .....	13



2.4	Specifications Review for Hydrostatic Performance .....	16
2.4.1	General .....	16
2.4.2	Internal Pressure Tests for Joint Quality .....	17
2.4.3	Internal Pressure Tests for Pressure Rating .....	17
2.4.4	In-field Tests for Infiltration .....	18
2.5	Gaps in Standard Specifications .....	20
2.6	Recent Development for Infiltration Test .....	22
2.7	Summary .....	24
2.8	References .....	26
CHAPTER 3 .....		30
3	Experiment Development .....	30
3.1	Testing Concept .....	30
3.2	Mechanical Apparatus .....	32
3.3	Testing Setup .....	34
3.4	Setup with Joint Gaps .....	36
3.5	Setup with Joint Offset .....	37
3.6	Testing Procedure .....	39
3.6.1	Measurements .....	39
3.6.2	Ultimate Capacity .....	39
3.6.3	Operating Capacity .....	41
3.7	Test Results for Condition Classification .....	41
3.8	Sample Selection .....	43
3.8.1	Pipe .....	43
3.8.2	Gasket .....	44
3.9	Summary .....	45

3.10References .....	46
CHAPTER 4 .....	47
4 Pipe Joint Design .....	47
4.1 Rubber Gasket.....	47
4.2 Joint Design .....	49
4.3 Gasket Specimens .....	52
4.4 Sealing Potential Calculation.....	56
4.5 Sealing Pressure and Joint Gap.....	56
4.6 Sealing Pressure and Geometrical Variations.....	57
4.7 Sealing Pressure and Joint Alignment .....	57
4.8 Summary .....	58
4.9 References.....	58
CHAPTER 5 .....	59
5 Testing Results.....	59
5.1 Ultimate Hydrostatic Capacity.....	59
5.2 Operating Hydrostatic Capacity.....	61
5.3 Joint Gap Monitoring.....	63
5.4 Leakage Monitoring.....	66
5.5 Additional Tests .....	68
5.6 Preliminary Findings.....	69
5.7 Ultimate Pressure Capacity Varying by Pipe Size.....	70
5.8 Water Level Reduction in Ultimate Pressure Evaluation .....	71
5.9 Water Level Reduction in 20-hour Operation Test.....	76
5.10Summary .....	77
5.11References.....	78

CHAPTER 6 .....	79
6 Joint Hydrostatic Performance Curves and Application .....	79
6.1 Hydrostatic Performance Implications .....	79
6.2 Reality Challenges in Maintaining Minimum Joint Gap .....	80
6.3 Performance Curve Development.....	81
6.4 Test Results.....	83
6.5 Prediction Using Gasket Load-deformation Tests .....	84
6.6 Discussion on Uncertainty of Data .....	85
6.7 Application of Performance Curves.....	86
6.7.1 Process .....	86
6.7.2 Infiltration Potential Factor.....	87
6.7.3 Illustrative Case Study .....	89
6.8 Summary .....	91
6.9 References.....	91
CHAPTER 7 .....	92
7 Hydrostatic Performance for Infiltration Prediction using Machine Learning Techniques .....	92
7.1 Recent AI Applications.....	92
7.2 Machine Learning Literature Review .....	94
7.2.1 Tree-based classifiers.....	94
7.2.2 Oversampling .....	96
2.4.1 K-Nearest Neighbours (KNN) .....	97
7.3 Model Development.....	98
7.3.1 Data Preparation.....	98
7.3.2 Data Statistical Distribution.....	99
7.3.3 Machine Learning Model.....	104

7.3.4	Classification Performance .....	105
7.4	Results and Discussions .....	108
7.4.1	General .....	108
7.4.2	Performance of Tree-based Models Before Oversampling .....	108
7.4.3	Oversampling Methods .....	112
7.4.4	SMOTE .....	113
7.4.5	DBSMOTE .....	115
7.4.6	Comparison between different models .....	117
7.4.7	Feature Importance .....	119
7.4.8	Design Approach: Recommendations for Future Work .....	120
7.5	Summary .....	120
7.6	References .....	121
CHAPTER 8	.....	125
8	Summary, Conclusions and Recommendations .....	125
8.1	Conclusions .....	126
8.1.1	Existing Standards and Literature .....	126
8.1.2	Experimental Development .....	127
8.1.3	Machine Learning Modeling .....	130
8.2	Recommendations .....	131
8.3	References .....	132
Bibliography	.....	133
Appendix A – Design of the Testing Apparatus	.....	1
Appendix B – Testing Results	.....	1
Appendix C – Machine Learning Source Code and Output	.....	1
Curriculum Vitae	.....	1

# LIST OF TABLES

Table 1: List of flexible pipe products.....	10
Table 2: List of RCP standards. ....	14
Table 3: Acceptance criteria for RCP. ....	14
Table 4: Population of studied area (Population Reference Bureau 2013).....	15
Table 5: Summary of Joint Performance Standards .....	16
Table 6: Hydrostatic performance test summary .....	18
Table 7: Infiltration Allowance for Sanitary Sewer.....	21
Table 8: Comparison between Infiltration Test and Conventional Hydrostatic Test .....	25
Table 9: Infiltration Test Result Conditions .....	42
Table 10: Infiltration Test Count Summary .....	42
Table 11: Pipe Joint Geometry .....	43
Table 12: List of Gaskets Used in the Research .....	45
Table 13: RCP Single Offset Joint Detail .....	51
Table 14: Gasket Properties .....	53
Table 15: Summary of Test Result for Ultimate Capacity with Aligned Position .....	60
Table 16: Summary of Test Result for Ultimate Capacity with Offset Position .....	61
Table 17: Summary of Test Result for Operating Capacity with Aligned Position .....	62
Table 18: Summary of Test Result for Operating Capacity with Offset Position .....	63
Table 19: Summary of Test Result for Other Pipes and Gaskets .....	69

Table 20: Gasket Mass to Annular Space Influence Ratio, $I_g$ .....	70
Table 21: Estimated Volumetric Change in Annular Space .....	72
Table 22: Recent Applications of Machine Learning in Civil Engineering .....	93
Table 23: Data Parameters for ML .....	99
Table 24: The Summary of Coefficient of Determination from the Regression Analysis ...	103
Table 25: Hyperparameters for Tuning ML Learning Models .....	112
Table 26: Hyperparameters for Tuning SMOTE and DBSMOTE Models .....	117
Table 27: The Confusion Matrix, Accuracy, And AUC using Various Splits of the Original Dataset.....	119

## LIST OF FIGURES

Figure 1: CCTV showing Type 3 Infiltration as per ASTM C1840 (2017). .....	7
Figure 2: A 40-year-old concrete pipe showing the level of sewage.....	13
Figure 3: Illustration of various hydrostatic test setup standard configurations. ....	19
Figure 4: Test setup for infiltration by Fenner (After Fenner, 1990).....	22
Figure 5: Test setup for joint alignment (top), offset (centre) and joint deflection (bottom) proposed by Moore and Garcia (2015). ....	23
Figure 6: Test Setup. ....	31
Figure 7: RCP Joint Test Detail. ....	32
Figure 8: Pressurization Apparatus. ....	33
Figure 9: Pressurization Mechanical System Scheme. ....	34
Figure 10: Test Pipe Section (left) Bell End (right) Spigot End. ....	35
Figure 11: Interior of Test Pipe Section. ....	35
Figure 12: (a) A spacer ring is placed in between the pipe sample to create the desired joint gap. (b) The gap spacer ring is placed below the secondary gasket to open the gap of the pipe joint. ....	36
Figure 13: Illustration for offset joint. ....	37
Figure 14: Hydrostatic test setup for infiltration with joint offset. ....	38
Figure 15 Moment of Failure. ....	40
Figure 16: RCP Joint Profile and Annular Space .....	44
Figure 17: Typical load-deformation curve for rubber gasket (After Czernik, 1996). ....	48

Figure 18: Gasket deformation test.....	49
Figure 19: Illustration of gasket geometry withstands internal pressure. ....	50
Figure 20: RCP Single Offset Joint Detail.....	51
Figure 21: Typical cross-section of self-lubricated single offset gasket.....	54
Figure 22: Gasket Geometric Properties.....	55
Figure 23: Offset joint.....	58
Figure 24: Hydrostatic Infiltration Performance for 600 mm RCP. ....	64
Figure 25: Hydrostatic Infiltration Performance for 900 mm RCP. ....	65
Figure 26: Hydrostatic Infiltration Performance for 1200 mm RCP. ....	65
Figure 27: Water Level Monitoring from WSCC.....	66
Figure 28: Minor External Leak During Test (1200 mm RCP, 375 kPa).....	67
Figure 29: Leakage from Outside. ....	67
Figure 30: Leakage from Inlet Tube Caulking (600mm at 300 kPa).....	68
Figure 31: Hydrostatic Infiltration Performance for Self-lubricated Single Offset Gasket Profile (T06).....	71
Figure 32: Water Reduction Chart for 600 mm RCP. ....	74
Figure 33: Water Reduction Chart for 900 mm RCP. ....	74
Figure 34: Water Reduction Chart for 1200 mm RCP. ....	75
Figure 35: Primary Gasket Displacement at Failure.....	76
Figure 36: Water Level Reduction for 20-hour Operation Test (T06). ....	77



Figure 37: (a) Left: Displaced gasket captured by CCTV and (b) Right: observed in the infiltration test.....	80
Figure 38: Joint gap on the (a) left, and (b) right side of the pipe created in the job site to account for the manufacturing tolerance to maintain sewer alignment. ....	82
Figure 39: 600 mm RCP infiltration Joint Test Performance Curves.....	82
Figure 40: 900 mm RCP infiltration Joint Test Performance Curves.....	83
Figure 41: 1200 mm RCP infiltration Joint Test Performance Curves.....	83
Figure 42: Infiltration Potential Assessment Model. ....	87
Figure 43: Infiltration Potential Assessment Illustration. ....	89
Figure 44: Profile View of a Potential Infiltration Case. ....	90
Figure 45: Decision Tree Scheme.....	95
Figure 46: Behaviour of Rubber used as RCP Joint Sealant. ....	101
Figure 47: Statistical Distribution and Trends of RCP Infiltration Test Results. ....	102
Figure 48: Regression Analysis. ....	103
Figure 49: Classification ML Model Framework for RCP Joint Performance Data. ....	105
Figure 50: Confusion Matrix. ....	106
Figure 51: Scheme ROC Curve. ....	108
Figure 52: Classification Report and Confusion Matrix from: (a), (b) and (c) Original Training Data; (d) SMOTE Training Data; and (e) DBSMOTE Training Data.....	110
Figure 53: Classification Report and Confusion Matrix from the Original Testing Data ....	111
Figure 54: Performance Comparison Among Tree-based Classifiers on Testing Data.....	112

Figure 55: Comparison of data counts between oversampling techniques.....	113
Figure 56: Accuracy and AUC Comparison between Original Testing Data and Oversampled Data using SMOTE.....	115
Figure 57: Accuracy Measurements Against eps Using DBSMOTE.....	116
Figure 58: Accuracy Measurements Against min_samples Using DBSMOTE.....	117
Figure 59: Comparison of performance using gradient boosting classifiers trained by the original, SMOTE and DBSMOTE training data.....	118
Figure 60: Feature Importance Using DBSMOTE.....	119

## LIST OF NOMENCLATURE

$A_s$	mm <sup>2</sup>	Annular space
$AS_c$	mm	Circumference of the annular space
$B$	mm	Single offset distance of the joint
$b$		Constant in regression analysis
$D_s$	mm	Diameter of the single offset step at the pipe spigot
$f$	mm	Spigot width
$F_1$		Score measuring the accuracy of ML model
$G$	mm	Joining gap
$H_c$	mm	Compressed height of the gasket
$H_g$	mm	height of unstretched gasket
$H_s$	mm	height of stretched gasket
$I_g$	g / mm <sup>2</sup>	influence ratio
$ID$	mm	Pipe inner diameter
$J$	mm	Joint depth
$j_s$	mm	Joint depth of the larger gap
$j_T$	mm	Joint depth of the smaller gap
$m$		Slope in regression analysis
$n$		Number of samples
$P$	N or lb	Applied force in gasket load-performance test

$P_f$	N or lb	Factored applied force in gasket load-deformation test
$R$		The square root of coefficient of determination
$r_s$		ratio of stretched length to unstretched length
$S$	mm	Larger gap between the bell and spigot of the single offset joint
$S'$	mm	Larger gap between the bell and spigot of the single offset joint with open joint gap
$T$	mm	Smaller gap between the bell and spigot of the single offset joint
$T'$	mm	Smaller gap between the bell and spigot of the single offset joint with open joint gap
$W$	mm	Base width of the gasket
$x$		Input variable
$y$		Output value
$y_i$		Output value, $i$
$\hat{y}$		Fitted or predicted output value
$\bar{y}$		Mean of output value
$\Delta S$	mm	Change in larger gap between the bell and spigot of the single offset joint due to the opening of the joint gap
$\theta$	°	Taper angle of the joint

## LIST OF ABBREVIATION

AUC	area under curve
AI	artificial intelligence
ANN	artificial neural network
CCTV	closed-circuit television
CSP	corrugated steel pipe
DBSMOTE	density-based synthetic minority over-sampling technique
ET	extra trees
ETC	extra trees classifier
FN	false negative
FP	false positive
FPR	false-positive rate
GBC	gradient boosted classifier
GB	gradient boosting
HDPE	high-density polyethylene
InI	Inflow and infiltration
KNN	K-nearest neighbours
ML	machine learning
MICC	microbiologically induced concrete corrosion
min	Minute

MTO	Ministry of Transportation Ontario
PE	polyethylene
PVC	polyvinyl chloride
RF	random forest
RFC	random forest classifiers
ROC	receiver operating characteristic
RCP	reinforced concrete pipe
SRHDPE	steel reinforced high-density polyethylene
SMOSTE	synthetic minority over-sampling technique
TN	true negative
TP	true positive
TPR	true positive rate
WSCC	water supply connecting cylinder

# **LIST OF APPENDICES**

Appendix A – Design of the Testing Apparatus

Appendix B – Test Results

Appendix C – Machine Learning Source Code and Output

## **PREFACE**

I spent the first half of my career in the precast concrete industry after graduating from my master's degree, specifically, with a reinforced concrete pipe manufacturer. When hearing about the superior performance of concrete pipe and many marketing articles on the embarrassing news of its counterparts, the industry was very slow in developing effective solutions to tackle two of its main challenges: leaky joints and hydrogen sulphide corrosion. These challenges led to a decline in the sanitary market in many places across the United States and Canada. In some parts of the United States, the market had vanished and was replaced with flexible pipes. As an engineer, we are trained to solve technical problems by applying sound engineering principles. Our solutions are built on a concrete research foundation. With great encouragement from my supervisor Prof. Moncef L. Nehdi, and the financial support from the president of my ex-employer, Brian Wood, I enrolled in the Ph.D. program at Western in 2017. Being a full-time student with a full-time job, these years were not easy. My experience in the industry allowed me to fast track the research making this possible. Despite the challenges in machine learning, which put me out of my comfort zone, the outcome was enjoyable. The knowledge of machine learning creates unlimited possibilities in this field because the industry is so behind in adopting the advantages of emerging technologies. This degree started another new chapter of my career.



# CHAPTER 1

---

## 1 Introduction

The ingress of groundwater into sewage pipeline systems, known as infiltration, has been a challenge for municipalities as early as the 1970s. Part of the issue was due to ageing infrastructure. However, many newly constructed pipe joints have exacerbated the problem. Research and development in the joint performance of reinforced concrete pipe (RCP) have been overlooked. Over the past century, the RCP industry has rather focused on material structural strength and design theory. Yet, the century-old RCP faced tremendous threats from emerging flexible synthetic pipe materials. Among many technical challenges, leaky joints and microbial induced concrete corrosion have been the most problematic. When dealing with hydrostatic joint performance, the industry does not have a standardized test to validate the capacity of the existing joint designs and joint materials against external pressure. The current hydrostatic test required by the standard is for quality control purposes; and is limited in measuring the ability of the joint to withstand the internal pressure for 10 minutes. The measurement is binary and is incorrectly interpreted by the end-user.

This thesis records the development of a new method to evaluate the RCP joint hydrostatic performance for infiltration. It offers a standard testing method, not only as quality control for concrete pipe manufacturers but also provides a channel of further development for better hydrostatic performance. The second part of the study takes the data collected from the experiment further into the artificial intelligence world. Advanced machine learning (ML) techniques are explored to allow predictions of leakage given predefined conditions.

Using supervised tree-based ML models and methods to account for the imbalanced data results in the best predictive accuracy of experimental results.

## 1.1 Research Needs and Motivation

Technological breakthroughs are needed to rejuvenate the RCP industry. In order to preserve the value of RCP, the foremost step is to mitigate the shortcomings of the existing aged specifications that fail to tackle leaky joints, deficient load tests, and microbiologically induced concrete corrosion (MICC) by hydrogen sulphate attack. In 2017, a university-industry research program via synergy between Western University and Con Cast Pipe was initiated to enhance the mechanical, hydrostatic, and durability performance of RCP. As an overall research scope, it aims at RCP production cost reduction, developing robust and unbiased specifications, mitigating biogenic corrosion problems, and better meeting end-user expectations. This thesis focuses on the specific issue of joint infiltration for newly installed RCP sewers.

## 1.2 Research Objectives

The research objectives are to provide a groundwork to the RCP industry so that the RCP infiltration potential can be better understood, evaluated and mitigated. These objectives can be achieved by pioneering a testing standard that can adequately evaluate the capacity of the RCP joint against infiltration in the factory setting, easy enough to be conducted as a satisfactory quality test, and reliable enough to reflect the in-situ hydrostatic conditions.

## 1.3 Thesis Outline and Format

This thesis has been prepared in accordance with the integrated-article format predefined by the Faculty of Graduate Studies at Western University, London, Ontario, Canada. The contents are presented in eight chapters. Substantial parts of the thesis have either published or submitted for publication in peer-reviewed technical journals (**Wong and Nehdi, 2018, Wong and Nehdi, 2020, Wong et al., 2020**). The outline of the chapters is as follows:

Chapter 1 provides an introduction, along with the research background and objectives of the study.

Chapter 2 provides a comprehensive literature review on RCP development history, the challenges on inflow and infiltration, specifications for RCP hydrostatic performance and the knowledge gap between the standards and the practical challenges. Chapter 2 also reviews the recent experimental developments on similar topics conducted by other researchers.

Chapter 3 details the experimental concept, physical setup, testing procedures and the anticipated results. Chapter 3 also provides descriptions of the pipe samples and gasket sample selections.

Chapter 4 provides information on pipe joint design and mechanical properties of rubber gaskets. The sealing potential created by both the gaskets and the pipe joints, and influence factors are covered in this chapter.

Chapter 5 reports the testing results and evaluates the ultimate and operating capacity. Other results obtained in the experimental program, such as joint gap monitoring, are also reported. This chapter also provides preliminary findings and experimental observations.

Chapter 6 presents joint the performance curves of three selected RCP sizes developed using the data collected from the experimental program. This chapter links the experimental and practical construction challenges in jointing RCP with respect to the hydrostatic performance for infiltration. An illustrative case study is presented to support the application of the performance curves developed from the experiment.

Chapter 7 presents the use of machine learning techniques to predict the experimental outcomes based on the data collected from the experiment. Several classification algorithms are reviewed. The ML model is developed to select the best algorithms for this application.

The entire study is summarized in Chapter 8. The main conclusions and recommendations that emanate from this work are outlined in this Chapter.

## 1.4 Original Contribution

This research bridges a major knowledge gap between existing industry standards in evaluating the hydrostatic performance of the RCP joint and the misunderstanding of the actual performance when the pipe is subjected to infiltration conditions from high groundwater tables in the job site. The reported research describes the development of a novel experimental set-up and an original database supporting the method of evaluation. The key influential parameters on joint performance, including joint gap, joint offset, gasket type, pipe size, and test duration, are revealed. The outcomes were further modelled using machine learning techniques to provide adequate predictions.

The study is divided into five phases with the following original contributions:

1. Providing critical analysis of pertinent existing codes and standards for RCP outlining the gap between standards and end-user expectations.
2. Developing a novel testing method including the mechanical apparatus, varied alignment setups, and procedures to evaluate the suitability of existing RCP joint designs and jointing materials.
3. Collecting a unique and versatile, capturing the key influential parameters to produce RCP joint infiltration performance curves.
4. Developing application procedures to quantify the RCP installation quality against site-specific groundwater conditions in order to mitigate the infiltration potential.
5. Developing, for the first time in the open literature, RCP infiltration prediction models based on machine learning methodologies in order to open the doors for the use of ML in such applications.

## 1.5 References

Wong, L. and Nehdi, M.L. (2018) Critical Analysis of Precast Concrete Pipe Standards, *Infrastructures* 2018, 3(3), 18;

Wong, L.; Nehdi, M. L. (2018). New Test Method for RCP Joint Hydrostatic Infiltration, CSCE Conference 2018, Fredericton, New Brunswick, Canada

Wong, L. and Nehdi, M.L. (2020) Quantifying Resistance of Reinforced Concrete Pipe Joints to Water Infiltration, *ASCE Journal of Pipeline Systems - Engineering and Practice*, Reston, Virginia, United States.

Wong, L. and Nehdi, M.L. (2020) Predicting Hydrostatic Infiltration in Reinforced Concrete Sewer Pipes Considering Joint Gap and Joint Offset, *ASCE Journal of Pipeline Systems - Engineering and Practice*, Reston, Virginia, United States.

Wong, L., Marani, A. and Nehdi, M.L. (2020, In peer-review) Hybrid Tree-Based Ensemble-Oversampling Prediction of RCP Joint Performance for Infiltration, *ASCE Journal of Pipeline Systems - Engineering and Practice*, Reston, Virginia, United States.

## CHAPTER 2

---

### 2 Literature Review

This chapter provides a brief history of RCP development and critical analysis of existing RCP standards worldwide, focusing on the challenges faced by the RCP industry in joint performance and concrete corrosion. Greater concerns regarding inflow and infiltration demand the need for this research. A review of several existing specifications and RCP infiltration research provides a background understanding of the research. Substantial parts of this chapter have been published in the journal *Infrastructures* (**Wong and Nehdi, 2018**).

#### 2.1 Inflow and Infiltration

In-situ joint performance has routinely become a focal point for RCP performance and a source of concern for infiltration (**Pipeline, 1999**). Given that the pipe materials are sound, and pipe structural design is adequate, two conditions must be met for infiltration to take place: (a) presence of groundwater, and (b) path where the groundwater can ingress through. Gapped, defected and displaced joints in newly installed pipes commonly contribute to the occurrence of infiltration (**Fenner, 1990**). In a recent report (**Norton Engineering Inc. 2017**), poor pipe jointing was claimed to be the main reason for infiltration. Leaky pipe joints are not an acceptable outcome for the owner. Singh and Adachi (**2013**) presented a theoretical bathtub curve of buried pipe indicating that the failure rate was relatively high, not only in aged pipelines but also in its earlier stage before entering the prime service period. Failure occurring right after installation is common,

considering possible infiltration caused by deficient and displaced joints during construction. Visual inspection sometimes may not be completely reliable because the evidence of InI varies based on the time of the year (**Robinson et al., 2019**). Yet, it is often too late to make appropriate accommodations at the time of the pipe project closing inspection. When leaks occur, fine particle migration is likely to follow. According to the industry mandate, a leak should not be accepted by the owner and should be sealed. The role of the RCP joints was reported in a 40 km sample of the pipe network, which showed that it had a major influence on the hydrostatic performance (**Buco et al. 2008**).

**Figure 1** shows a typical case of a severe infiltration (Type 3 as per ASTM C1840) through an RCP joint in a newly constructed sewer line observed in closed-circuit television (CCTV) inspection. To repair this type of problem, trenchless technologies such as injection grouting can be deployed (**Collection Systems Committee, 2017**). The repair cost can be extremely high in comparison to the cost of the pipe material and construction, especially in smaller diameter pipes, e.g. 1200 mm or smaller, where human access is restricted. The repair will often cause construction delays, increased cost and prolonged social impacts. Any field repairs, such as chemical grouting or structural lining, could fix the problem, but generally, make RCP less attractive to the designer.



**Figure 1: CCTV showing Type 3 Infiltration as per ASTM C1840 (2017).**

A typical concrete pipe joint is considered as a moment-release joint, where no moment transfer takes place (**Moore and Sheldon, 2012**). The joint can rotate and cause separation of one side with respect to the opposite side of the pipe. RCP sections can respond to external loading and ground movement, which may cause joint rotation and/or displacement. Changing construction practice from one pipe section to another and non-uniform bedding conditions can lead to earth load effects with shear force and moment rotation across the joint. Current RCP design codes only consider in-plane stresses and strains, ignoring the longitudinal effects due to the condition of the surrounding soil. Under-performing RCP joints may cause infiltration and subsequent loss of surrounding soil support. Sewer pipe allowing ingress of water can affect the soil-structure under roadways. In the case of corroded steel pipes, sinkholes can be created, causing economic loss, possible injury and even life loss (**CBC, 2012**).

The RCP industry has often focused on promoting the superior mechanical strength of RCP over that of emerging pipe materials. Indeed, the support of the surrounding soil usually plays a less important role in RCP than that in the flexible pipe installations due to the higher pipe stiffness than that of the surrounding soil. The field joint performance is generally perceived as the responsibility of the contractor, not the manufacturer or sealing material supplier. This is reflected in the existing method of joint evaluation using a factory-performed test. This common test, required by the standards to evaluate hydrostatic performance, only examines exfiltration over a very short time period (**Wong and Nehdi, 2018**), while infiltration is not assessed (**CSA A257, 2014**). Hence, it does not evaluate true performance but is rather a go-or-no-go quality assurance check. This test does not capture actual in-situ performance when the pipe incurs infiltration of groundwater. The hydrostatic performance requirements of the joint are usually stated in regional or municipal standards (**ASSHTO 2009, MTO 2014, York Region 2011**). Owners also commonly require the RCP to be watertight, resisting infiltration and exfiltration, zero leakage, or any other means of protecting groundwater from entering the sewage system. Engineers are responsible for explaining how water tightness of the underground pipes and structures are to be achieved at elevations below the prevailing groundwater level, or at least how the risk of infiltration leakage due to groundwater is to be mitigated.



## 2.2 Reinforced Concrete Pipe Development

### 2.2.1 History of RCP

Archeological evidence shows that sewer type construction has existed for thousands of years (**OCPA, nd.**). The documented history of gravity sewer pipe using rigid materials such as concrete, clay and bricks in North America can be traced back to the late 19th century (**Schladweiler, 2017**). Through scientific research, engineers have continuously evolved the pipe's strength, durability, and joint performance. For instance, Marston and Anderson (**1931**) were the first to develop a rational design approach for a rigid pipe. They discovered that the installation conditions influenced the load acting on the pipe. Orlander (**1950**) and Spanglar (**1960**) further enhanced Marston's theory by better describing the stress distribution around the pipe.

In the mid-1960s, Frank Heger (**1963**) studied the structural behaviour of reinforced concrete pipe (RCP) under the three-edge bearing test. This test is still being used today as a primary structural testing method for rigid concrete pipes. The use of welded deformed wire fabric as pipe reinforcement was also reported by Frank Heger. It enhanced crack control and offered better bonding between the concrete and reinforcing steel, resulting in a substantial reduction of the needed reinforcing steel (**Heger 1967**). With advancements in computational technology, finite element modelling was used to simulate the pipe-soil interaction, which provided a better approximation of the earth pressure envelope around the pipe. In the 1970s and 1980s, Heger developed earth pressure distribution based on four standard installation methods. This was later published by the American Society of Civil Engineering (ASCE) (**1993**), AASHTO LRFD (**2009**) and the Canadian Highway Bridge Design Code (**2014**). Going into the new millennium, fibre-reinforced concrete pipe was investigated by the industry. Steel fibre for pipe reinforcement was adopted in European Standard BS EN 1916 in **2002**. The use of steel fibre as primary pipe reinforcement was first published in ASTM C1765 in **2013**, followed by using synthetic fibre-reinforced concrete pipe (FRCP) (**ASTM C1818**) in **2015**. Several studies of fibre-reinforced concrete in Canada were published between 2012 and 2016 (**Mohamed et. al. 2012**).

## 2.2.2 Industry Challenges

### 2.2.2.1 Competition from Flexible Pipe Industry

Since the commercialization of polyvinyl chloride (PVC) pipe in the 1950s, its lightweight, longer lay length, chemical resistance and leak-free features made a significant impact on the concrete pipe industry. Subsequent developments of other flexible pipe materials, such as corrugated steel pipe (CSP), high-density polyethylene (HDPE), polypropylene (PP), fiberglass pipe, and steel-reinforced high-density polyethylene (SRHDPE) offered a multitude of options to engineers when selecting pipe materials to suit design criteria. CSP and SRHDPE can be designed to 3600 mm and 2400 mm, respectively (**Table 1**).

**Table 1: List of flexible pipe products.**

Pipe Materials	Size Range (mm)	Length (m)	Introduced	Joint	Source
Polypropylene Pipe	300–1500	4–6	NA	10.8 psi @ 1000 h	ADS SaniTite HP
Corrugated Polyethylene	100–1500		1987	Watertight	ADS N-12WT
HDPE	100–900	6–10	1960s (Lester, 2017)	Soil-tight	Armtec BOSS 1000, 2000
	600–1500	6	NA	Pressure rated at 5 psi with 10 psi surge	ADS N12 Low Head
Steel Reinforced PE	600–2400	4.2 or 6.6	NA	Welded joint leak-free Test to 15 psi–3 psi load head, soil-tight	Armtec DuroMax
Fiber Glass Reinforced	450–3150	0.75–6	1960s (Curran, 2013)	Pressure classes 0–250 psi	Hobas
PVC	100–1500	--	1950s (Walker 1990)	Pressure rated at 50 psi	Ipex Ring Tite PVC DR35
Corrugated Steel Pipe	150–3600	--	1896 (Rinker Materials 1994)	Soil-tight	Armtec—HelCor
RCP	300–3600	2.4	>100 year (OCPA, nd)	Watertight, test to 15 psi	OCPA

The difference between flexible pipes and concrete pipes is that the flexible pipe relies on the soil as part of the structural support. Flexible materials interact with the surrounding soil under overburden load by deformation. The stiffness of the surrounding soil resulting from the level of compaction provides resistance to the deformation of the pipe. This is also known as the positive arching effect. Consequently, the installation of flexible pipes is more stringent than that for concrete pipe in terms of the geometry of the trench and

compaction effort of the backfill materials. However, the common misunderstanding of the differences in installation requirements between flexible and rigid pipes often puts concrete pipe at a disadvantage.

Going into the 21st century, many flexible pipe companies introduced various innovative wall profiles to improve the pipe stiffness and reduce its deformation. With improved technology, hybrid materials, stronger mechanical properties and effective marketing, the flexible pipe increased its size range significantly, reaching 2400 to 3000 mm in diameter. **Table 1** provides a list of the flexible pipe materials currently available in the North American market, showing their advantages over the rigid concrete pipe. With strong marketing, flexible pipe materials pose a real challenge for concrete pipe, despite that the durability of such pipes is yet to be proven considering that, other than PVC, these products have been on the market for less than 25 years.

#### 2.2.2.2 Hydrostatic Performance Challenges

There is a need to preserve the advantages of reinforced concrete pipe through understanding the expectations of the end-user and the advent of technological advancements and innovations that can propel its performance and bridge the gap between the market needs and current standards. A pipeline is expected to resist the infiltration of groundwater or soil and resist the exfiltration of the flow (**MTO, 2014**). The pipe joint is expected to withstand movements of the pipe, such as deflections, without causing leakage. Profiled gaskets, O-ring gaskets or welded joints are needed where the groundwater level is above invert, and infiltration cannot be tolerated, especially in sanitary applications. The term “water-tightness” is commonly used by specifiers to describe this condition, but this is usually misinterpreted by the pipe manufacturers. Pipe manufacturers usually perform limited routine hydrostatic tests internally and assume that the joint performs equally to the corresponding external pressure. The watertightness of a joint is interpreted based on laboratory results from the gasket supplier. Hydrostatic pressure was quantified, for instance, by the Ministry of Transportation Ontario (MTO) Gravity Pipe Design Guideline (**MTO 2014**) at 10.5-m head for RCP and 7.5-m for HDPE and PVC without a leak. This

quantifies the hydrostatic performance expectations and conditions of any gravity sewer, including RCP. The joint performance of RCP was mentioned in several reports and publications (MTO 2014, Pratt et al. 2011). Joint failures were reported due to ground movement (e.g., soil settlement), infiltration and exfiltration caused by installation and joint sealant materials, and inadequate design and application.

### 2.2.2.3 Bio-Corrosion Challenges

The challenges of microbiologically induced concrete corrosion (MICC) pose a significant threat to RCP used to carry sewage. Concrete corrosion due to the exposure to hydrogen sulphide in the sewerage environment was first reported by Parker (1945) in 1945. Hydrogen sulphide gas induced by bacteria growth on the interface between the sewage and the pipe forms sulfuric acid. The acidic environment rich in sulphate corrodes the upper part of the concrete pipe, causing peeling and reduction in wall thickness and subsequent reinforcing steel corrosion. **Figure 2** exhibits a 40-year old pipe removed from its service, showing the level of the sewerage. The deterioration results in mechanical strength reduction and hence, service life reduction. **Wu et al. (2018)** recently reported a reduction in service life from 75 and 100 years to less than 20 years for a concrete tunnel segment in Edmonton, constructed in 2001. 50% reduction in the service life of concrete truck sewers were reported in their findings, indicating various deterioration due to the biogenic corrosion of concrete. In recent years, various researchers have explored developing prediction models for the concrete pipe wall reduction rate and service life span (**Vollertsen et al. 2011, Sulikowski et al. 2016, Bielefeldt et al. 2017**) by considering factors that influence MICC. New findings, however, still require implementation in concrete pipe standards so that innovative improvements can be introduced in full-scale RCP production.



**Figure 2: A 40-year-old concrete pipe showing the level of sewage.**

## 2.3 Specification Review

In order to develop technical solutions for the abovementioned challenges, the critical analysis was performed in the selected area by comparing existing RCP specifications. The manufacturing standards of RCP used in five concrete pipe consumption countries representing a quarter of the world's population were compared. These include Canada, the United States of America (US), the United Kingdom (UK), Australia and New Zealand, and the People's Republic of China (China). These countries are hereafter called the study area. The governing RCP standards in the study area are listed in **Table 2**. In addition to the geometry and tolerance requirements, the RCP acceptance criteria in the study area consist of structural strength, hydrostatic performance, and concrete quality. **Table 3** exhibits the similarities and differences between the various acceptance criteria.

**Table 2: List of RCP standards.**

Study Area	Design Standard and Reference	Materials and Manufacturing Specification	Structural Strength Testing Standard	Hydrostatic Performance Testing Standard
Canada	CSA S6 OCPA Concrete Pipe Design Manual	CSA A257.2 (RCP)	CSA A257.0	CSA A257.0
USA	ASCE15 ACPA Concrete Pipe Design Manual	ASTM C76 (RCP) ASTM C1765 (SFRCP) ASTM C1818 (SynFRCP)	ASTM C497	ASTM C443 ASTM C1628
United Kingdom	BS EN 1295	BS EN 1916 (RCP, SFRCP)	BS EN 1916	BS EN 1916
Australia & New Zealand	AS/NZS 3725	AS/NZS 4058 (RCP) AS4139 (FRCP)	AS/NZS 4058	AS/NZS 4058
China	CECS 143	GB/T11836 (RCP)	GB/T16752	GB/T16752

**Table 3: Acceptance criteria for RCP.**

Study Area	Materials	Durability Test	Visual Inspection	Concrete Strength	Reinforcement Placement and Amount	Load Test	Hydrostatic Test
Canada		Absorption	Yes	Yes		Yes	Note 1
USA 1	Yes	Absorption	Yes			Yes	Note 2
USA 2	Yes	Absorption	Yes	Yes	Cover and amount		Note 2
UK		Yes	Yes		Cover only	Yes	Yes
Australia & New Zealand		Absorption	Yes		Cover only	Yes	Yes
China			Yes	Yes	Cover only	Yes	Yes

*Note 1—owner required; Note 2—joint conform to ASTM C443, C990, C1628 or other specifications.*

The study area was selected to cover countries having well-established concrete pipe associations and/or related industrial, non-profit regulatory bodies. The US and Canada are selected as a representation of North American standards. The American Standards of Testing and Materials (ASTM) are widely adopted and referenced around the world. British Standards were selected as a representation for European countries and many Commonwealth Nations. Countries such as Malaysia also adopt British Standards for reinforced concrete pipe. Hong Kong, a former British oversea colony, also adopts British Standards for drainage design guides. Australia and New Zealand are part of the front end of pipe technology advancement and were also selected. China, with about 19% of the world's population, is one of the fastest-growing economies in the world, was also selected. Its densely populated metropolises experience rapid urbanization along with high demand for infrastructure development, including drainage systems, and thus the rationale for including it in this study. **Table 4** showed the total population in 2013 covered by the standards studied in this Chapter.

**Table 4: Population of studied area (Population Reference Bureau 2013).**

Study Area	Population (Million)	%
Canada	35	0.5
USA	316	4.4
United Kingdom	64 (700)	0.9 (9.8) *
Australia & New Zealand	27	0.4
China	1357	19.0
Total (Study Area)	1799	25.2 (34.1) *
Total Population	7137	

\* ( ) population of Europe.

The study endeavours to reveal the shortcomings of current standards and the discrepancy between them and the owners' expectations, aiming at supporting the need for change and the potential development of standards that capture recent technological RCP advancements. In particular, hydrostatic pressure performance evaluation from those specifications is presented in subsequent sections. Full study focussing on comparing structural strength examination and concrete durability measurement provisions in current RCP standards was published by Wong and Nehdi (2018).

## 2.4 Specifications Review for Hydrostatic Performance

### 2.4.1 General

Three approaches were categorized in the specifications reviewed from the study areas (**Table 5**): joint quality tests, pressure rating evaluations, and commissioning tests. The first two methods are performed by pipe suppliers in the factory, while the latter method is completed by contractors in the field after installation of the pipeline.

**Table 5: Summary of Joint Performance Standards**

Standard	Ori. *	No. of Pipe	No. of Jt.	Med. **	Dir. ***	Pressure Limit (kPa) <sup>#</sup>	Test Duration	Accept. Criteria	Leak Exam.
<b>Joint Quality</b>									
CSA A257	H	3	2	W	I	103(A),90(D),35(O)	10 min	No leak	Visual
ASTM C443	X	2	1	W	I	90 (A), 70 (D)	10 min	No leak	Visual
ASTM C990	V	2	1	W	I	90 (A)	10 min	No leak	Visual
ASTM C1628	X	2	1	W	I	90 (A), 70 (D)	10 min	No leak	Visual
ASTM C497	H	2	1	W	E	Owner spec.	Owner spec.	No leak	Visual
AS/NZS 4058	H	4	3	W	I	90 (A)	60 min	Limit Leakage	Measure
					I	90		Limit Leakage	Measure
	V/H	1	0	W	I	50, +20% of Operating	90 sec/10 mm wall	Limit Leakage	Visual
BS EN 1916	H	2	1	W	I	50 (A), 50 (D), 50 (O)	15 min		Visual
GB/T 16752	V/H	1	0	W	I	60 CL1, 100 CL2,3	10 min	No leak	Visual
<b>Pressure Rated</b>									
AWWA C302	H	2 +	1+	W	I	Operating	48 hours	No leak	Visual
					I	120 % of operating	20 min	No leak	Visual
ASTM C361	X	2	1	W	I	120% of spec 75-300 375 (A), 375 (O)	Not specified	No leak	Visual
<b>In-field Quality</b>									
ASTM C1214	H	V ar	Va r.	A	E	Initiate at 23.7 (B)	0.3 – 6 min/100ft based on size	Limit Leakage	Measure
ASTM C969	H	< 70 0ft	Va r.	W	I/E	Min. 6 (B) (2ft or 0.6m head)		Limit Leakage	Measure
ASTM C1103	H	2	1	A/ W	E	24 > GWT (B)	5 sec	Limit Leakage	Measure

\*Orientation: H – Horizontal, V – Vertical, X – Not specified,

\*\*Testing Media: W – Water, A- Air,

\*\*\*Pressure Direction: I – Internal pressure, E – External Pressure,

# Testing Position: A – Aligned, D – Deflected, O – Offset, B – as built



## 2.4.2 Internal Pressure Tests for Joint Quality

Standard practices such as **CSA A257.2 (2019)**, **ASTM C443 (2012)**, **ASTM C1628 (2017)** and **BS EN 1916 (2002)**, **AS/NZ 4058 (2007)** and **GB/T 16752 (2006)** evaluate the joint performance by internal hydrostatic pressure. Pipes are horizontally or vertically connected and plugged using bulkheads at each end. One to four test pipes are required in the setup. **Figure 3** illustrates various hydrostatic test setups adopted in the study areas, and **Table 6** summarized the internal hydrostatic performance requirements of each study area. This is a common method and is widely adopted by pipe manufacturers. The duration of the test varies from 2 min to 10 min, depending on the standard. The target pressure is maintained, and the technician is required to observe whether leakage occurs. This test also evaluates the performance with open joint, i.e. while deflecting the pipe alignment to force an open joint. **CSA A257.2** and **BS EN 1916** also evaluate the performance when the joint is subject to a shear force creating a joint offset. In the joint offset, the annular space (space in the joint), when maximized at one side, creates minimum compression in the rubber material, hence the worst hydrostatic performance. However, the main purpose of these tests conducted by the pipe manufacturer is mere quality assurance of the product. Most of these tests have a target pressure, e.g. 103 kPa for CSA A257.2 and 90 kPa for ASTM C443. The test results are binary: pass or fail, and rarely evaluate the true capacity of the joint. The tests also evaluate the ability of the joint to withstand internal pressure and do not correlate to external pressure. In addition, the duration of tests is short, and the pipe sizes are limited to smaller diameters in the interest of safety. No working pressure is determined from this group of testing methods, leading to some misinterpretation or misuse of the standards.

## 2.4.3 Internal Pressure Tests for Pressure Rating

Similar to the test methods described above, **AS/NZS 4058 (2007)**, **AWWA C302 (2016)** and **ASTM C361 (2014)** adopt the same testing methodology and provide pressure ratings. Among these standards, AWWA C302 and ASTM C361 are technically considered to be used for examining pressure pipe. The pressure rating is determined by testing the pipe

assembly to a pressure higher than the specified level, usually 20%. These standards are more stringent and are sometimes being specified in gravity sewer applications that require an elevated joint performance. ASTM C361 requires evaluating the pressure rating under both aligned and offset positions. However, like those tests performed by the manufacturer described in the previous section, these tests only examine the internal pressure rating and do not correlate to field performance.

**Table 6: Hydrostatic performance test summary**

Study Area	# of Test Pipes	Test Ori.	Straight Alignment	Deflection	Differential (Shear) Load	Joint Shear Test	Other Requirements
Canada (CSA A257)	3	Horizontal	103 kPa (10 min)	90 kPa (10 min)	35 kPa at 10 min 45 kN shear load	Shear load during hydro	Owner's requirement Not required if size larger than 1200 mm
US (ASTM)	2	Horizontal or Vertical	90 kPa (10 min)	69 kPa (10 min)	Not required	Shear load without hydro	Owner's requirement
UK (BS EN 1916)	2	Horizontal	50 kPa (15 min)	50 kPa (15 min)	50 kPa for 15 min	50 kPa for 15 min	Not required if wall is thicker than 125 mm
China (GB/T 16752)	1	Horizontal or Vertical	60 kPa CL1 (10 min) 100 kPa CL2 & 3 (10 min)	Not specified	Not specified	--	Not required if wall is thicker than 150 mm
Australia/New Zealand (AS/NZ 4058)	1	Horizontal Vertical	90 kPa (90 s/10 mm wall thickness)	Not specified	Not specified	--	--
Australia/New Zealand (AS/NZ 4058)	4	Horizontal	90 kPa ≤ 0.6 mL/mm/m loss rate in 1 h	Not specified	Not specified	--	--
Australia/New Zealand (AS/NZ 4058)	4	Horizontal	$P_{spec}$ = pressure rating $P_{test} = 1.2 P_{spec}$ $P_{ult} = 1.5 P_{spec}$ for 30 s	Not specified	Not specified	Yes	Contract requirement

#### 2.4.4 In-field Tests for Infiltration

In-field tests are far more effective in detecting leaks under service conditions. They allow the contractor to measure the amount of leakage using air or water after installation of the pipeline. These tests are part of sewer pipe acceptance requirements against infiltration. However, some of these tests can be cumbersome and time-consuming to perform. About 69% of municipalities in Canada do not require these tests (**Norton Engineering Inc., 2017**). For an infiltration test such as **ASTM C1103 (2014)**, a certain level of groundwater is needed, which may not be available at the time of the test. Other standard tests, such as

ASTM C969 (2017) and ASTM C1214 (2013), allow pressure reduction over a long section of pipe. If the total leakage exceeds the limit, it is difficult to identify which joints are the source of the problem. In addition, these tests are usually difficult to execute during construction and only examine the pressure resistance for a short period. These tests are the only way to examine the quality of pipe installation, and many municipalities and regions adopt them for commissioning infiltration acceptance criteria. Criterial limits vary from location to another, as shown in **Table 5**.

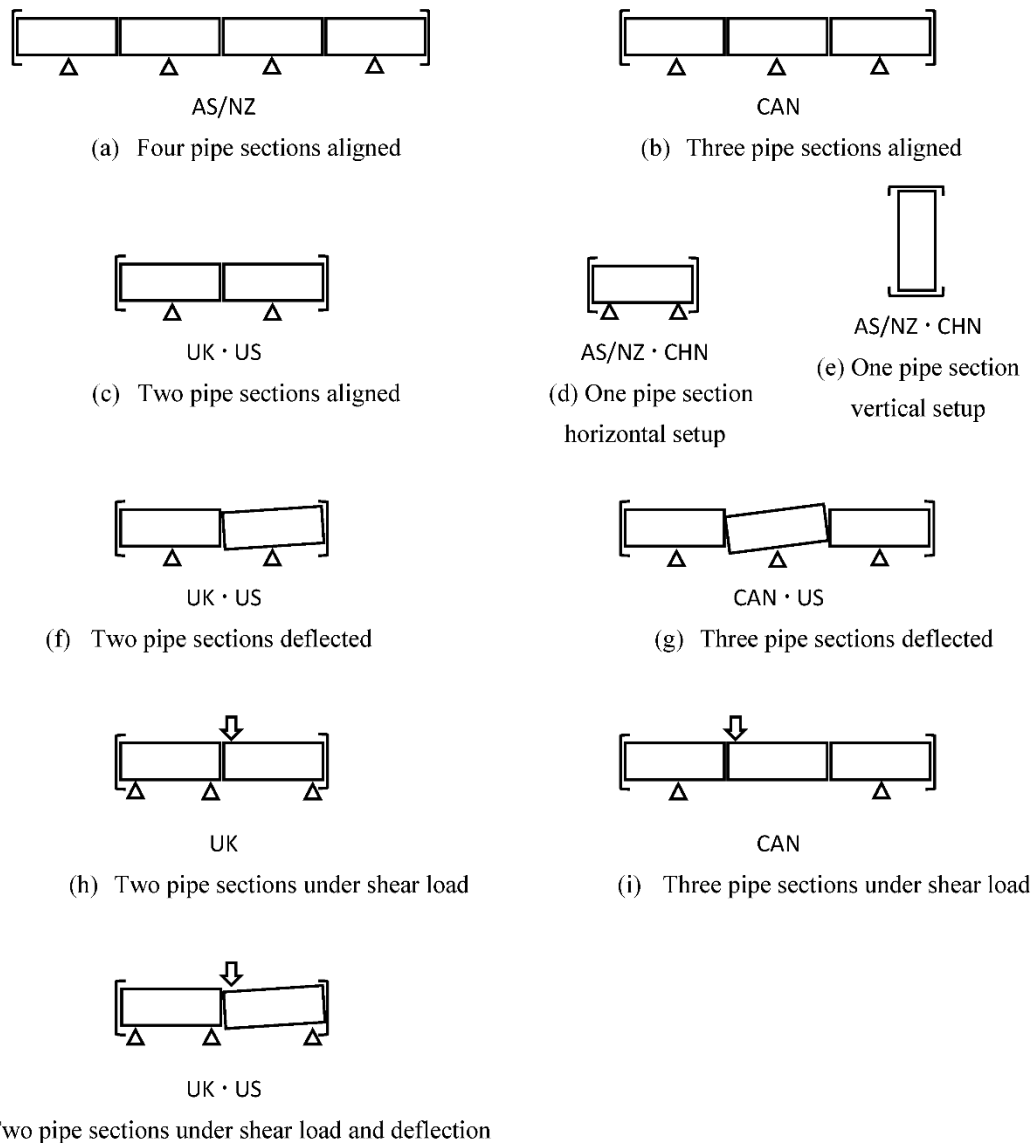


**Figure 3: Illustration of various hydrostatic test setup standard configurations.**

## 2.5 Gaps in Standard Specifications

In the case of sanitary sewer applications, watertight joints are expected to provide flow continuity. A watertight joint is defined as one that provides zero leakage against water infiltration and exfiltration for a specific head or pressure (**ASSHTO, 2009**). The Ontario Ministry of Transportation (**2007**) specifies that all pipe joints shall provide resistance to infiltration of groundwater with specified pressure to match the typical exfiltration performance of 103 kPa (10.5 m of hydraulic head). In most municipalities, infiltration criteria are considered in designing pipelines, as shown in **Table 7**. For example, infiltration criteria in the York Region, Ontario, Canada (**2011**) and OPSS 410 (**2012**) are limited to 0.075 litres per millimetre of pipe diameter per 100 metres per hour. In the case of a 600 mm diameter pipe, the maximum permissible leakage due to infiltration is calculated to be 45 litres per 100 metres length per hour. Other municipalities have specific pipe joint requirements against infiltration. For instance, the City of Surrey, British Columbia, Canada (**2016**) requires an appropriate design of pipe joints for infiltration if the high groundwater table rises above the pipe invert.

To validate the performance of RCP against infiltration, in-situ testing after pipe installation is required to demonstrate the limit of infiltration and exfiltration. ASTM C969 (**2017**) limits infiltration to 200 gallons per inch pipe diameter per mile in 24 hours (0.0927 litres per millimetre diameter per 100 metres per hour). OPSS 410 (**2012**) limits leakage to 0.075 litres/millimetre diameter per 100 metres of pipe per hour, which is less than the ASTM C969 requirement. Such performance requirements are referenced in designing the hydraulic capacity but usually have no relationship to the groundwater conditions, joint design, and installation quality. Moreover, the Region of Peel, Ontario, has recently updated its manhole design standards for new sanitary sewers to completely restrict the ingress of water by specifying multiple levels of joint protection and adopting the use of pressure pipes (**Region of Peel, 2019**). However, there is neither routine evaluation nor validation against infiltration being conducted by pipe manufacturers.

The presence of groundwater is one of the performance criteria that should be adequately considered for RCP joints. Presently, design requirements generally neither consider nor

require validating infiltration performance by the pipe manufacturer. If the pipe is buried 5 m, 9 m or 12 m below the groundwater level, the joint infiltration resistance shall be designed to withstand at least 50 kPa, 90 kPa, and 120 kPa, respectively. The groundwater level is maintained stable for a long duration, which puts the pipe under sustained pressure. Most existing hydrostatic tests and in-situ infiltration tests for system commissioning conduct measurements over a very short period. Existing practices do not warrant the long-term hydrostatic performance of RCP under sustained pressure. This reveals a gap between end-user expectations and industry practices. Without proper standard validation of RCP infiltration prior to installation, the manufacturer and contractor are exposed to high risk, including litigation and financial obligations.

**Table 7: Infiltration Allowance for Sanitary Sewer**

<b>Municipalities</b>	<b>Location</b>	<b>Reference Year</b>	<b>Reference Section</b>	<b>Infiltration Criteria</b>
Region of Peel	Ontario, Canada	July 2009	Section 2.3	0.0002 m <sup>3</sup> /s/ha (0.2 L/s/ha)
City of Edmonton	Alberta, Canada	December 2014	Section 8.7.1	0.28 L/s/ha
City of Toronto	Ontario, Canada	November 2009	Chapter 2	0.26 L/s/ha
Region of York	Ontario, Canada	March 2017	Section 26.12.2	0.075 L/mm/100m/hr
City of Surrey	BC, Canada	March 2008 Kerr Wood Leidal Associated Engineering (2008)	Section 4.1.4 Section 4.3.2	11200 L/day/ha (0.13 L/s/ha)
OPSS 410	Ontario, Canada	November 2012	Clause 07.16.03	0.075 L/mm/100m/hr
ASTM C969	US	2017		200 Gallon/inch/mile/day (0.0927 L/mm/100m/hr)

## 2.6 Recent Development for Infiltration Test

A few non-standard methods for evaluating infiltration were developed by gasket suppliers. The concept was to use a secondary gasket to create a space in the joint for pressurization. These tests require horizontal alignment with visual examination during the test (Hamilton Kent, Ltd.). This test method was recently included in **ASTM C497 (2019)** as part of the standard test for infiltration. The test duration and pressure level are owners specific, and the test result is usually binary: “leak” or “no-leak”. Unlike exfiltration, where visual inspection is conducted from the outside of the pipe, it is nearly impossible to conduct visual inspection effectively on the inside of the pipe if the pipe is less than 1200 mm.

Fenner (1990) developed a method to test a 300 mm clay pipe joint for infiltration by clamping the joint with the surrounding rubber sleeve (**Figure 4**). The maximum pressure exerted on the rubber seal was a 5-meter hydraulic head (50 kPa) equaling to the height of the water level in the standpipe. The leakage was monitored through the piezometer tube. Fenner also examined the joint performance under a vertical angular deflection between two pipes, similar to the deflected alignment and with the damaged joint. Despite the sample only limited to 300 mm, and the material was not reinforced concrete, this method was the earliest reported testing method for infiltration.

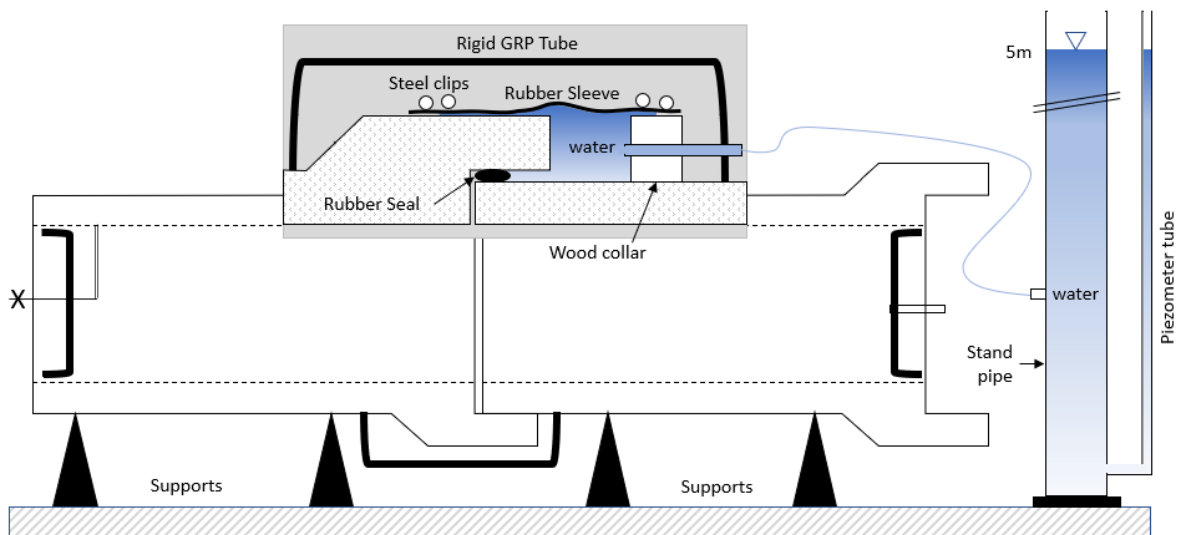


**Figure 4: Test setup for infiltration by Fenner (After Fenner, 1990).**

A new testing protocol for a water tightness of culvert joints was proposed to AASHTO by Moore and Garcia (2015). The testing method was designed to accommodate any pipe and sealing material so as to have a universal method of evaluation. Two pipe sections plugged on both ends are evaluated horizontally with either an internal or external pressure. The testing frame allows the pipe joint to deflect or to be offset under shear load (Figure 5). The external pressure is applied with a partial vacuum, which may not truly examine infiltration. Leakage is visually observed externally. In their study, Moore and Garcia conducted a total of nine tests using 600 mm RCP, including eight tests with 90 kN to 100 kN applied shear force on the joint. Among those eight tests, three involved a combination of joint deflection up to 19 mm. One of the tests was pressurized internally with no shear force but an increasing joint gap. Leakage was observed when the gap reached 38 mm. This test can universally adopt any pipe materials; however, the size of the test set-up is costly, considerably large, and may only accommodate up to a certain pipe size. The test is also an internal test at low-pressure levels. Elevated pressures may create safety concerns. Eye witnessing of a leak is still the main step in the determination of the test.

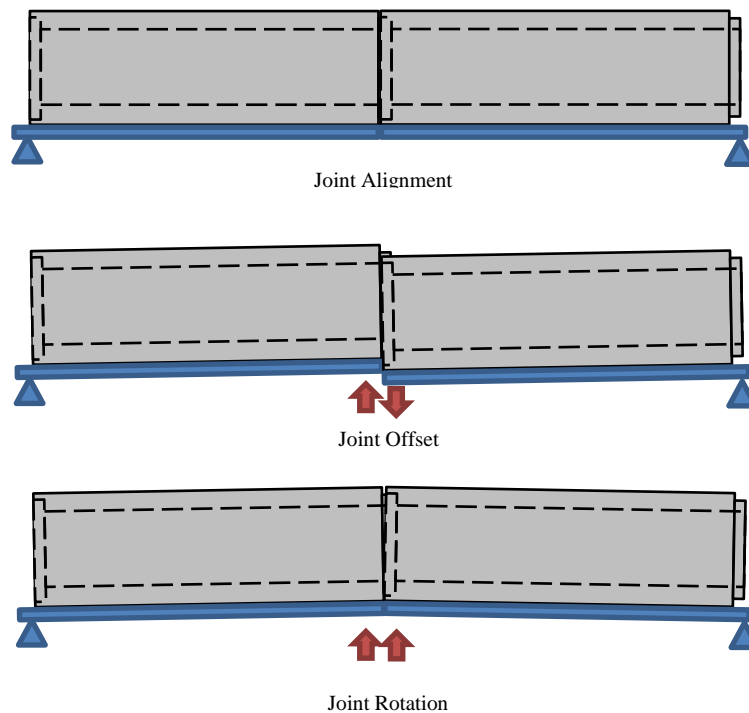


**Figure 5: Test setup for joint alignment (top), offset (centre) and joint deflection (bottom) proposed by Moore and Garcia (2015).**

A novel RCP joint infiltration test was developed and reported in this thesis based on a vertical setup of two pipe sample sections (spigot and bell). This simple test can easily be performed by RCP manufacturers in their production facilities. The detailed test setup and procedure will be described in **Chapter 3. Table 8** compares the tests reported by Wong and Nehdi (2018), Moore and Garcia (2015), Fenner (1990) and the conventional CSA A257 exfiltration test.

## 2.7 Summary

In summary, this chapter provides a background understanding of RCP joints, industry standards related to hydrostatic performance, and the divide between existing standards and the water-tightness requirements set by the end-users. It concludes that:

1. The standard tests do not effectively evaluate the external pressure induced by groundwater through infiltration.
2. The standard tests do not meet the owner's watertight requirement against infiltration.
3. Infiltration is currently a major issue faced by most of the municipalities.
4. An effective, reliable and robust RCP standard infiltration testing method is yet to be developed, standardized and adopted by RCP manufacturers.
5. No literature was found that reports the hydrostatic performance of the RCP joint against infiltration.

In order to preserve RCP products as a major drainage material, further research is needed to mitigate the weaknesses of the RCP joint performance against infiltration. It is important to develop a simple, user-friendly and reliable test for the industry to adopt.



**Table 8: Comparison between Infiltration Test and Conventional Hydrostatic Test**

<b>Reference</b>	<b>Wong and Nehdi (2018, 2020)</b>	<b>Moore and Garcia (2015)</b>	<b>CSA A257.2 (2014)</b>	<b>Fanner (1990)</b>
<b>Scope of the test</b>	Evaluation of joint hydrostatic performance for infiltration	Standardized test for infiltration and exfiltration for all pipe materials	Quality control of RCP joint for exfiltration in the factory	Infiltration and exfiltration of Pipe Joint
<b>Samples</b>	600 mm to 1200 mm diameter RCP 0.45 m long pipe spigot end 0.45 m long pipe bell end	600 mm diameter (2) 2.44 m long	300 mm to 1200 mm (3) 2.4 m full-length pipe	300 mm clay pipe
<b>Ori.</b>	Vertical aligned Vertical gapped Vertical offset and gapped	Horizontal straight Horizontal deflected	Horizontal straight Horizontal deflected Horizontal offset	Horizontal straight Horizontal deflected
<b>Amount of water</b>	Annular space and volume of cylinder	Internal volume of pipes	Internal volume of pipes	Circumferential collar around the joint
<b>Max. Target (kPa)</b>	685	55	105	50
<b>Results</b>	Ultimate pressure, working pressure (80%), gasket movement	Observation of leakage	Pass or fail of target pressure	Measurement of leak rate
<b>Duration of test (excluding setup)</b>	Ultimate (30 – 45 mins) Operating (20 hours)	Up to 96 hours	10 minutes	Not reported
<b>Testing footprint</b>	Based on cross-section of the pipe	Based on two pipes horizontally positioned	Based on three pipes horizontally positioned	Based on two pipes horizontally positioned
<b>Preparation</b>	Cut pipe samples Less than 10 min filling	Full pipe Minimum 1-hour filling depends on pipe size	Full pipe Minimum 1-hour filling depends on pipe size	Full pipe Special designed rubber sleeve and rigid GRP tube setup

## 2.8 References

- American Association of State Highway and Transportation Officials (AASHTO), “LRFD Bridge Design Specification”, Washington, D.C., USA, 2014.
- American Association of State Highway and Transportation Officials (AASHTO), “Pipe Joint Selection for Highway Culvert and Storm Drains”, Washington D.C., USA, 2009, pp. 63-09.
- ASCE 15, “Standard Practice for Direct Design of Buried Precast Concrete Pipe Using Standard Installation”, American Society of Civil Engineers, Reston, VA, USA, 1993, 48 p.
- ASTM C1103-14, “Standard Practice for Joint Acceptance Testing of Installed Precast Concrete Pipe Sewer Lines” ASTM International, West Conshohocken, PA, USA, 2 p.
- ASTM C1214-13, “Standard Test Method for Concrete Pipe Sewerlines by Negative Air Pressure (Vacuum) Test Method”, ASTM International, West Conshohocken, PA, USA, 4 p.
- ASTM C1628-17 “Standard Specification for Joints for Concrete Gravity Flow Sewer Pipe, Using Rubber Gaskets”, ASTM International, West Conshohocken, PA, USA, 2017, 7 p.
- ASTM C1765-13, “Standard Specification for Steel Fiber Reinforced Concrete Culvert, Storm Drain, and Sewer Pipe”, ASTM International, West Conshohocken, PA, USA, 2013, 6 p.
- ASTM C1818-15, “Standard Specification for Synthetic Fiber Reinforced Concrete Culvert, Storm Drain, and Sewer Pipe” ASTM International, West Conshohocken, PA, USA, 2015, 8 p.
- ASTM C1840-17, “Standard Practice for Inspection and Acceptance of Installed Reinforced Concrete Culvert, Storm Drain, and Storm Sewer Pipe” ASTM International, West Conshohocken, PA, USA, 2017, 9 p.
- ASTM C361M-14, “Standard Specification for Reinforced Concrete Low-Head Pressure Pipe”, ASTM International, West Conshohocken, PA, USA, 26 p.
- ASTM C443-12, “Standard Specification for Joints for Concrete Pipe and Manholes, Using Rubber Gasket” ASTM International, West Conshohocken, PA, USA, 2012, 3 p.
- ASTM C497-19, Standard Testing Methods for Concrete Pipe, Concrete Box Sections, or Tile; ASTM C497, ASTM International: West Conshohocken, PA, USA, 17 p.
- ASTM C969-17, “Standard Practice for Infiltration and Exfiltration Acceptance Testing of Installed Precast Concrete Pipe Sewer Lines” ASTM International: West Conshohocken, PA, USA, 2017, 3 p.
- AS/NZS 4058, “Precast Concrete Pipes (Pressure and Non-Pressure)”, Australian Standard: Environmental Health Directorate, East Perth, Australia, 2007, 65 p.
- AWWA C302, “Reinforced Concrete Pressure Pipe, Non-cylinder Type, American Water Works Association, Denver, CO, USA, 2016, 40 p.

- Bielefeldt, Gutierrez-Padilla, Ovtchinnikov, Silverstein, Hernandez. Bacterial, “Kinetics of Sulfur Oxidizing Bacteria and Their Biodeterioration Rates of Concrete Sewer Pipe Samples”, *Journal of Environmental Engineering*, Vol. 136 Issue 7, 2017.
- BS EN 1916:2002, “Concrete Pipes and Fittings, Unreinforced, Steel Fibre and Reinforced”, British Standards Institution (BSI), London, UK, 2002, 94 p.
- Buco, J., Emeriault, F., Kastner, R., “Full-Scale Experimental Determination of Concrete Pipe Joint Behavior and Its Modeling”, *Journal of Infrastructure Systems*, Vol .14, Issue 3, 2008, pp. 230-240.
- CBC News, “2011 video shows 'very serious' storm sewer damage”, Canadian Broadcasting Corporation, Toronto, Ontario: <https://www.cbc.ca/news/canada/ottawa/2011-video-shows-very-serious-storm-sewer-damage-1.1139040>, Assessed, Feb 10, 2020, 2012.
- City of Surrey, “Design Criteria Manual”, Engineering Department., British Columbia, Canada, 2016, 193 p.
- Collection Systems Committee, “Sanitary Sewer Rehabilitation Fact Sheet”, Water Environment Federation: Alexandria, VA: <https://www.wef.org/globalassets/assets-wef/direct-download-library/public/03---resources/wsec-2017-fs-009---csc---sewer-rehabilitation---final---9.27.17.pdf>. Assessed, Feb 10, 2020, 2017.
- CSA A257, “Standards for Concrete Pipe and Manhole Sections”, CSA Group, Mississauga, ON, Canada, 2019, 40 p.
- CSA S6, “Canadian Highway Bridge Design Code”, CSA Group: Mississauga, ON, Canada, 2014, 894 p.
- Curran, S.D. “Fiberglass Pipe Past, Present and Future”, Fiber Glass Tank and Pipe Institute: Houston, TX, USA, 2013, p 5.
- Fenner, R. A. “Excluding Groundwater Infiltration into New Sewers”, *Water and Environment Journal*, Vol. 4, Issue 6, 1990, pp. 544-551.
- GB/T 16752, “Test Methods of Concrete and Reinforced Concrete Drainage and Sewer Pipe”, China, 2006.
- Heger, F. “Structural Behaviour of Circular Reinforced Concrete Pipe – Development of Theory”, *Journal of the American concrete Institute*, 1963, p 48.
- Heger, F.; Gillespie, “J. Design of Circular Concrete Pipe Reinforced with Welded Deformed Wire Fabric”, *Transportation Research Board*: 1967, p 34.
- Lester, H.G. “Corrugated Polyethylene Pipe Design Manual & Installation Guide”, Plastic Pipe Institute: Irving, TX, USA, 2017.
- Marston, A.; Anderson, A.O. “The Theory of Loads on Pipes in Ditches and Test of Cement and Clay Drain Tile and Sewer Pipe”, Iowa State College of Agriculture and Mechanic Arts: Ames, IA, USA, 1913.
- Ministry of Transportation Ontario. “MTO Gravity Pipe Design Guideline”; Ministry of Transportation Ontario: St. Catharines, ON, Canada, 2014, p 233.
- Mohamed, N.; Soliman, A.M.; Nehdi, M.L. “Utilization of steel fibres in precast concrete pipes”, In *Proceedings of TAC 2012, Tunnel and Underground Space: Sustainability and Innovations*, Montreal, Canada, 2012-10-17 (TAC Paper 158), 2012.

- Mohamed, N.; Soliman, A.M.; Nehdi, M.L. “Full-scale pipes using dry-cast steel fibre-reinforced concrete”, *Construction Building Materials*, 2012, 72, pp. 411–422.
- Mohamed, N.; Soliman, A.M.; Nehdi, M.L. “Mechanical performance of full-scale precast steel fibre-reinforced concrete pipes”, *Engineering Structures*, 2012, 84, pp. 287–299.
- Mohamed, N.; Nehdi, M.L. “Rational finite element assisted design of precast steel fibre-reinforced concrete pipes”, *Engineering Structures*, 2012, 124, pp. 196–206.
- Moore and Garcia “Test Methods for Watertightness of Culvert Joints”, National Cooperative Highway Research Program Project 20-07, Task 347. Transportation Research Board: USA, 2015.
- Moore, I., Sezen, H., Sheldon, T. “Structural Design of Culvert Joint”, NCHRP Transportation Research Board of the National Academies, Web-only Document 190, <http://www.trb.org/Publications/Blurbs/167506.aspx>, 2012, 388 p.
- Norton Engineering Inc, “Unacceptable Inflow and Infiltration in New Subdivisions Phase 1 Final Report. Phase 1 Final Report, 59 p., available at: [http://web.archive.org/web/20190403210735/https://www.nortonengineeringinc.ca/I&I%20in%20NS%20Final%20Report%202017\\_Oct%2016%202017.pdf](http://web.archive.org/web/20190403210735/https://www.nortonengineeringinc.ca/I&I%20in%20NS%20Final%20Report%202017_Oct%2016%202017.pdf), 2017.
- OCPA, “Concrete Pipe Design Manual”, Ontario Concrete Pipe Association, Kitchener, ON, Canada, nd., 145 p.
- OPSS 410 “Construction Specification for Pipe Sewer Installation in Open Cut”, Ontario Municipal Provincial Standards, 2012.
- Orlander, H.C. “Stress Analysis of Concrete Pipe”, Engineering Monograph No. 6; US Bureau of Reclamation, Washington, DC, USA, 1950.
- Parker, C.D. “The Corrosion of Concrete”, The Sewage Branch of the Melbourne and Metropolitan Board of Works, Aust. J. Exp. Biol. Med. Sci. 1945, 23, pp 81–90.
- Pipeline “Infiltration and Inflow Can be Costly for Communities”, National Environmental Service Center, Vol. 10, Issue No. 2, 1999, 8 p.
- Population Reference Bureau “2013 World Population Data Sheet”, Population Reference Bureau: Washington, DC, USA, 2013.
- Pratt, C.; Yang, H. “Hodkiewicz, M. Factors Influencing Pipe Failures in the West Australia Environment”, CEED Proceeding: 2011.
- Region of Peel Standard Drawing 2-5-2, “New Sanitary Sewer Construction, Typical Precast Circular Maintenance Hole Details (1200 mm – 3000 mm)”, Region of Peel Public Works Standard Drawing, Brampton, Ontario, Canada, 2019.
- Rinker Materials, “Corrugated Steel Pipe”, Info Series, Rinker Materials, 1994.
- Robinson, B, Sandink, D, Lapp, D. “Reducing the Risk of Inflow and Infiltration (I/I) in New Sewer Construction”, Institute for Catastrophic Loss Reduction: Toronto, Ont., Canada, No. 64, Nov. 2019, 72p.
- Schladweiler, J.C. “The History of Sanitary Sewer”. 2017. Available online: <http://www.sewerhistory.org/> (accessed on June 14, 2018).

- Singh, A. and Adachi, S. “Bathtub curves and pipe prioritization based on failure rate”, *Built Environment Project and Asset Management*, Vol. 3 (1), 2013, pp.105-122.
- Spangler, M. “Soil Engineering”; International Textbook Company: Scranton, PA, USA, 1960.
- Sulikowski, J.; Kozubal, J. “The Durability of a Concrete Sewer Pipeline Under Deterioration by Sulphate and Chloride Corrosion”, *Procedia Eng.* 2016, 153, pp 698–705.
- Walker, R. “The Early History of PVC Pipe”, *thePlumber.com*, <https://theplumber.com/early-history-of-pvc-pipe/>, assessed on Feb 20, 2020, 1990.
- Wong, L. and Nehdi, M.L, “Critical Analysis of Precast Concrete Pipe Standards”, *Infrastructures*, 3(3), 18, 2018, 18p.
- Wong, L. and Nehdi, M.L. “New Test Method for RCP Joint Hydrostatic Infiltration”, *CSCE Conference 2018*, Fredericton, New Brunswick, Canada, 2018.
- Wu, L.; Hu, C.; Liu, W. “The sustainability of Concrete in Sewer Tunnel—A Narrative Review of Acid Corrosion in the City of Edmonton Canada”, *Sustainability* 2018, 2018, 10, pp 517.
- Vollertsen, J.; Nielsen, A.H.; Jensen, H.S.; Rudelle, E.A.; Hvitved-Jacobsen, T. “Modeling the Corrosion of Concrete Sewer”, In *Proceedings of the 12th International Conference on Urban Drainage*, Porto Alegre, Brazil, 11–16 September 2011.
- York Region “Sanitary Sewer System Inspection, Testing and Acceptance Guideline”, Section 2.4: Ontario, Canada, 2011.

## CHAPTER 3

---

### 3 Experimental Development

This chapter provides details of the experimental developments, including the concept of the tests, the experimental apparatus, and the testing setup. Two testing procedures, for ultimate and operating joint capacities, and the results classifications are also detailed in this chapter. Later in the chapter, the selection of the pipe samples and gasket samples are provided. Substantial parts of this chapter have been published in Wong and Nehdi (2018).

#### 3.1 Testing Concept

The tests developed in this study were to provide easy setup, safe operation and quantitative measurements of RCP joint leakage, to quantify the RCP short-term ultimate pressure and to evaluate its long-term performance during operation. **Figure 6** shows the unique vertical setup with a section of the bell and spigot of a pipe that provides ease of access to the inside face of the pipe sample. **Figure 7**, an enlarged cut face of the test joint illustration, shows a small annular space between the primary and secondary gaskets to be pressurized. The pressure is created using compressed air to push the water into the annular space through a small inlet tube. The hydrostatic pressure variation inside the annular space is constant in the vertical setup because the joint gap is on the horizontal plane. Conversely, in the horizontal setup described in **ASTM C497 (2019)**, the pressure varies inside the annular space due to the elevation differential. The primary gasket is used to seal the RCP after the pipe is placed in service. The purpose of the secondary gasket is to force failure in the primary gasket during the test; therefore, those gaskets are carefully selected based on the joint detail of the test RCP. Suppliers are consulted for the adequate gasket based on the target testing pressure, material

properties, and available space. Small inlet and outlet holes are drilled at 180 degrees through the pipe and in between the primary and secondary gaskets. Plastic tubes are sealed with epoxy before conducting the test to allow water to be introduced into the space. To ensure a safe testing process, the equipment was designed to handle a maximum pressure of 685 kPa, equivalent to 68.5-m of hydraulic head. Unlike traditional hydrostatic tests, only a very small amount of water is used in the confined annular space and the testing system. Hence, the filling time is much shorter during the setup. In addition, the new test has no flooding hazard of the testing area when a failure occurs because the maximum amount of water that is possible to leak out is in the water supply connecting cylinder. The operator is expected to monitor and quantify leakage during the test in addition to visual inspection.



**Figure 6: Test Setup.**

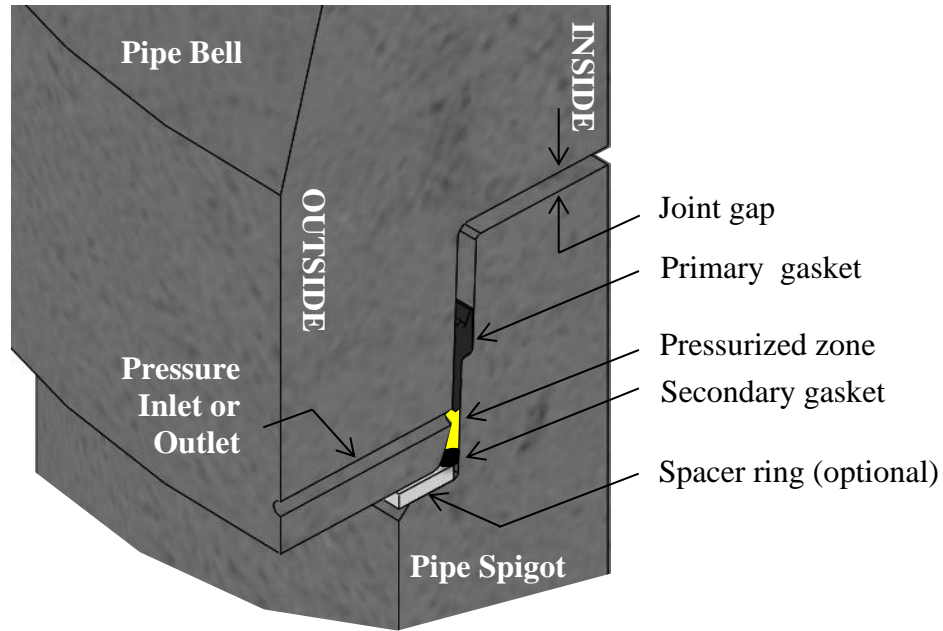


**Figure 7: RCP Joint Test Detail.**

### 3.2 Mechanical Apparatus

The mechanical apparatus shown in **Figure 8** is used to control the compressed air pressure introduced into the annular space of the RCP joint. The pressurization scheme is shown in **Figure 9**. The apparatus includes an air inlet valve, pressure regulator, pressure gauge, water supply connecting cylinder (WSCC), connecting hoses, and a water outlet valve. The pressure regulator allows the operator to control the incoming pressure and maintain the required target testing pressure, which is displayed in the pressure gauge. The WSCC made of a 4-inch diameter semi-transparent fiberglass pressure cylindrical chamber contains enough water at the time of the test to supply the water demand in the annular space. The cylinder allows the water loss during the test to be monitored and measured if a system leakage and/or joint leakage occur. The water outlet valve is used to introduce water to the system during the setup process. When filling the annular space using the inlet valve, the space is considered filled when water escapes from the outlet valve. The outlet valve is then kept closed during the entire test. The design of the apparatus is included in **Appendix A**.



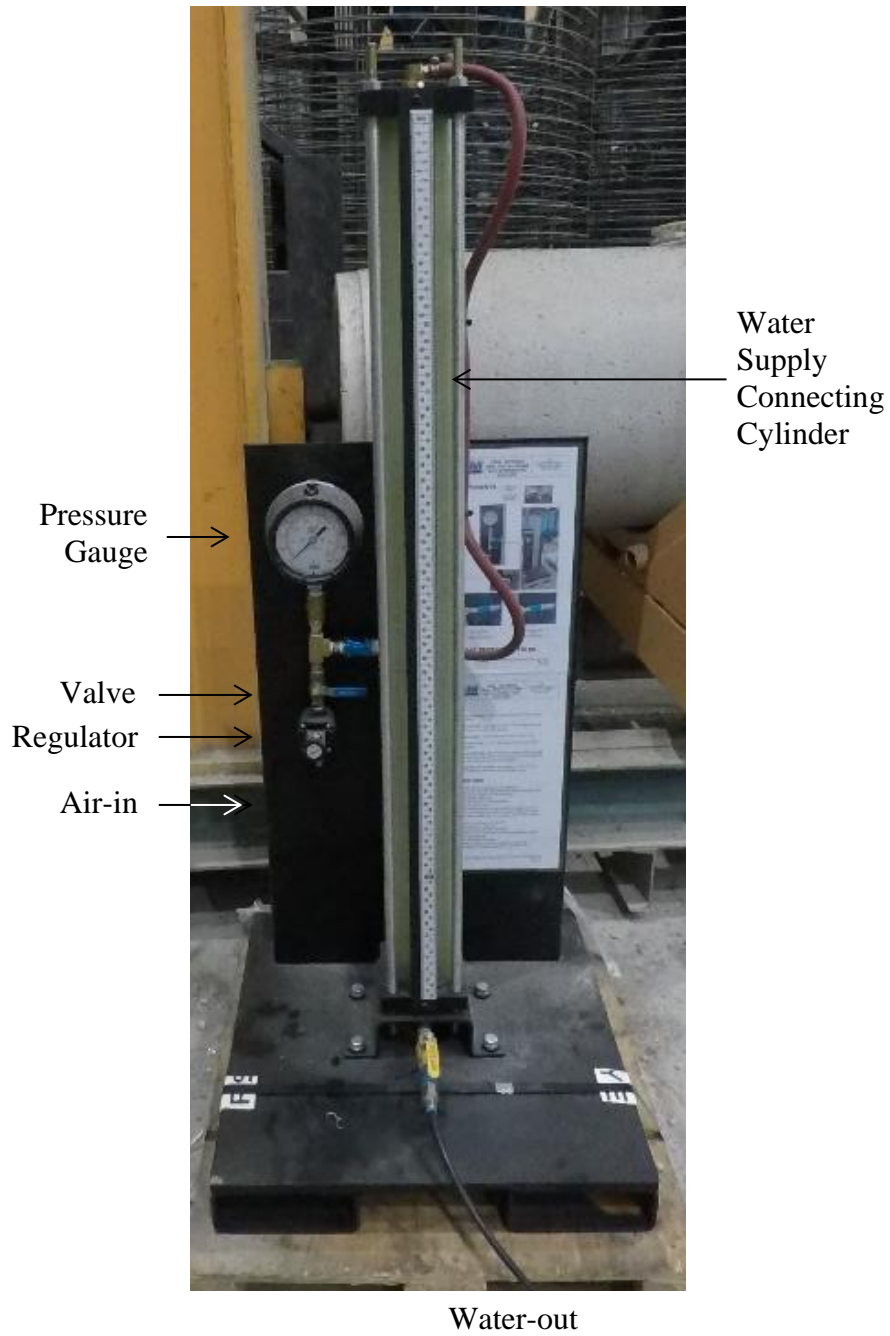


**Figure 8: Pressurization Apparatus.**

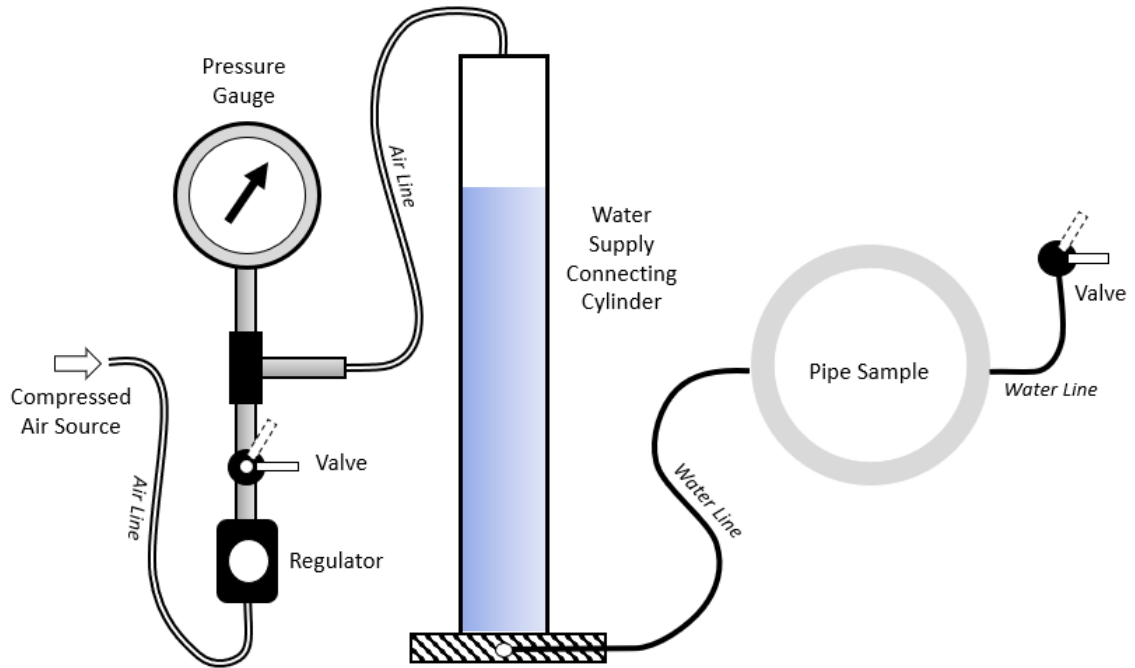


**Figure 9: Pressurization Mechanical System Scheme.**

### 3.3 Testing Setup

Two pipe sections consisting of a bell end and spigot end, as shown in **Figure 10**, are aligned and stacked vertically (**Figure 6**). These sections are saw-cut from the same random pipe sample. The total height of the combined pipe sections is between 700 and 1000 mm for ease of assessment and monitoring of the interior pipe face during the test. **Figure 11** shows the interior of the test assembly setup. Shorter test pipe sections allow the operator to safely monitor the inside of the pipe during the test. The test joint is created by carefully joining two pipe sections sealed with a primary gasket and a secondary gasket. The primary gasket is seated in its design location, and the secondary gasket is placed between the shoulder of the pipe spigot, and the bell end face to create the confined space for pressurization. When a larger gap is required, a plastic spacer ring is sandwiched in between the pipe samples below the annular space. Both joined pipe sections are strapped down to the supporting steel base frame to create restraint from separation during the test. Due to the internal pressure generated, a large uplift force is expected. The number of tie-down straps and the strap rating are calculated based on the target testing pressure and the geometry of the annular space. The base frame is specially designed to carry the expected forces from the strap. In comparison to the field condition, the



### 3.4 Setup with Joint Gaps

In the conventional test, the pipe alignment is deflected to examine the opened joint's hydrostatic performance. The deflected alignment is difficult to achieve because it creates a non-uniform annular space for the secondary gasket to work. Producing a non-uniform gasket is not cost-effective. In order to examine the joint with open gaps under the infiltration condition, a plastic spacer ring is introduced in between the joint. The purpose of this additional ring spacer is to increase the annular space and provide a larger area for the gasket to move during the test. This simulates the joint gap described in the earlier section of this Chapter. Following the same testing procedure, different thicknesses of rings from 6 mm to 13 mm are used in the study to monitor the effect on the hydrostatic performance with respect to the joint gap. **Figure 12(a)** shows a white plastic spacer ring below the secondary gasket that is sandwiched between the pipe samples in the joint. **Figure 12(b)** shows the placement of the spacer ring during the test setup.

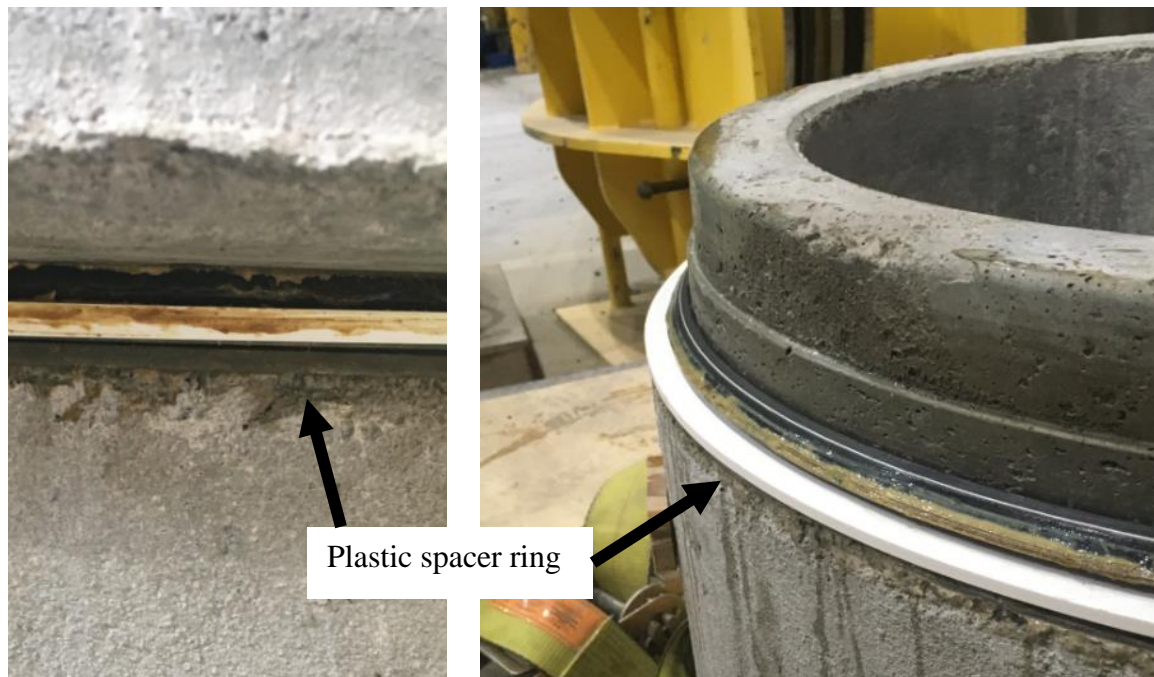


**Figure 12:** (a) A spacer ring is placed in between the pipe sample to create the desired joint gap. (b) The gap spacer ring is placed below the secondary gasket to open the gap of the pipe joint.

### 3.5 Setup with Joint Offset

RCP joints can be offset by external factors such as the differential settlement of bedding materials, differential loads from the backfill or other construction loads. When the joint is offset, the annular space is reduced on one side and increased on the opposite side. This leads to a reduction in hydrostatic performance on the side, having increased joint gap. The joint detail used in this research allows the joint to be offset by 3 mm. To simulate the joint offset, a lateral load is applied using a hydraulic jack on the upper test section with two reaction back supports on the lower test section. **Figure 13** illustrates the test setup for offset joints. To provide a safe operating condition and maintain the offset during the test, a jacking post with a hydraulic pump is mounted on the base frame in addition to the typical setup described earlier. Two back support posts are mounted on the opposite side at about 30 degrees apart. The pump is then connected to a jacking device. Before offsetting the joint, the distance between the pump and the post is measured as a reference. **Figure 14** shows the complete test setup with joint offset and the measurement of the offset joint.

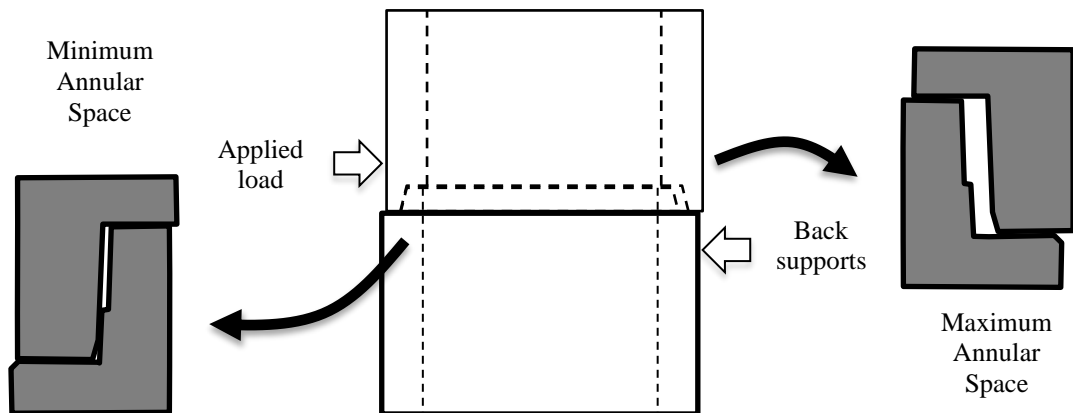


**Figure 13: Illustration for offset joint.**



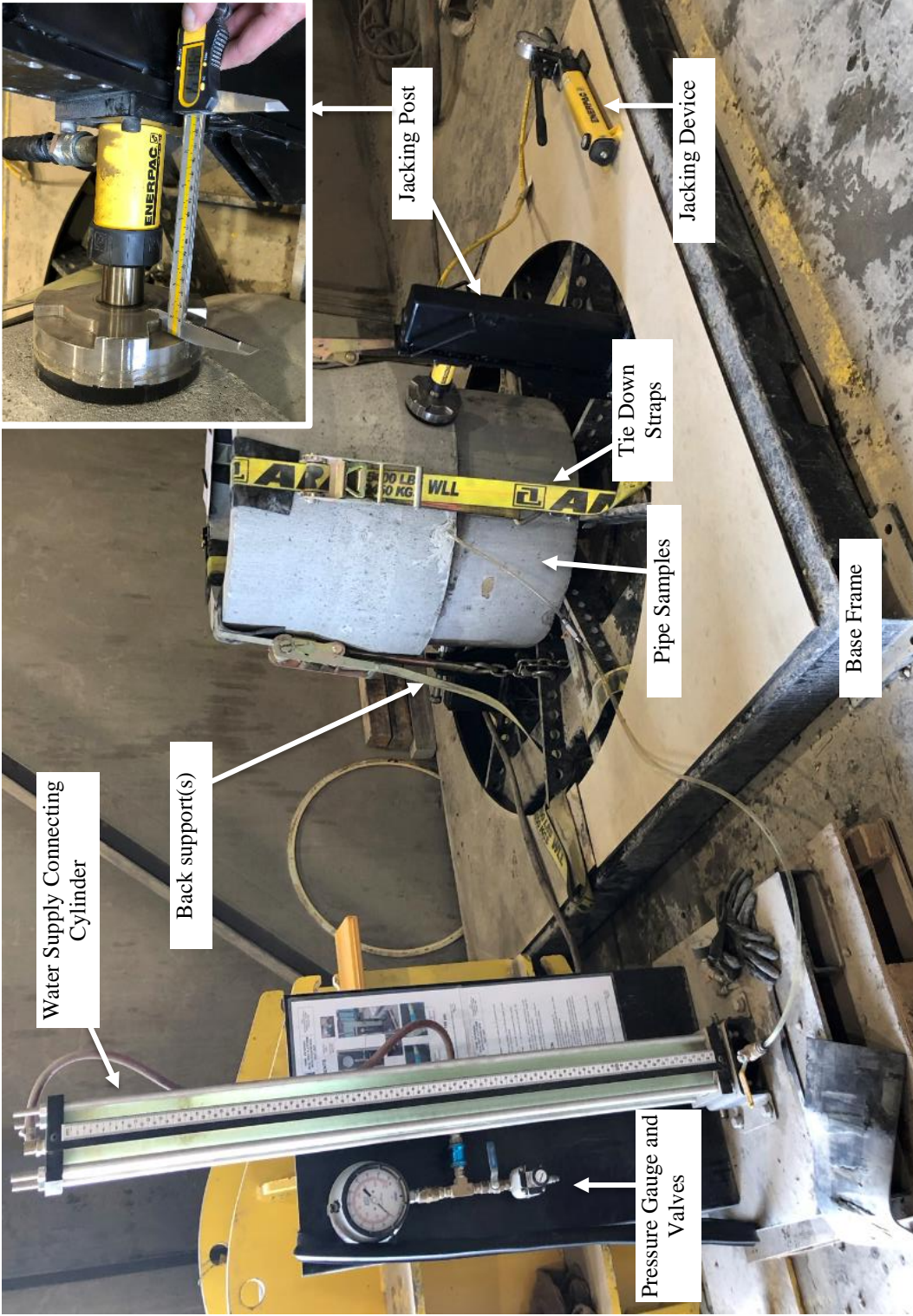


Figure 14: Hydrostatic test setup for infiltration with joint offset.

## 3.6 Testing Procedure

### 3.6.1 Measurements

During the test, the following parameters are monitored and recorded: pressure, time, water level in the WSCC, and joint gap movement. The testing pressure is measured in kilopascal (kPa) at a minimum of 25 kPa intervals. Time measurements are conducted using a digital stopwatch displayed near the pressure gauge. The water level in the WSCC with respect to the starting point is measured in millimetres at each pressure interval using callipers. The change in water level is recorded and converted to litres based on the calculation of cylinder volumetric change, which indicates the loss of water in the WSCC, as discussed below. Joint gap and its movement are critical in the joint hydrostatic performance; therefore, the initial joint gap and its change are measured in millimetres using a ruler at a minimum of two points around the pipe. The change of the joint gap during the pressure test should be minimal.

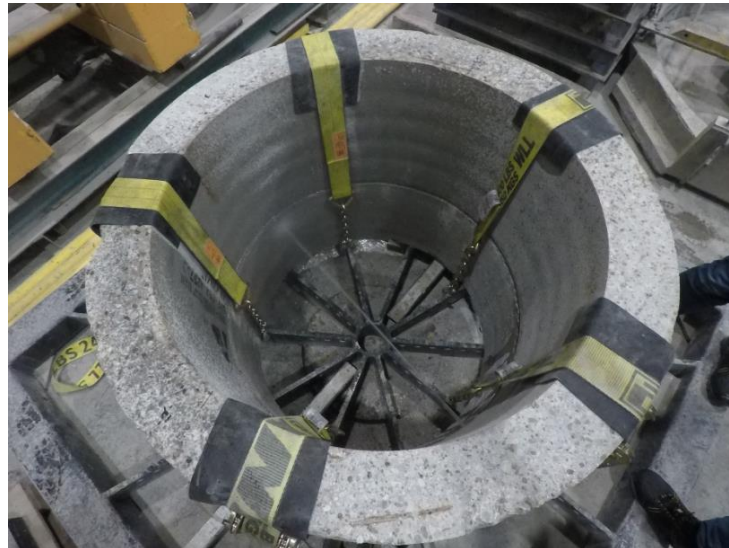
### 3.6.2 Ultimate Capacity

The first target of the test is determining a short-term ultimate hydrostatic capacity of the RCP joint, which is when the joint can no longer hold the test pressure for 10 minutes. The test begins with a selected starting pressure based on the CSA A257 requirement of 105 kPa, the recommendation of the gasket supplier, or previous test experience, whichever is greater. As more test results are collected, higher starting pressure can be selected to reduce the duration of the test. The pressure is then gradually increased at intervals of 25 kPa or 50 kPa and held for a minimum of 10 minutes at each increment, followed by visual inspection for leaks. The measurement of the water level in the WSCC is also recorded. The duration of 10 minutes is selected based on similar evaluations from most hydrostatic standard tests. Any leakage observed at the inside of the pipe joint is considered a failure. The ultimate capacity is rated at the previous pressure level. All other leakage observed, such as outside the joint, inlet and/or outlet pipes or other locations, will not be considered as failure. If those leakages can be controlled and do not impact the test, the test can be continued. Adjustment of the straps can

also be made to mitigate exterior leakage during the test. The time for each incremental attempt is recorded by the operator using a stopwatch. **Figure 15 (a) and (b)** show two typical failures of primary gaskets. A test using 600 mm RCP failed at 250 kPa when water seeped down the inner face of the joint. A test using 900 mm RCP failed at 475 kPa when water suddenly shot out.



(a) 600 mm RCP, 250 kPa,



(b) 900 mm RCP, 475 kPa.

**Figure 15 Moment of Failure.**



### 3.6.3 Operating Capacity

The hydrostatic performance of the RCP joint is affected by the exposure to sustained groundwater pressure. Hence, to evaluate the RCP operating capacity, the annular space is subjected to sustained pressure for a minimum of 20 hours to allow the gasket and joint to be stabilized. The target operating pressure is set to 80% of the ultimate capacity; therefore, the test is usually completed after the ultimate capacity is determined. A new set of gaskets from the same lot are used in this test to avoid damage caused during the previous establishment of the ultimate pressure. It is recommended to begin the test by holding the pressure at 100 kPa, followed by 10 minutes at 70% of the ultimate pressure. This is to ensure that the test setup is performing as expected. If no leakage is observed, the pressure is then held at 80% of the ultimate capacity for the next 20 hours. Visual examination for leakage shall be made within 10 minutes after reaching the 80% mark, followed by periodic inspection at 4-hour intervals. The water level in the WSCC versus time shall be recorded at each inspection. After 20 hours, full inspection for leakage is conducted, and the water level in the final WSCC is recorded. If no leak is observed from the inside of the pipe, the test is successful, and the operating capacity of the pipe joint is determined at 80% of the ultimate capacity.

## 3.7 Test Results for Condition Classification

More than 100 tests were conducted. For both the ultimate and operating performance conditions, the result of the test has four unique success conditions, as outlined in **Table 9**. The summary of the infiltration test count is provided in **Table 10**. For the ultimate capacity, a successful test terminated based on the failure of the primary gasket with minor or no external leak is categorized into Condition 1. The test is considered as Condition 2 when an external leak is observed during the test without a complete failure of the secondary gasket. In this case, the ultimate capacity of the primary gasket is considered when an interior leak occurs. The test is considered as Condition 3 when the secondary gasket is unable to hold the pressure in the annular space during the test. Here, the ultimate capacity of the primary gasket is not reached.

For the operating capacity, Condition 1 considers a successful test with minor or no external leak, and the target duration is reached or exceeded. Condition 2 considers that external leak

is observed, the target pressure is maintained, and the target duration is reached. The test is considered as Condition 3 when the target duration is not reached due to external leak or other types of leakage. The test is considered unsuccessful, i.e. Condition 4, when the setup was unable to hold any pressure, or major leakage occurs at the early stage of the test setup. The tests categorized as Condition 4 are not included in this Chapter.

**Table 9: Infiltration Test Result Conditions**

<b>Condition</b>	<b>Description</b>
<b>Ultimate Test</b>	
1	<ul style="list-style-type: none"> <li>No significant external leak was observed during the test. A minor external leak can be eliminated by adjusting the tension of the straps.</li> <li>The test is terminated based on the leakage or failure of the testing gasket.</li> <li>The ultimate capacity of the test gasket is determined based on the failure of testing gasket or equipment capacity.</li> </ul>
2	<ul style="list-style-type: none"> <li>The external leak is substantial during the test, but the water tank is not fully drained at the end of the test. The test is terminated based on the leakage or failure of the testing gasket.</li> <li>The Target pressure level can be maintained during the test.</li> <li>The test is terminated based on the leakage or failure of the testing gasket.</li> <li>The ultimate capacity of the testing gasket is determined based on the failure of testing gasket or equipment capacity.</li> </ul>
3	<ul style="list-style-type: none"> <li>External leak substantial during the test.</li> <li>The test is terminated based on the leakage or failure of the secondary gasket.</li> <li>The ultimate capacity of the test gasket is determined based on the pressure level prior to the termination of the test.</li> </ul>
4	<ul style="list-style-type: none"> <li>The test is not completed due to the setup issue.</li> <li>No pressure data is collected.</li> </ul>
<b>Operating Test</b>	
1	Target pressure and duration are both reached with no external leak. A minor external leak, when observed during the test, is corrected.
2	Target pressure and duration are reached despite the external leak.
3	The test is terminated before the target duration is reached due to an external leak or testing gasket failure.

**Table 10: Infiltration Test Count Summary**

<b>Results</b>	<b>Ultimate</b>	<b>Operating</b>	<b>Grand Total</b>
Condition 1	38	30	68
Condition 2	19	12	31
Condition 3	13	2	15
<b>Grand Total</b>	<b>68</b>	<b>44</b>	<b>114</b>

## 3.8 Sample Selection

### 3.8.1 Pipe

In the initial phase of developing this test method, conventional RCP sizes of 600 mm, 900 mm and 1200 mm in diameter were selected. These three sizes were selected for this research partly because the cost of repair is relatively higher than that for the larger size pipes due to the restriction of operator entry, and partly because they are easier to handle compared to a larger size. In addition, the industry claims that these sizes have a higher competition from other emergent pipe materials. The pipe samples were made by the sponsor plant in Oakville, Ontario, Canada in compliance with CSA A257.2 using a vibration and pressing process, with a conventional dry cast concrete mixture that exceeded a compressive strength of 40 MPa at 28 days and reinforced with a spiral cold drawn wire cage(s). The joint was comprised of a single offset spigot end jointing into a groove bell end, as shown in **Figure 10**. A detail of the joint cross-section is shown in **Figure 16**, and the geometry is listed in **Table 11**.

**Table 11: Pipe Joint Geometry**

<b>Size</b>		<b>600</b>	<b>900</b>	<b>1200</b>
ID		610	914	1219
S	mm	8.3	8.3	7.6
T	mm	3.2	3.2	3.7
js	mm	48.8	48.8	63.5
j <sub>r</sub>	mm	49.6	49.6	44.5
J	mm	98.4	98.4	108
f	mm	61.5	61.5	53
A <sub>s</sub> Annular Space	mm <sup>2</sup>	564	564	882
Spigot Diameter	mm	733	1037	1325
ID + 2f				
Spigot Circumference	mm	2303	3258	4163

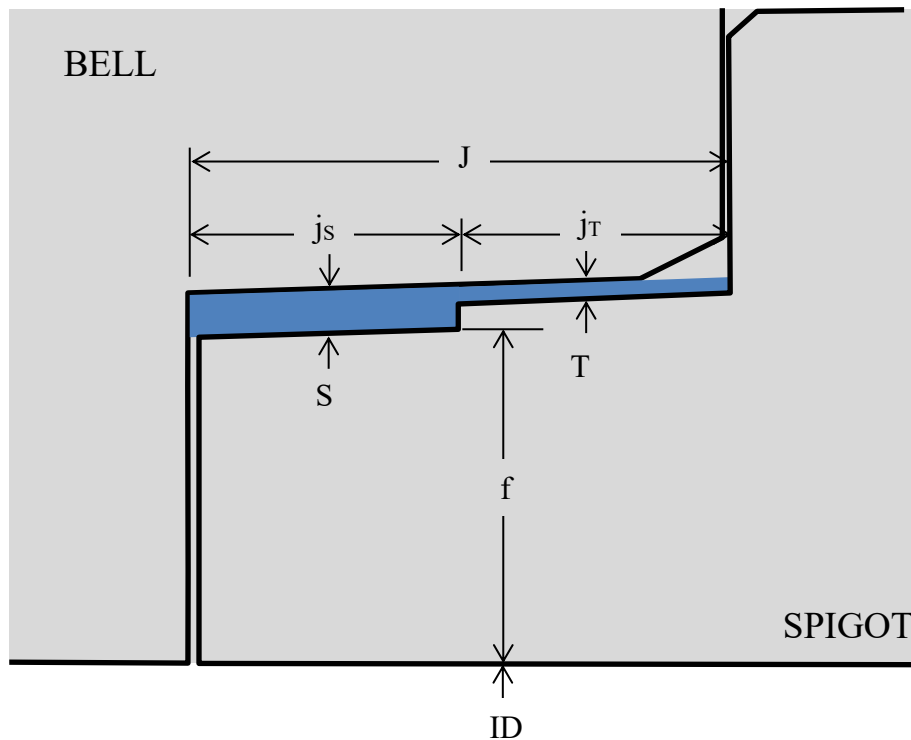


**Figure 16: RCP Joint Profile and Annular Space**

### 3.8.2 Gasket

The various models of primary gaskets tested are commonly used by the industry and were pre-lubricated and made of synthetic rubber, meeting requirements of **ASTM C443**, **ASTM C425**, **ASTM C1619**, and **CSA A257**. The secondary gaskets having profiles recommended by industry suppliers were used to provide sealing to contain the annular space for pressurization. The purpose of the study was to develop and validate the new test method and not to compare the performance of commercial gasket brands. Therefore, the actual gasket brands in **Table 12** were not disclosed and are rather represented by a prefix letter “T” for primary testing gasket and “S” for the secondary gasket. For those primary testing gaskets, the mass and the unstretched cut length were measured prior to the test. When installing the gasket on to the pipe spigot, the gasket is stretched from its original cut length because the circumference of the pipe spigot is larger than the unstretched cut length. The increase in the stretched length varies between 10 % and 16%. The average stretched unit mass is calculated

by dividing the average mass measured by the spigot circumference or stretched length. The influence ratio,  $I_g$ , is defined in **Eq. 1** as the ratio of the mass of the gasket to the effective annular space that confines the gasket, which provides an important explanation of the ultimate capacity of the gasket against the infiltration pressure. The effective annular space is shaded in **Figure 16**. In the case of the single offset joint of the test pipe, the annular space,  $A_s$ , is estimated using **Eq. 2**.

$$\text{Eq. 1} \quad I_g = \frac{\text{average gasket mass (g)}}{\text{effective annular space (mm}^2\text{)}}$$

$$\text{Eq. 2} \quad A_s = S \times j_S + T \times j_T$$

**Table 12: List of Gaskets Used in the Research**

<b>Profile ID</b>	<b>Type</b>	<b>Supplier</b>	<b>Design Capacity</b>	<b>Remark</b>
S01	Wedge	1		Secondary
S03	Wedge	2		Secondary
S04	Wedge	2		Secondary
T02	Self-lubricated 135	1	105	Primary
T03	Self-lubricated 165	2	105	Primary
T04	Self-lubricated 185	2	105	Primary
T05	Double Tilting Gasket with PP coupler	3	250	Primary
T06	Self-lubricated 135	2	105	Primary
T07	Self-lubricated 185	1	105	Primary
T08	Wedge Profiled	1	140	Primary

### 3.9 Summary

This chapter provides a detailed description of a novel infiltration testing method that RCP manufacturers can easily set up and conduct in a factory setting. The test is much safer to conduct owing to the much lower water consumption needed to achieve a much higher-pressure target in comparison to conventional exfiltration tests. Although the pipe sizes and gaskets were listed, larger pipe sizes and other types of gaskets can be easily accommodated using the same setup and procedure. The test has been proven reliable based on the repeatability of the results in this research.

### 3.10 References

ASTM C497 “Standard Testing Methods for Concrete Pipe, Concrete Box Sections, or Tile”, ASTM International: West Conshohocken, PA, USA, 2019, 17 p.

ASTM C443-12, “Standard Specification for Joints for Concrete Pipe and Manholes, Using Rubber Gasket” ASTM International, West Conshohocken, PA, USA, 2012, 3 p.

ASTM C425-04, “Standard Specification for Compression Joints for Vitrified Clay Pipe and Fittings” ASTM International, West Conshohocken, PA, USA, 2004, 3 p.

ASTM C1619-19, “Standard Specification for Elastomeric Seals for Joining Concrete Structures” ASTM International, West Conshohocken, PA, USA, 2019, 3 p.

CSA A257, “Standards for Concrete Pipe and Manhole Sections”, CSA Group, Mississauga, ON, Canada, 2019, 40 p.

# CHAPTER 4

---

## 4 Pipe Joint Design

This chapter discusses the properties of the rubber, the design of gaskets, and the properties of the gasket specimens in greater detail. Theoretic calculation of sealing pressure based on the load-deformation curve of the gasket sample is presented. The sealing potential based on the calculation is subsequently used to compare the results obtained by the infiltration test.

### 4.1 Rubber Gasket

The hydrostatic capacity of RCP depends on the properties of rubber gaskets, a primary material used in sealing RCP joints. Its mechanical properties, geometric dimensions, and the pipe joint design also contribute to the sealing potential. Rubber maintains its volume under applied load by deformation. The cross-section of the rubber increases when it is compressed and reduces when it is stretched. The mechanical properties in compression can be derived using ASTM D575 (2001). The ability to deform under applied load can be described in three phases: elastic, viscoelastic, and viscous phase (Czernik 1996). **Figure 17** illustrates the relationship between the applied load and deformation due to the compression of a typical rubber. In the early stage of loading or elastic response, the deformation of a rubber specimen due to compression forces increases linearly and returns to its initial shape when the applied force is removed. When the applied load reaches the viscoelastic response phase, the change in deformation diminishes at the same load increment. The change in performance is time-dependent but is totally recoverable. However, if the load causes the rubber to deform into the viscous response phase, the deformation is no longer recoverable. In this Chapter, the rubber gasket samples were tested to the viscoelastic phase assuming that the rubber gasket is intended not to exceed the viscoelastic properties in its service life.

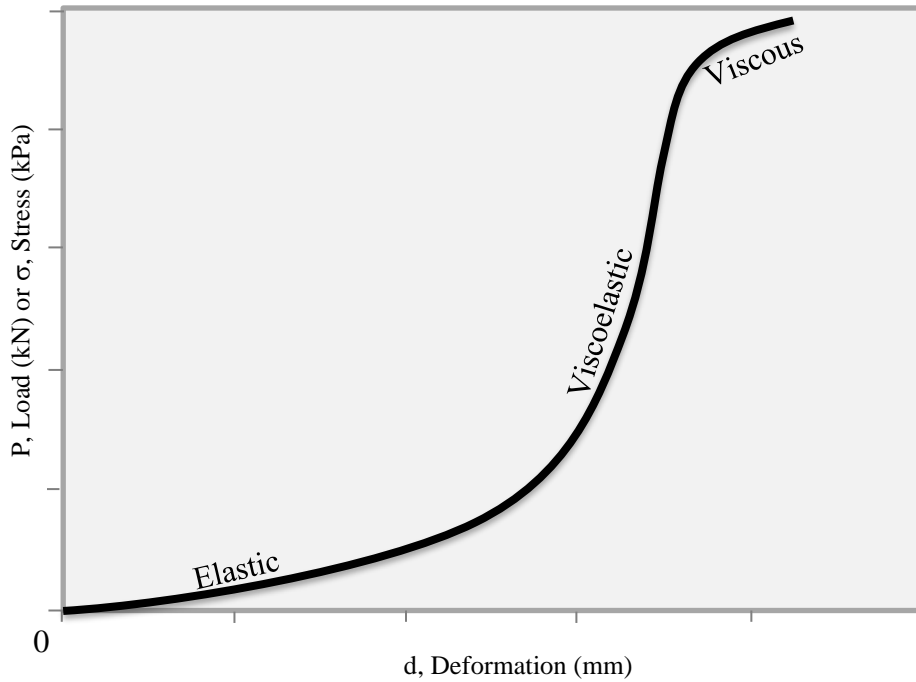


**Figure 17: Typical load-deformation curve for rubber gasket (After Czernik, 1996).**

Rubber also relaxes under load over time, incurring stress relaxation or creep. The load-deformation curve is empirically developed by measuring the actual deformation of the gasket sample in accordance with ASTM D575 (2001). **Figure 18** displays a typical test conducted by gasket manufacturers to determine the load-deformation curve. The curve describes the material behaviour for a specific rubber compound and gasket design. However, the surface boundary and the actual media of the pressure are ignored in the test. The load-deformation behaviour of rubber also depends on the durometer, hardness of the material, in accordance with ASTM D2240 (2015). These properties also impact the sealing potential of the gasket.



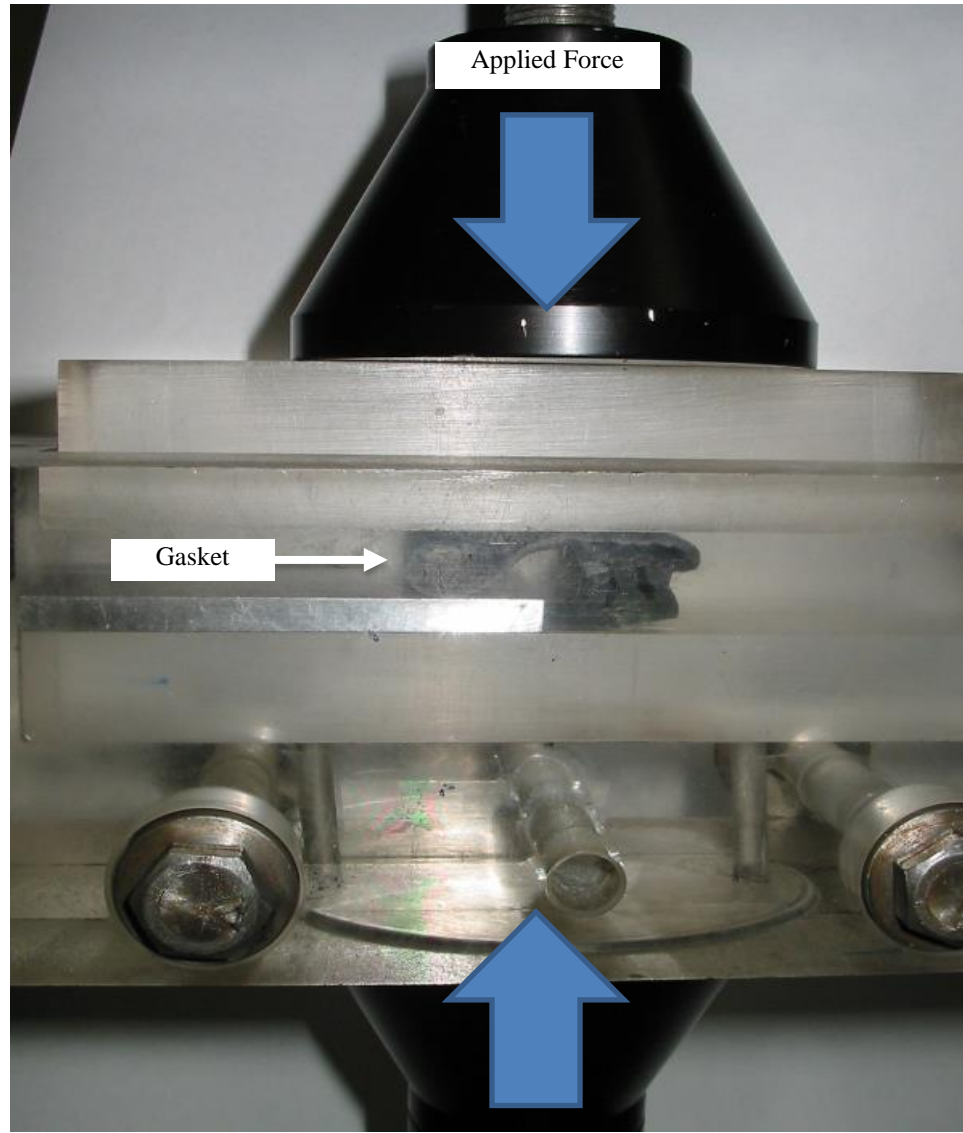


**Figure 18: Gasket deformation test.**

## 4.2 Joint Design

In addition to the aforesaid material mechanical properties, the sealing potential of a rubber gasket also depends on its cross-sectional geometry. The face of the gasket in contact with the applied hydrostatic pressure determines the amount of frictional force required to keep the gasket in equilibrium. **Figure 19** illustrates that the orientation of the gasket dictates the amount of contact area; and thus, affects the amount of frictional resistance provided.

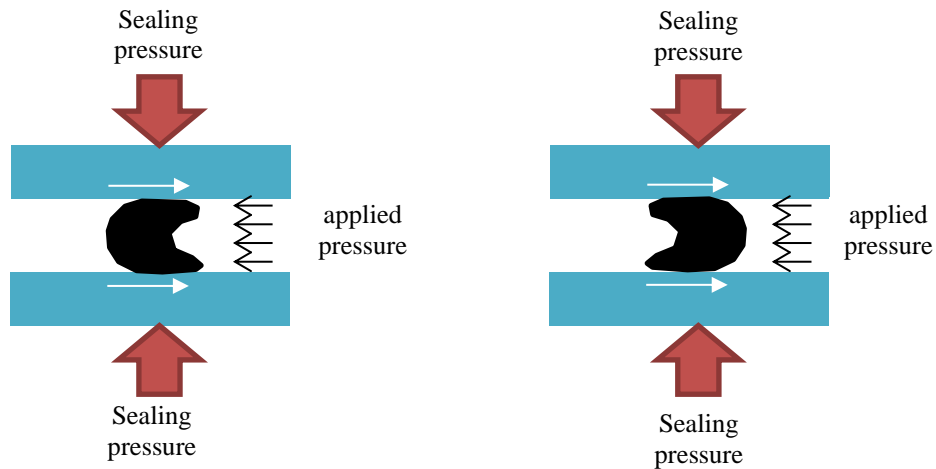
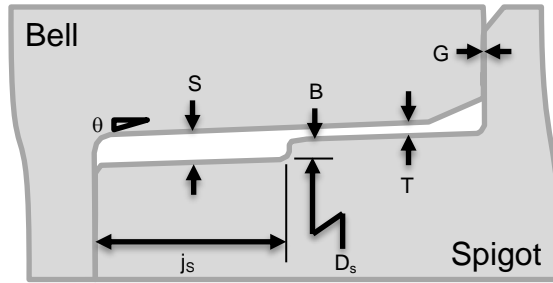


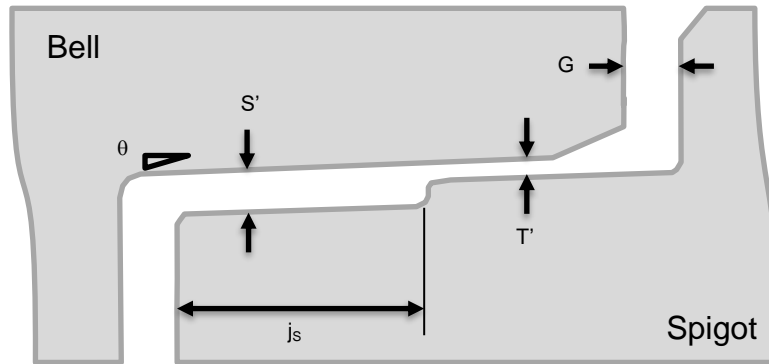
**Figure 19: Illustration of gasket geometry withstands internal pressure.**

The amount of stretch at the time of loading and the ratio of the cross-sectional area to the confined space also determines the sealing potential. The confined space, also known as annular space, generates compression of the rubber, creating the sealing potential (ACPA, 2019). The joint design defined in the plant certification published by the American Concrete Pipe Association (APCA) provides a mathematical calculation for the minimum and maximum compression of two common RCP joints for confined circular gaskets and single offset profiled gaskets. These values can be used to calculate the maximum and minimum sealing potential based on the load-performance curve of the rubber.

The joint design of the RCP in this experimental program is shown in **Figure 20 (a)** and **Table 13**. This design has been commonly used by the RCP industry to offer self-balancing ability during pipe installation without manually equalizing the tension such as in traditional wedge or O-ring gasket. The female end of the pipe, known as the bell, receives the male end, known as the spigot, with a 2-degree taper in the wall of the slot. The spigot of the pipe has an offset,  $B$ , of 6.7 mm, 6.7 mm and 7.6 mm for 600 mm, 900 mm, and 1200 mm pipes, respectively. This offset creates two sizes of annular space,  $S$  and  $T$ . The tapered face reduces the annular space,  $S$ , when the pipe is being jointed together, inducing compression in the sealing material. This is a common design for all concrete pipes. The tube section of the sample gasket is rolled into the annular space, denoted “T,” for its final resting position. The joint design has a taper angle,  $\theta$ , for an easier homing process as illustrated in **Figure 20**. The effect of the taper angle on the sealing potential will be discussed later. The 600 mm and 900 mm pipes share the same gasket profile, while the 1200 mm pipe sample uses a different gasket profile due to its larger annular space.



(a) Ideal position by design



(b) With joint gap

**Figure 20: RCP Single Offset Joint Detail.**

**Table 13: RCP Single Offset Joint Detail**

Size	600	900	1200
$j_s$	48.8	48.8	63.5
B	6.7	6.7	7.6
$\theta$ (°)	2	2	2
S	8.3	8.3	11.3
T	3.2	3.2	3.7
$D_s$	733	1037	1325
$AS_c$	2303	3258	4163

Read this table in conjunction with **Figure 20**

Unit of Measure: *millimetre*

$AS_c$  – *Circumference of annular space*

### 4.3 Gasket Specimens

The gaskets used in this study are the self-lubricating, profiled type, that is designed for the single offset joint described above. The typical cross-section of an unstretched gasket, illustrated in **Figure 21(a)**, consists of two sections: the deformation section and the rolling tube section. **Figure 21(b)** shows the stretched cross-section after the gasket is placed onto the pipe spigot. There was a reduction in gasket height due to the increase in gasket length. The maximum stretch limit was 20% in addition to the unstretched length (ACPA, 2019). The stretched height can be calculated using **Eq. 3**.

$$\text{Eq. 3} \quad H_s = \frac{H_g}{\sqrt{r_s}}$$

Where  $H_g$ : height of unstretched gasket;  $H_s$ : height of stretched gasket;  $H_c$ : Height of compressed gasket;  $r_s$ : a ratio of stretched length to unstretched length.

**Figure 21(c)** shows the cross-section of the gasket after being compressed when two pipe sections were jointed. The rolling tube section was lubricated inside by silicone during gasket manufacturing to assist the jointing process of the concrete pipe. The rolling action during the homing process self equalizes the gasket tension along the entire length. Thus, additional equalization was not necessary compared to conventional profiled wedges or O-ring gaskets. The gasket height in the compressed state was limited to the available annular space shown in **Figure 21(c)**. The force required to compress the gasket from the stretched state into the compressed state creates the sealing potential, which is discussed in the next section. Gasket samples were also randomly selected in terms of dimension and weight. The number of samples, minimum, average and maximum values listed in **Table 14** exhibit a certain degree of variations. The unstretched length and mass were plotted against each other, as shown in **Figure 22(a)-(c)**, as well as the height and base width in **Figure 22(d)-(f)**. The scale of the x-axis and y-axis were maintained similarly in the figures for ease of comparison. The degree of variation is believed to explain the variation of sealing potential. This will be discussed further in the later section.

**Table 14: Gasket Properties**

<b>Pipe Size</b>		<b>600</b>	<b>900</b>	<b>1200</b>	<b>600</b>	<b>900</b>	<b>1200</b>
<b>Gasket Ref ID</b>		<b>T02</b>	<b>T02</b>	<b>T07</b>	<b>T06</b>	<b>T06</b>	<b>T03</b>
<b>Supplier<sup>3</sup></b>		<b>A</b>	<b>A</b>	<b>A</b>	<b>B</b>	<b>B</b>	<b>B</b>
<b>Spigot Dia. (mm)</b>		733	1037	1325	733	1037	1325
<b>Spigot Cirf.<sup>2</sup>, L<sub>s</sub> (mm)</b>		2303	3258	4163	2303	3258	4163
<b>Annular Space, A (mm)</b>		8.3	8.3	11.3	8.3	8.3	11.3
<b>Max limit of Annular Space (mm) 1.1 × A</b>		9.13	9.13	12.43	9.13	9.13	12.43
<b>Unstretched Length<sup>1</sup>, L<sub>u</sub> (mm)</b>	<b>Count</b>	20	19	21	14	17	21
	<b>Min</b>	2088	2957	3591	1994	2854	3678
	<b>Avg</b>	2103	2971	3623	2030	2882	3707
	<b>Max</b>	2119	2987	3674	2056	2930	3749
	<b>Max % Stretch</b>	10.3%	10.2%	15.9%	15.5%	14.1%	13.2%
	<b>Min % Stretch</b>	8.7%	9.1%	13.3%	12.0%	11.2%	11.0%
	<b>Stretch</b>						
<b>Mass<sup>1</sup> (g)</b>	<b>Count</b>	20	19	21	14	17	21
	<b>Min</b>	566	764	1456	590	852	1366
	<b>Avg</b>	577	805	1501	617	914	1442
	<b>Max</b>	590	826	1537	636	949	1472
	<b>Var</b>	24	63	81	46	97	106
<b>Unit Mass (g/m)</b>	<b>Count</b>	20	19	21	14	17	21
	<b>Min</b>	246	234	350	256	261	328
	<b>Avg</b>	251	247	361	268	280	347
	<b>Max</b>	256	254	369	276	291	354
	<b>Var</b>	11	19	19	20	30	26
<b>Unstretched Height, H<sub>g</sub>* (mm)</b>	<b>Count</b>	7	6	17	3	11	16
	<b>Min</b>	15.3	15.8	18.5	16.1	16.2	18.9
	<b>Avg</b>	15.8	16.6	19.4	16.1	16.7	19.6
	<b>Max</b>	16.0	17.3	20.3	16.3	17.4	20.5
	<b>Var</b>	0.7	1.5	1.9	0.2	1.3	1.6
<b>Base Width, W<sup>1</sup> (mm)</b>	<b>Count</b>	7	6	17	3	11	16
	<b>Min</b>	17.1	17.2	21.0	16.8	16.5	18.9
	<b>Avg</b>	17.3	17.5	21.9	17.1	16.8	20.1
	<b>Max</b>	17.5	17.8	22.4	17.3	17.2	21.1
<b>Stretched Height, H<sub>s</sub> (mm)</b>	<b>Min</b>	14.6	15.1	17.2	14.9	15.2	17.8
	<b>Avg</b>	15.2	15.9	18.1	15.1	15.7	18.5
	<b>Max</b>	15.3	16.5	19.0	15.4	16.5	19.4
	<b>Var</b>	0.7	1.4	1.7	0.5	1.3	1.6
	<b>%Min</b>	4.4%	4.7%	6.6%	7.0%	5.8%	5.8%
	<b>%Max</b>	4.3%	4.4%	6.6%	5.5%	5.2%	5.2%
<b>Reduction in Gasket Height or Compressed Height, H<sub>c</sub> (mm)</b>	<b>Min</b>	5.50	5.95	4.81	5.81	6.08	5.37
	<b>Avg</b>	6.03	6.73	5.64	5.97	6.57	6.10
	<b>Max</b>	6.21	7.39	6.53	6.27	7.38	6.95
	<b>% Min</b>	37.6%	39.5%	27.9%	38.9%	40.0%	30.2%
	<b>% Max</b>	40.5%	44.7%	34.4%	40.7%	44.7%	35.9%

<sup>1</sup>Value obtained by measurement; <sup>2</sup>Also known as gasket stretched length; <sup>3</sup>Durometer for Gasket A is 40D, and Gasket B is 45D

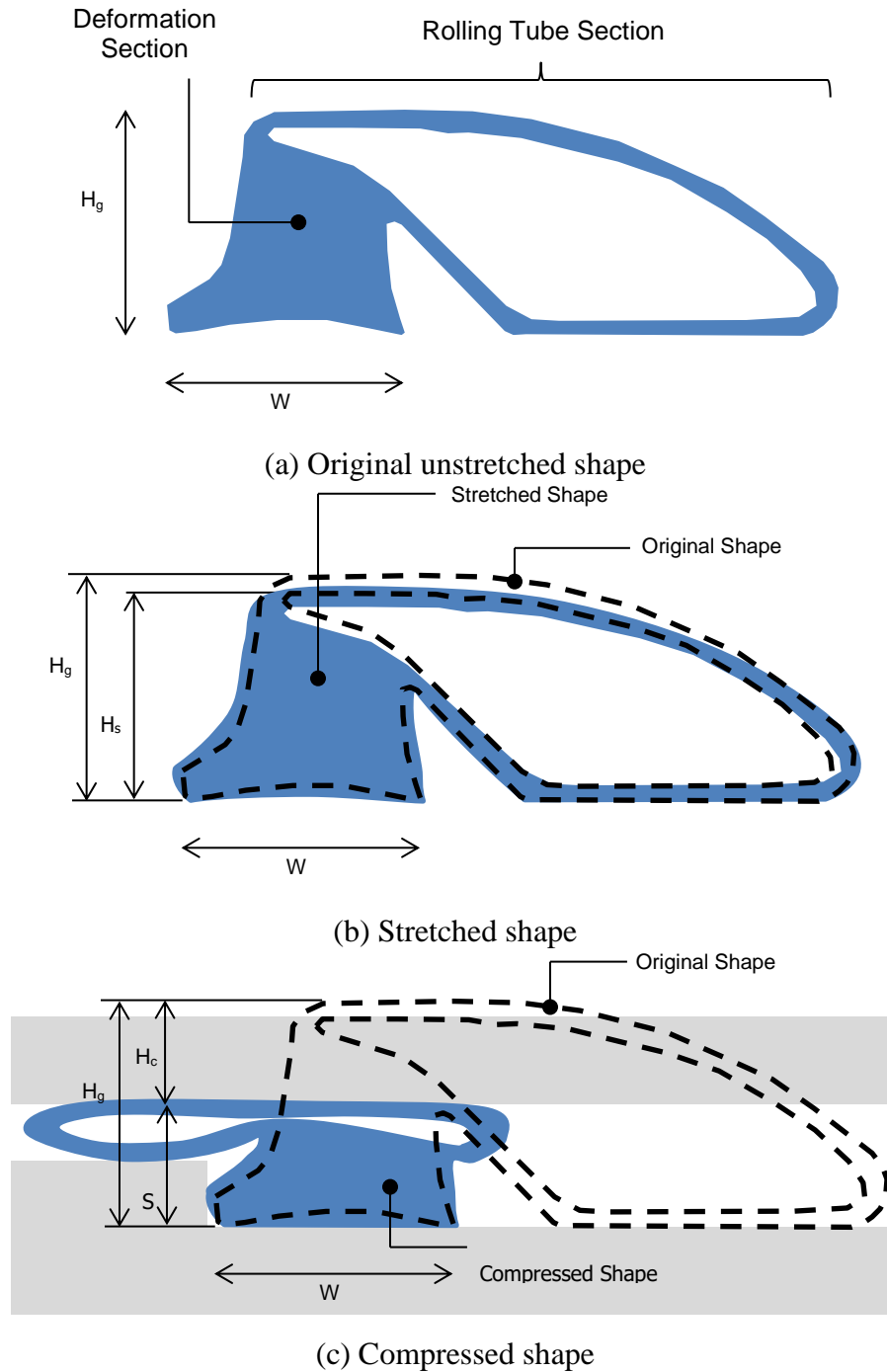
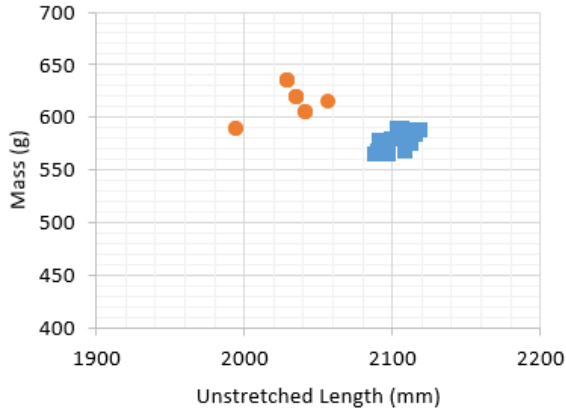
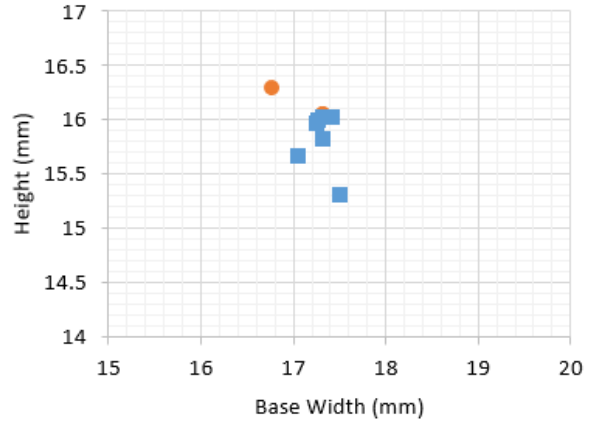


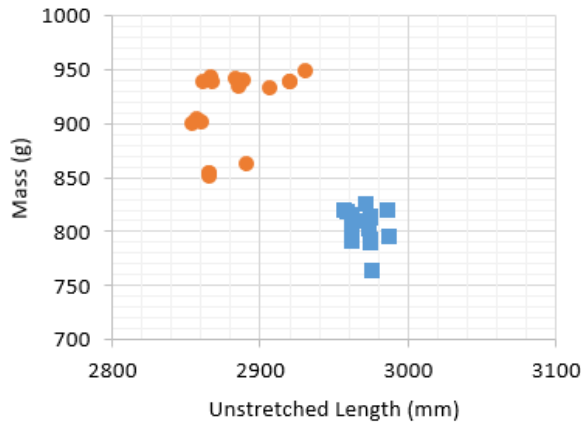
**Figure 21: Typical cross-section of self-lubricated single offset gasket.**



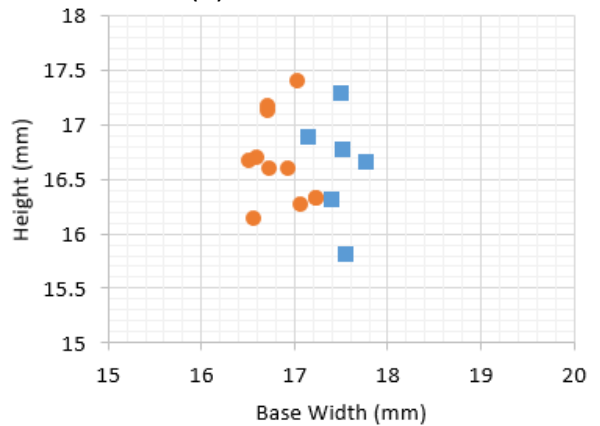
(a) 600 mm RCP



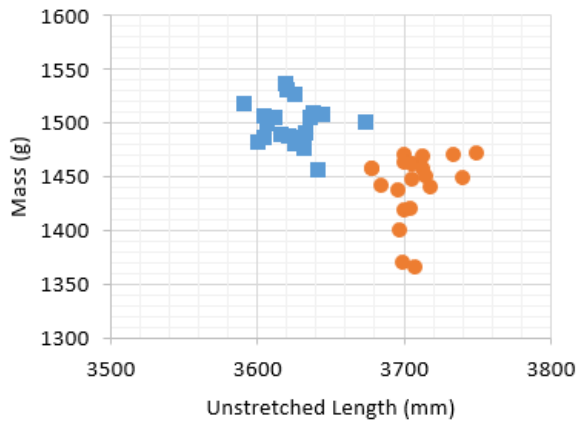
(d) 600 mm RCP



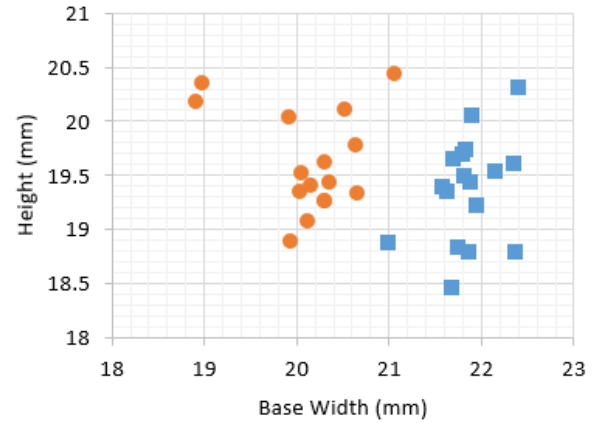
(b) 900 mm RCP



(e) 900 mm RCP



(c) 1200 mm RCP



(f) 1200 mm RCP

Legend: ■ A ● B

**Figure 22: Gasket Geometric Properties.**

## 4.4 Sealing Potential Calculation

The sealing potential was estimated based on the deformation properties of the rubber under the load, i.e. load-deformation behaviour obtained from **ASTM D575**. The compensation was made to account for the reduction in the cross-section area during the stretch, i.e. increase in length when installing the gasket on the spigot of the pipe. In the final compressed condition (**Figure 20(c)**), the reduction of the gasket height,  $H_c$ , was computed by subtracting the annular space,  $S$ , from the stretched height,  $H_s$ . The required force,  $P_f$ , to compress the gasket to have a reduction,  $H_c$ , can be empirically determined based on its load-deformation behaviour obtained from the load-deformation curve using **Eq. 4**. 20% factor was applied to the force in the load-deformation test to account for relaxation. In this study, when comparing to the short-term ultimate test, the relaxation factor was omitted. The sealing pressure was computed by dividing the applied force by the sample contact area.

$$\text{Eq. 4} \quad P_f = \frac{P}{(1-20\%)}$$

## 4.5 Sealing Pressure and Joint Gap

The sealing pressure is also impacted by the change in annular space due to the joint gap and the geometrical variation of the gasket itself. The spigot of the pipe sample has 2% taper angle on the conic surfaces of the bell and the outer surface of the spigot by design. This is typical as per ASTM C443, which limits the angle to be 3.5% measured from the pipe axis. As shown in **Figure 20 (b)**, the 2% taper angle increases the annular space as the joint gap increases at the rate of the joint gap,  $G$ , multiplying the tangent of the taper angle,  $\theta$  (**Eq. 5**).

$$\text{Eq. 5} \quad \Delta S = G \cdot \tan\theta$$

With 2% taper angle, the annular space increases by 0.87 mm when the joint gap increases to 25 mm. For 600mm and 900 mm pipe sample, the increase is 10.5%; and for 1200 mm pipe sample, the annular space increases by 7.7%. This increase reduces the force required to compress the gasket; hence, reduce the sealing pressure. For the gasket samples used in this study, the reductions are ranged between 30% to 36% when the joint gap increases to 25 mm.



## 4.6 Sealing Pressure and Geometrical Variations

The sealing pressure is also impacted by the geometrical variation of the gasket itself. **Figure 22** shows the mass of the gasket varies against the unstretched length, and the unstretched height varies against the base width. The variation of unstretched length for Gasket A in 1200 mm diameter pipe seems to be higher and that in 600 mm. So does Gasket B in 1200 mm pipe, when comparing to 600 mm pipe and 900 mm pipe, the variation in unstretched length is higher. The amount of the gasket stretched, increase in length, after being positioned at the pipe spigot are ranged between 8.7% and 15.9% (**Table 14**), smaller than the maximum stretch limit of 20% as per ACPA (2019). This increase results in a reduction in the gasket height by 4.3% to 6.6%. This variation of the compressed height varies between 27.9% and 44.7% of the stretched height. For non-circular gasket (i.e. single offset gaskets), the minimum and maximum compression should be within 15% and 40%. This large variation impacts the force required to compress the gasket in the annular space, which indicates that the sealing pressure is very sensitive to the geometric variation of the gasket.

## 4.7 Sealing Pressure and Joint Alignment

Practically speaking, the straight alignment describing the ideal installation does not usually govern the sealing capacity. The maximum predicted sealing potential depends on the joint gap,  $G$ , or joint offset, or a combination of both, as illustrated in **Figure 23**. The maximum allowable joint offset is the secondary annular space  $T$ . In this study, the maximum allowable joint offset is 3.2 mm, 3.2 mm, and 3.7 mm for 600 mm, 900 mm, and 1200 mm pipes, respectively. By offsetting the joint, the annual space increases on one side and decreases on the other side (**Figure 23 (a)**). In other words, the sealing potential at the side with larger annular space is reduced. The minimum sealing potential at the location of maximum annular space is calculated using Error! Reference source not found.. **Figure 23 (b)** illustrates a more extreme condition where the joint is offset with a joint gap. The maximum annual space,  $S'_{max}$ , can be calculated using **Eq. 7**, which is rewritten from **Eq. 6** to account for both joint offset,  $T$ , and joint gap,  $G$ .

$$\text{Eq. 6} \quad S_{max} = S + T$$

$$\text{where } T_{max} = 2T \text{ when } T_{min} = 0$$

$$\text{Eq. 7} \quad S'_{max} = G \tan \theta + S_{max} = G \tan \theta + S + T$$

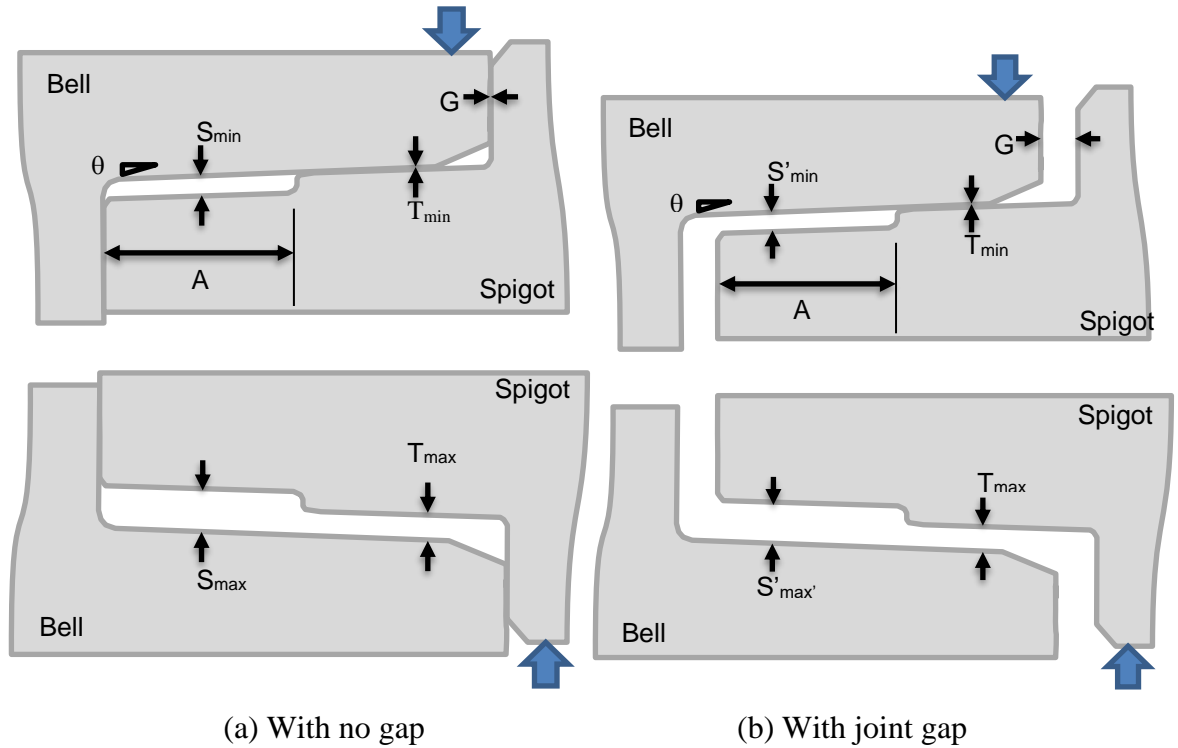


**Figure 23: Offset joint.**

## 4.8 Summary

This chapter provides a basic understanding of the behaviour of rubber gaskets in preparation for explaining the experimental observations. The theoretic calculation of the sealing potential further provides a baseline for experimental comparison. The influential parameters, such as geometric variation and joint alignment, are to be further studied based on the experimental measurements reported in the next chapter.

## 4.9 References

ACPA “2019a ACPA QCast Plant Certification Manual”, American Concrete Pipe Association, Irving, Texas, US

ASTM D575 “Standard Test Methods for Rubber Properties in Compression”, ASTM International: West Conshohocken, PA, USA, 2001, 4 p.

ASTM D2240 “Standard Testing Method for Rubber Property – Durometer Test”, ASTM International: West Conshohocken, PA, USA, 2015.

Czernik, D. “Gaskets Design, Selection, and Testing”, McGraw-Hill, New York, USA, 1996.

## CHAPTER 5

---

### 5 Testing Results

This chapter reports results from a total of 122 infiltration tests, in which 114 tests were conducted at an industry scale manufacturing facility on standard pipe sizes of 600 mm, 900 mm, and 1200 mm made at the same location. Eight tests were conducted using other pipe sizes and gaskets. The results exhibit the influence of the joint gap and other input variables. The observations of gasket movement under pressure and at failure are also reported. Preliminary findings provide insights into key parameters that influence the results. Substantial parts of this Chapter will be published in **Wong and Nehdi (2020)**.

#### 5.1 Ultimate Hydrostatic Capacity

A total of 68 tests were conducted to examine the ultimate hydrostatic capacity of the RCP joint against infiltration. The test results for the aligned position and offset position were presented in **Table 15** and **Table 16**, respectively. Among these tests, 55 of those tests (Condition 1 and 2) were terminated due to the failure state of the primary gasket when water seeped through the joint from inside of the pipe (**Figure 15a**) or shot out from the testing pressure due to gasket displacement (**Figure 15b**). Twelve tests had a failure of the secondary gasket before the primary gasket, leading to termination of the test (Condition 3). A parallel objective of the testing was to examine the performance of the test apparatus. Accordingly, two tests were terminated without showing a failure state at 86% and 95% of the test set-up design capacity. The test of 600 mm diameter RCP reached 650 kPa (Test #9) for 10 minutes, followed by 20-hour at an operating pressure of 525 kPa with no sign of leakage for both tests.

**Table 15: Summary of Test Result for Ultimate Capacity with Aligned Position**

Gasket	Size	Gasket ID	Test ID	Pressure (kPa)	Gap (mm)	Terminated Reason	Data Points	Result Condition
A	600	T02	21	300	5.6	Failure of primary gasket	11	1
			47*	105	6.0	Failure of primary gasket	5	1
			46	150	6.3	Failure of primary gasket	5	1
			1	225	8.6	Failure of test gasket	9	1
			37	50	9.5	Failure of primary gasket	4	1
			13	250	9.8	Failure of test gasket	11	1
			48	50	12.9	Small leak at inside	6	1
	900	T02	23	600	4.8	86% of equip. cap.	21	1
			11	425	9.0	Failure of test gasket	11	1
			71	175	10.1	Leak from primary gasket	15	1
			66*	175	10.6	Leak from primary gasket	6	1
			65	250	11.3	Leak from primary gasket	9	1
			70	100	11.4	Leak from primary gasket	5	1
73			150	15.9	Leak from primary gasket	15	1	
1200	T07	91	350	3.6	Leak from primary gasket	11	1	
		94	375	6.5	Leak from primary gasket	13	2	
		15	350	10.8	Leak from primary gasket	15	1	
		59	300	11.0	Failure of primary gasket	7	2	
		124	225	11.1	Leak from primary gasket	7	2	
		60	300	11.4	Leak from secondary	11	3	
		132	250	14.0	Leak from primary gasket	12	2	
B	600	T06	9	650	5.5	95% of equip. cap.	15	3
			41	400	6.6	Failure of test gasket	11	1
			31	450	6.9	Failure of primary gasket	13	1
			40	350	10.0	Failure of test gasket	13	1
			45	200	13.3	Failure of primary gasket	9	1
			126	450	14.5	Leak from primary gasket	17	2
			900	T06	7	550	8.1	2nd gasket displaced
	62	550			9.7	Leak from secondary	18	3
	69	250			11.0	Leak from primary gasket	9	1
	1200	T03	75	325	14.3	Leak from primary gasket	24	1
			89	450	4.3	Leak from secondary	16	3
			3	480	7.3	Failure of Secondary	16	1
			105	275	8.1	Leak from primary	15	2
98			9.03	175	Leak from secondary	6	3	
92			475	9.8	Leak from primary gasket	19	2	
125			275	9.8	Leak due to concrete's quality	7	3	
1200	T04	131	400	11.2	Leak from primary gasket	15	2	
		61	350	11.3	Leak from secondary	7	3	
		58	350	12.4	Leak from secondary	13	3	
		103	225	13.0	Leak from primary gasket	7	1	
		133	450	14.1	Leak from primary gasket	14	2	
		99	325	14.4	Leak from secondary	13	3	
		5	500	8.0	Failure of Secondary	11	3	

\* Tests were conducted under operating pressure. Leaks were discovered before the target duration was achieved but still meeting the ultimate test duration requirement. These two tests were considered an ultimate test.

**Table 16: Summary of Test Result for Ultimate Capacity with Offset Position**

Gasket	Size	Gasket ID	Test No.	Gap (mm)	Pressure (kPa)	Terminated Reason	Data Points	Result Condition
A	600	T02	35	4.72	150	Failure of primary gasket	6	1
			117	8.83	350	Leak from primary gasket	17	2
			119	10	250	Leak from primary gasket	13	2
			121	13.63	250	Leak from primary gasket	12	1
			55	16.41	150	Failure of primary gasket	11	2
	900	T02	38	3.82	275	Failure of primary gasket	11	1
			79	9	350	Leak from primary gasket	17	1
			74	10.02	150	Leak from primary gasket	11	1
			77	12.98	150	Leak from primary gasket	12	1
			1200	T07	100	2.99	450	Leak from primary gasket
108	6.04	300			Leak from primary gasket	11	2	
136	11.88	250			Leak from primary gasket	9	2	
134	13.6	300			Leak from primary gasket	11	2	
B	600	T06			43	4.2	650	Equipment capacity
			127	7.96	650	Leak from primary gasket	16	2
			56	12.9	500	No Failure	21	1
	900	T06	50	5.23	550	Failure of Secondary	13	3
			83	5.53	300	Leak from primary gasket	10	1
			82	6.63	200	Leak from primary gasket	5	1
			84	8.61	400	Leak from primary gasket	15	1
			87	11.53	225	Leak from primary gasket	9	1
			110	16.62	500	Leak from primary gasket	23	2
			1200	T03	107	3.38	500	Leak from primary gasket
54	7.3	375			Failure of secondary gasket	15	3	
129	7.95	600			Leak from primary gasket	17	2	
140	16.06	450			Leak from primary gasket	11	1	

## 5.2 Operating Hydrostatic Capacity

A total of 44 tests were conducted for evaluating the operating hydrostatic capacity of the joint. Among those, 24 and 20 tests were examined under aligned and offset positions presented in **Table 17** and **Table 18**, respectively. In the case of determining the hydrostatic capacity under sustained operating pressure, pressure from the previous test was first removed. The pipe sections were then taken apart for gasket inspection. Replacements were made to ensure that the subsequent operation pressure test was not conducted using damaged gaskets or pipe sections. A total of 30 tests (Condition 1) were completed for at least 20 hours of maintaining

80% of the established ultimate capacity. Twelve tests were completed for 20 hours with an external leak observed during the test (Condition 2). Two tests were terminated within the first 10 min due to the failure of the primary gasket (Condition 3).

**Table 17: Summary of Test Result for Operating Capacity with Aligned Position**

Gasket	Size	Gasket ID	Test No.	Gap (mm)	Pressure (kPa)	Terminated Reason	Data Points	Result Condition	Duration (min)
A	600	T02	22	5.58	280	Completed	4	2	1200
			2	8.6	180	Completed	4	1	1200
			123	9.65	50	Completed	14	2	1200
			14	9.8	175	Test gasket displaced	2	3	8
	900	T02	24	4.8	480	Completed	2	1	1200
			67	7.73	200	Completed	7	1	1200
			72	11.8	140	Completed	10	1	1200
			81	13.61	120	Completed	10	1	1200
	1200	T07	93	3.12	320	Completed	13	1	1200
			96	6.27	300	Completed	11	2	1200
			147	9.97	180	Completed	12	2	1200
			16	10.8	280	Leak from primary gasket	4	3	2
			139	14.82	200	Completed	13	2	1200
B	600	T06	10	5.5	525	Completed	4	1	1200
			42	6.61	320	Completed	5	1	1200
			128	14.11	360	Completed	8	1	1200
	900	T06	64	9.8	480	Completed	19	1	1200
			114	11.81	225	Completed	14	1	1200
			116	16.32	295	Completed	11	1	1200
	1200	T03	90	3.45	400	Completed	11	1	1200
			4	7.34	414	Completed	2	1	1320*
			95	7.48	420	Leak from primary gasket	12	3	120
			138	16.51	360	Completed	11	1	1200
	T04	6	7.8	414	Completed	2	1	1200	

\* The duration exceeded 20 hour because the 20-hour target was reached before the office hour.

**Table 18: Summary of Test Result for Operating Capacity with Offset Position**

Gasket	Size	Gasket ID	Test No.	Gap (mm)	Pressure (kPa)	Terminated Reason	Data Points	Result Condition	Duration (min)
A	600	T02	36	4.42	125	Completed	6	1	1200
		T02	118	7.25	280	Leak from primary gasket	10	3	960
		T02	120	9.21	200	Leak from primary gasket	11	3	1080
		T02	122	13.26	160	Leak from primary gasket	9	1	30
	900	T02	39	3.82	220	Completed	5	1	1200
		T02	80	8.51	280	Leak from primary gasket	13	2	1200
		T02	76	10.5	120	Completed	8	1	1200
		T02	78	14.76	120	Completed	7	2	1200
1200		T07	146	3.29	240	Completed	12	1	1200
		T07	101	3.3	360	Leak from primary gasket	7	1	1200
		T07	106	3.38	360	Completed	10	2	1200
		T07	148	9.71	200	Completed	11	2	1200
		T07	144	13.34	240	Completed	12	2	1200
B	600	T06	44	4.2	520	Completed	2	1	1200
		T06	57	13.1	400	Completed	2	1	1200
900		T06	113	5.75	270	Completed	13	1	1200
		T06	85	8.99	320	Completed	9	1	1200
		T06	115	11.53	205	Completed	12	1	1200
		T06	111	15.5	400	Completed	15	1	1200
1200		T03	142	3.77	400	Completed	10	2	1200

### 5.3 Joint Gap Monitoring

The joint gap is achieved by placing the wedge style secondary gasket in between the shoulder of the pipe and the end face of the spigot (**Figure 7**). The gasket was compressed, but complete jointing of the pipe sections was avoided. The maximum gaps achieved in the tests ranged between 3.9 mm and 10.8 mm. With an additional plastic spacer ring having a thickness of 6 mm, 9 mm or 13 mm to be sandwiched in the joint, a maximum joint gap of 16.5 mm can be achieved (Test #138). This can simulate a large spectrum of in-field construction conditions of the resulting joint gap. Joint gaps at a minimum of three locations around the pipe were measured and monitored throughout the test. Variations and fluctuations of the joint gap

measurement observed during the test were minor and considered insignificant. These observed results were attributed to the flexible straps and degree of compression of the secondary gasket. If larger variations were observed during the test, or minor leakage was observed on the secondary gasket, adjustments of the straps were made to ensure proper restraint was provided to prevent further joint separation. The largest gap for each test is reported in **Table 15**. The ultimate hydrostatic pressure from each test is plotted against the maximum joint gap in **Figure 24, Figure 25, and Figure 26** for 600 mm, 900 mm and 1200 mm diameter RCP, respectively. The findings are further discussed below.

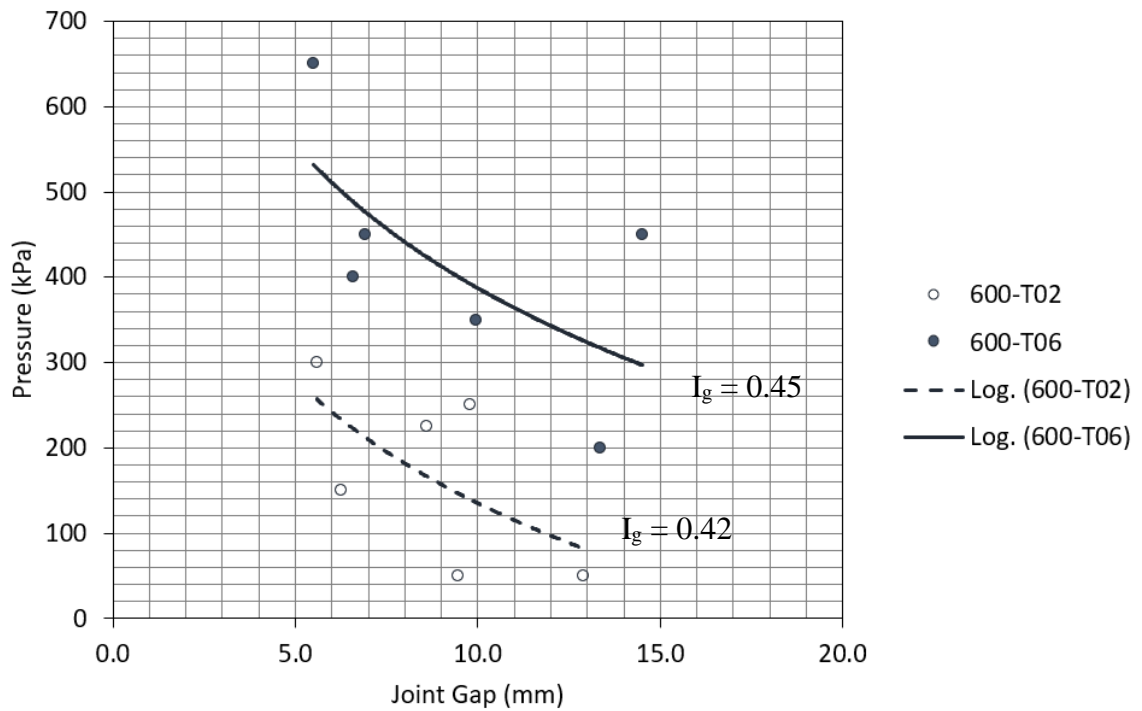


**Figure 24: Hydrostatic Infiltration Performance for 600 mm RCP.**



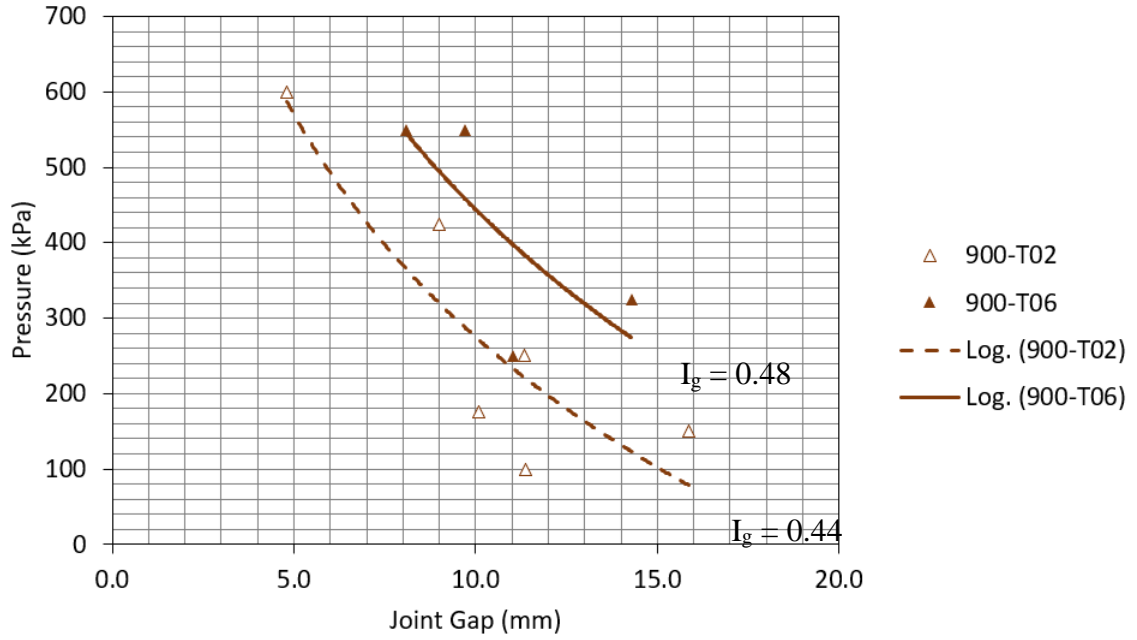


**Figure 25: Hydrostatic Infiltration Performance for 900 mm RCP.**

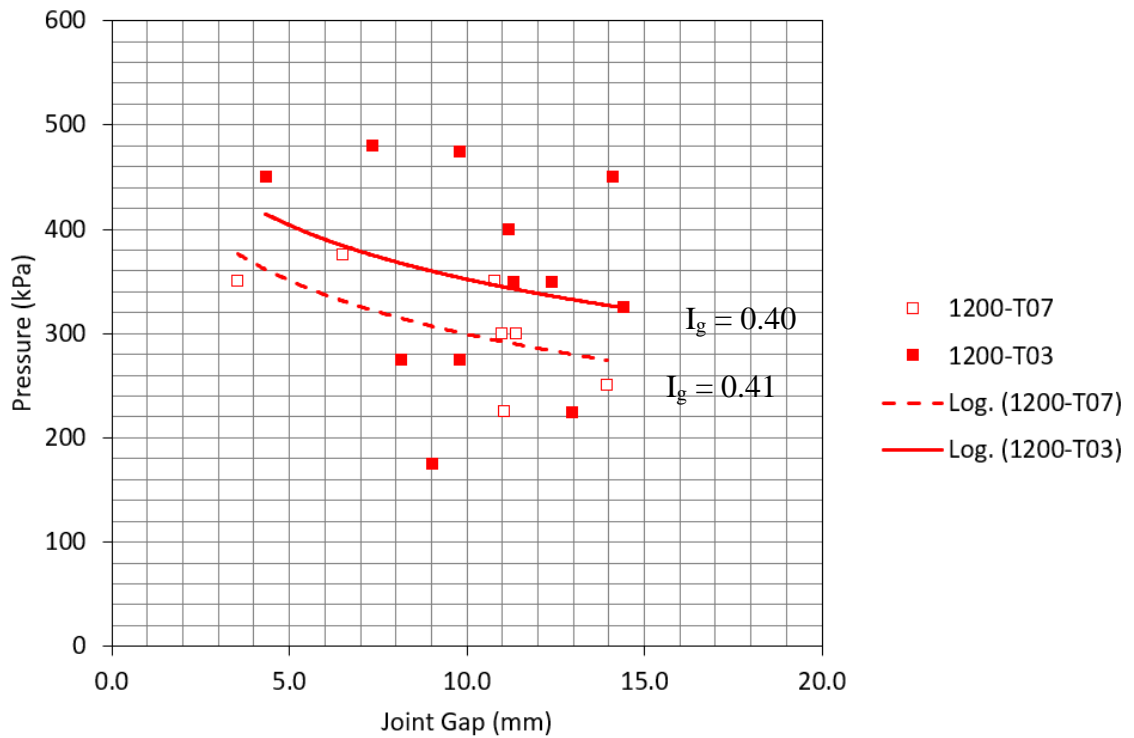


**Figure 26: Hydrostatic Infiltration Performance for 1200 mm RCP.**

## 5.4 Leakage Monitoring

In addition to visual inspection for leakage, the use of the WSCC allows monitoring the amount of water leaving the system (**Figure 27**). The water level in the WSCC was marked as a datum before pressurization. At each pressure increment, the water level was measured at the beginning and at the end of the 10-minute holding period. **Figure 28** shows minor leakage from outside of the pipe joint. **Figure 29** exhibits typical leakage through the secondary gasket from the outside face of the pipe sections, while **Figure 15** shows typical leakage through the primary gasket from the inside face of the pipe sections. Leakage usually starts when a watermark appears in between the joint gap and through the gasket. The intensity of water seepage increases until significant water is lost in the WSCC. Adjustment of the straps is made in some cases to reduce and/or stop the leakage from the secondary gasket, as long as the required pressure for the corresponding increment was not compromised. Other minor leaks from the inlet pipe connecting the WSCC and the joint can also be observed (**Figure 30**). The recorded water levels throughout the test at each pressure level are then plotted versus time. The rate of change in the water level is discussed below.

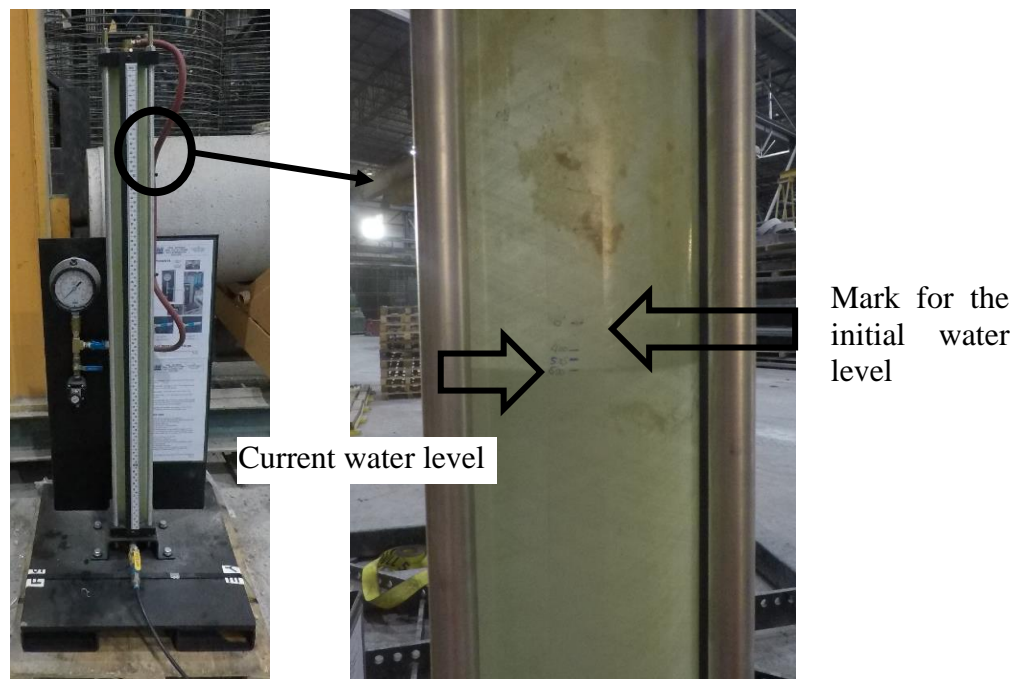


**Figure 27: Water Level Monitoring from WSCC.**



**Figure 28: Minor External Leak During Test (1200 mm RCP, 375 kPa).**



**Figure 29: Leakage from Outside.**



**Figure 30: Leakage from Inlet Tube Caulking (600mm at 300 kPa).**

## 5.5 Additional Tests

To demonstrate the validity of the testing method, eight additional tests were conducted, and the results are reported in **Table 19**. These tests use 675 mm and 750 RCP with self-lubricated gasket, 675 mm RCP with profiled wedge gasket, 1800 mm lined RCP with single offset joint, 600 mm lined pipe with joint coupler and double tilting gaskets. Although the tests did not take the primary gasket to failure, the results show the infiltration pressure level reached, representing the target ultimate capacity of the joint and gasket combination. The purpose of these tests was to demonstrate that the developed test method could be used to test a variety of pipe joint profile and gasket combinations. These tests were outside the original scope of the research. Thus, the results were not included in developing the performance charts. The effects

of the added variation, including the liner, joint coupler, and new wedged profile may influence the performance. More control may be introduced for complete performance evaluation.

**Table 19: Summary of Test Result for Other Pipes and Gaskets**

Gasket	Size	Gasket Ref. ID	Test ID	Pressure (kPa)	Joint Gap (mm)	Term. Reason	Duration (min)
C	600*	T05	18	250	NA	Coupler drop (upper gasket)	10
C	600*	T05	19	200	NA	Completed	1200
B	750	T06	25	600	3.9	Tube leak at 500kPa, reset the water level, 86% of equipment capacity	10
B	750	T06	26	480	3.9	Completed	1200
B	675	T06	27	600	4.1	86% of equip. cap.	10
B	675	T06	28	480	4.1	Completed	1200
B	675	T08	29	500	4.4	Ball valve blew off	10
B	1800 <sup>!</sup>	T04	104	200	7.7	Leaks from secondary	10

\* Lined concrete pipe with double tilting gasket and plastic coupler joint

! Lined concrete pipe with single offset joint

## 5.6 Preliminary Findings

**Figure 24, Figure 25, and Figure 26** exhibit the ultimate pressure reached during the tests versus the maximum joint gap for 600 mm, 900 mm and 1200 mm diameter pipes. Each figure contains two sets of data, i.e. two gasket sources with two different influence ratios,  $I_g$ , derived in **Table 20**. The scatter of data points indicates a moderate negative relationship, as shown via the best fit logarithmic curve. For 600 mm pipes (**Figure 24**), a capacity reduction of 200 kPa was observed between a joint gap of 6 mm to 14 mm in Gasket Profile T06, while 140 kPa reduction between 6 mm and 12 mm was measured for Gasket Profile T02. For 900 mm pipes (**Figure 25**), 200 kPa capacity reduction was found between 9 mm and 13.5 mm joint gap for Gasket Profile T06, while 180 kPa capacity reduction was registered for Gasket Profile T02. For gasket profile T02, the capacity was estimated at 100 kPa when the gap exceeded 15 mm. For 1200 mm pipes (**Figure 26**), the data for both gasket profiles seemed to be overlap. The capacity reduction trends between 5 mm and 14 mm joint gap at 80 kPa were somewhat parallel.

The larger the joint gap, the lower will be the ultimate hydrostatic infiltration pressure. Larger gasket profile (heavier average stretched unit mass) results in a larger difference in influence

ratios; hence higher ultimate pressure can be achieved with a given joint gap. The high variation observed is likely due to the gasket's mechanical properties that are sensitive to the applied pressure and the condition of the concrete surface at the pipe joint. In addition, the lesser capacity reduction for 1200 mm pipes compared to its 600 mm and 900 mm counterparts is caused by bigger joint height,  $J$ . The pipe joint height for 1200 mm RCP was 108 mm, while it was 98 mm for 900 mm and 600 mm RCP. Longer single offset joint offers a longer distance for the gasket to travel before failure. The gasket movement under pressure during the test can be observed through monitoring the water level, as discussed later in this text.

**Table 20: Gasket Mass to Annular Space Influence Ratio,  $I_g$**

Size	Gasket Profile ID	Spigot Dia. (mm)	Spigot Circumf. (mm)	Average unstretched length (mm)	Average mass (g)	Estimate Stretch %	Average stretched unit mass (g/m)	Annular space (mm <sup>2</sup> )	$I_g$ (g/mm <sup>2</sup> /m)
600	T02	733	2303	2074	550	11%	239	564	0.42
900	T02	1037	3258	2967	803	10%	247	564	0.44
1200	T07	1325	4163	3616	1496	15%	359	882	0.41
600	T06	733	2303	1994	590	16%	256	564	0.45
900	T06	1037	3258	2885	885	13%	272	564	0.48
1200	T03	1325	4163	3703	1452	12%	349	882	0.40

## 5.7 Ultimate Pressure Capacity Varying by Pipe Size

**Figure 31** shows the ultimate pressure capacity against infiltration from the data collected on 600, 675, 750, and 900 mm RCP using the same self-lubricated gasket profile 135 (T06). All pipe sizes had an identical joint profile with a joint height ( $J$ ) of 98.4 mm, a joint step ( $j_s$ ) of 48.8 mm by 8.3 mm ( $S$ ) and 49.6 mm ( $j_T$ ) by 3.2 mm ( $T$ ) (**Figure 16**). The data show a similar moderately negative relationship discussed earlier, as illustrated by the best fit logarithmic curve. The logarithmic trendline is used instead of the linear trendline because of the non-linear relationship between the gasket movement and joint gap under various pressure. When the joint gap is small, the gasket tends to be confined, resulting in higher sealing pressure. When the joint gap increases, the gasket relies on the friction between the concrete and rubber to maintain stationary position. This relationship between the ultimate pressure capacity and the joint gap is not believed to be linear. In addition, the reduction in capacity changed from 600



kPa at a 4 mm joint gap to 320 kPa at a 14 mm joint gap, indicating that it is **more** sensitive to the joint gap but **less sensitive** to the pipe size.

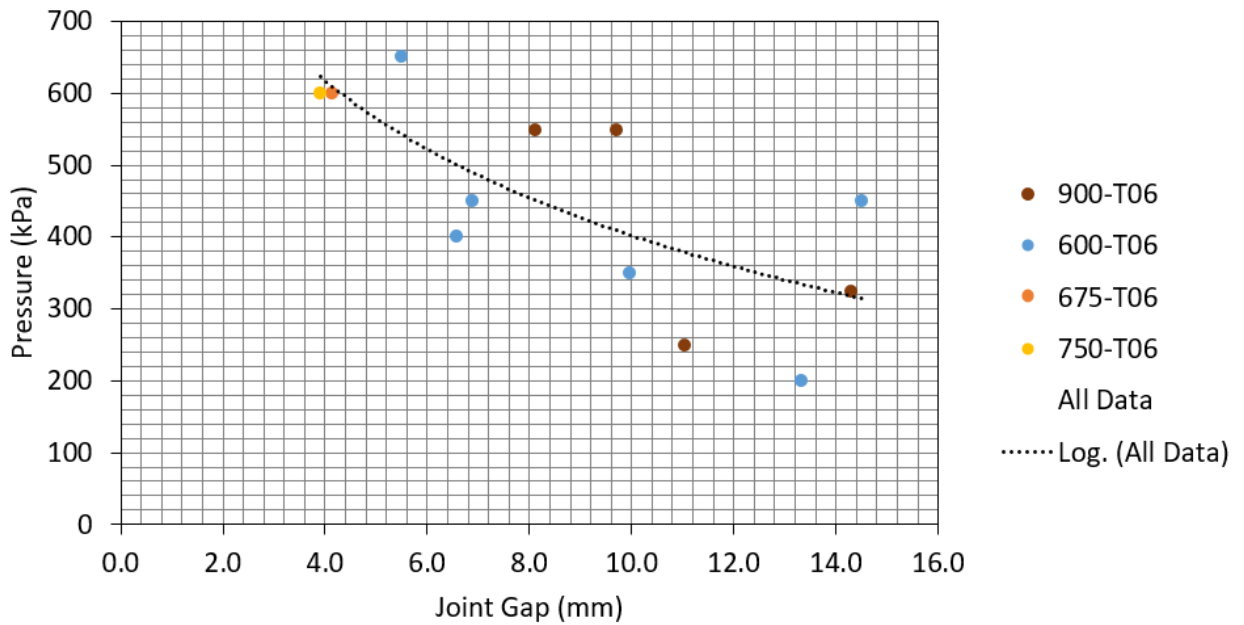


**Figure 31: Hydrostatic Infiltration Performance for Self-lubricated Single Offset Gasket Profile (T06).**

## 5.8 Water Level Reduction in Ultimate Pressure Evaluation

Measurement of the water level reduction with respect to the datum was converted into volume (litres) and plotted against the progress of the applied pressure in **Figure 32**, **Figure 33**, and **Figure 34** for 600 mm, 900 mm and 1200 mm diameter pipes, respectively. The trend was somewhat linear with a different rate, depending on the size of the pipe, pressure capacity and joint gap. The linear volumetric reduction rates in millilitres per 100 kilopascals of joint annular space from each test are listed in **Table 21** for selected tests. In 600 mm diameter RCP (**Figure 32**), the volumetric loss from three tests was plotted against the hydrostatic pressure. A linear reduction rate of 20 mL per 100 kPa was observed for the test with a 5.5 mm joint gap. A higher rate of 33 mL per 100 kPa was observed for the test with a 9.8 mm joint gap due to the larger annular space. For the test with a 5.6 mm joint gap, the reduction should be comparable to that with a 5.5 mm gap. However, due to the leakage observed at the inlet tube caulking, the reduction rate was 33 mL per 100 kPa, higher than that with a 5.5 mm joint gap. In 900 mm diameter RCP (**Figure 33**), both tests with 8.1 mm and a 9.0 mm joint gap exhibited

a volumetric reduction rate of 40 mL per 100 kPa. The test with a 4.8 mm joint gap had a reduction rate of 28 mL per 100 kPa until 500 kPa, followed by an escalated reduction rate of 260 mL per 100 kPa due to severe leak at the inlet tube. In the 1200 mm diameter RCP (**Figure 34**), the test with an 8.0 mm joint gap exhibited a reduction rate of 30 mL per 100 kPa until 350 kPa, where an exterior leak was observed. The test with a 7.3 mm joint gap showed a somewhat linear trend until 200 kPa, followed by a severe escalation in the reduction rate due to exterior leak. Similarly, the test with a 10.8 mm joint gap exhibited a reduced rate of 100 mL until 350 kPa, followed by a higher rate caused by an exterior leak.

**Table 21: Estimated Volumetric Change in Annular Space**

Pipe Size (mm)	Primary Gasket	2nd Gasket	Gap (mm)	kPa	Vol. Chg. mL/ 100 kPa <sup>1</sup>	Test ID
600	T02	S01	8.6	225	33	21
600	T02	S01	10.0	250	27	13
600	T06	S03	5.5	650	20	9
750	T06	S03	3.9	600	16	25
675	T06	S03	4.1	600	33	27
900	T02	S01	9.0	425	43	11
900	T06	S03	8.5	550	40	7
1200	T07	S01	11.0	350	30	23
1200	T04	S04	7.3	500	56	17
1200	T03	S03	8.0	480	33	5

<sup>1</sup> Volumetric change in mL / 100 kPa at the initial linear behaviour of the gasket movement

Reduction of the water volume is attributed to various reasons: (a) volume reduction of water under pressure, (b) absorption of concrete, (c) increase in joint gap causing an increase in annular space, (d) compression of rubber causing an increase in annular space, (e) displacement of the primary gasket, and (f) leakage. The reduction of water volume under pressure between 0 kPa and 685 kPa at room temperature is trivial. The change in the joint gap was found to be within 1 mm in most cases. The change in water level in the WSCC due to (a), (b) and (c) was not found to be a primary cause of the measured water loss.

The observed differences in water reduction rates are likely related to compression of rubber followed by displacement of the primary test gasket in its annular space. **Figure 31** shows the water reduction rate impacted by the joint gap. Other than one outlier, there is a linear trend indicating that the reduction rate increased when the joint gap increased. **Figure 35** indicates that the gasket was visible at the failure state in between the joint gap for the 900-mm diameter



pipe tested to (a) 475 kPa and (b) 525 kPa, indicating that significant movement has taken place during the test. The single offset pre-lubricated gasket is designed to roll into the narrower gap from the step of the spigot during the jointing process of the pipe. This leaves space behind the gasket from the inside of the pipe bell. The existing design of the joint is more favourable to withstand internal pressure when it pushes the gasket outward into the narrower annular space. However, it is not favourable in resisting external pressure since it pushes the gasket towards the wider part of the annular space to the bell. Therefore, the primary cause of the reduction in the water level is the gasket displacement into the volumetric increase of the annular space.

It was also observed in the case of the 900 mm RCP with T02 and T03 gaskets that the joint failed when the joint gap was greater than 9 mm and 9.8 mm, respectively. At the time of failure, the gasket in both cases had left the annular space. The amount of displacement is related to the mechanical properties and size of the rubber, the friction between the gasket and the concrete, the degree of compression resulting from the joint gap, the joint and concrete conditions. However, a more quantitative assessment needs a dedicated investigation. Leakage observed during the tests is often progressive at the beginning, but sudden at the time of imminent failure. This behaviour can easily be observed and measured using the test method proposed herein, indicating its potential value for consideration into relevant standard guidelines.

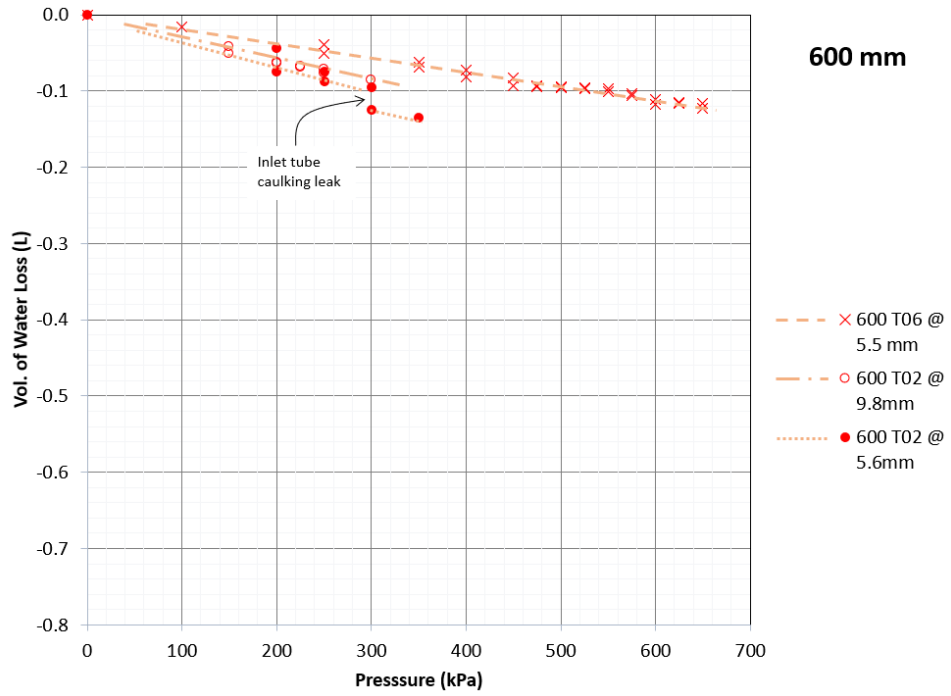


**Figure 32: Water Reduction Chart for 600 mm RCP.**

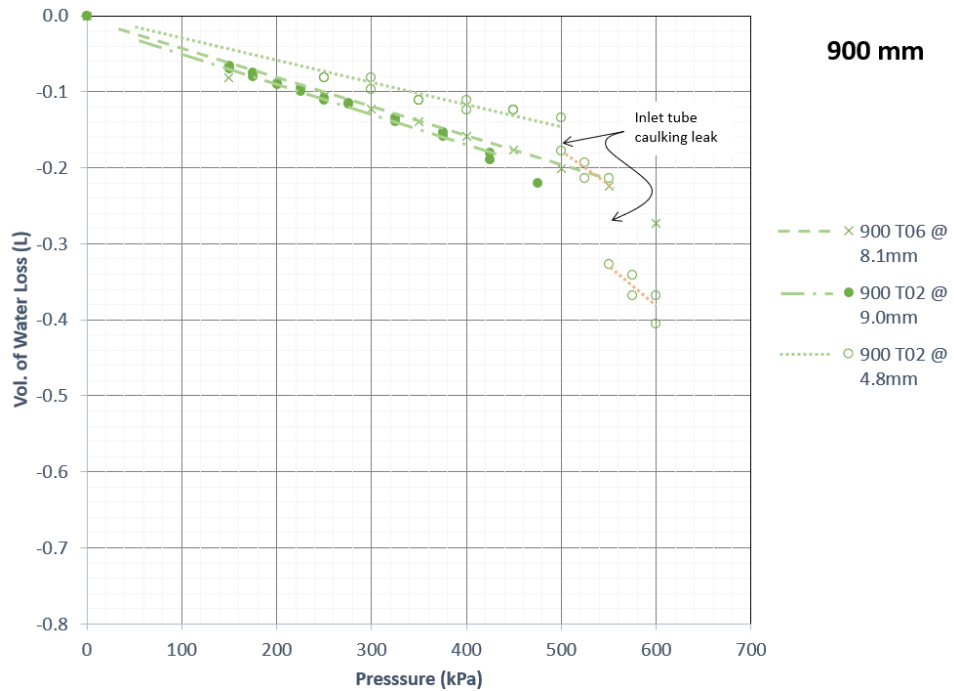


**Figure 33: Water Reduction Chart for 900 mm RCP.**

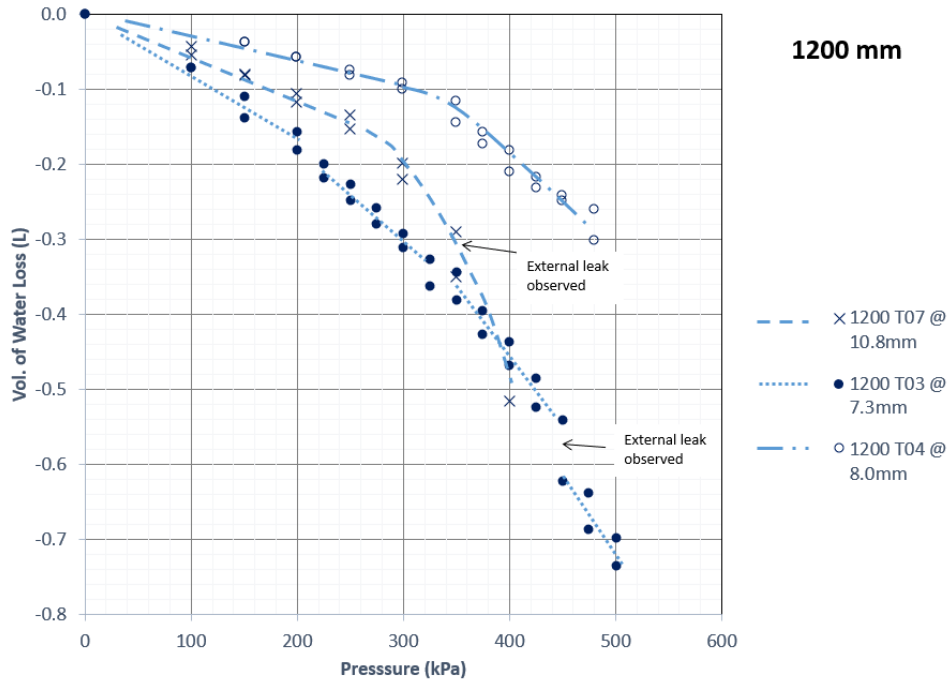


**Figure 34: Water Reduction Chart for 1200 mm RCP.**



(a) Test #11 900 mm RCP, 475 kPa, Gasket Profile T02, 9 mm gap



(b) Test #92 900 mm RCP, 525 kPa, Gasket Profile T03, 9.8 mm gap

**Figure 35: Primary Gasket Displacement at Failure.**

## 5.9 Water Level Reduction in 20-hour Operation Test

The water level was monitored for a total of 20 hours duration for three tests using 900 mm RCP (Test # 67, 81, and 114). The results are plotted in **Figure 36**. The rate of reduction in water level reached up to 2.5 mL in the first 10 minutes, but diminished thereafter, indicating that the movement of the gasket slows down with time. The measurement taken at the end of the 20-hour duration for Tests #67 and #81 were 2.8 mL and 3.1 mL, respectively. For test #114, the final reading was 4.4 mL, higher than tests #67 and #81. This was attributed to the method of measurement using a calliper on the marked water level. The accuracy of this method is rather modest when the water level remains unchanged over a long period. In general, the position of the gasket under pressure over time stabilized, based on the trend observed over 20 hours.

Based on the observation of the gasket movement reported earlier, one would question the behaviour over a longer period. Few operation tests for 900 mm pipe with various joint gaps were selected to include additional measurement of the water level from the WSCC. No apparent leakage from neither inside nor outside of the pipe joint was observed. The measurement was reported in **Figure 36**. The reduction in water level has a logarithmic relationship with the duration under sustained pressure. The water reduction was reported as 1.1 mm, 3 mm, and 7.2 mm for the joint gaps 7.7 mm, 9.3 mm and 11.8 mm, respectively,

indicating that the larger the gap, the more severe is the movement. The level of the movement reduced over time. Gasket movement tended to stabilize in a longer duration compared to the conventional 10-minute test. If the joint gap was relatively large at the beginning, under sustained high pressure, the leakage was expected to eventually occur.

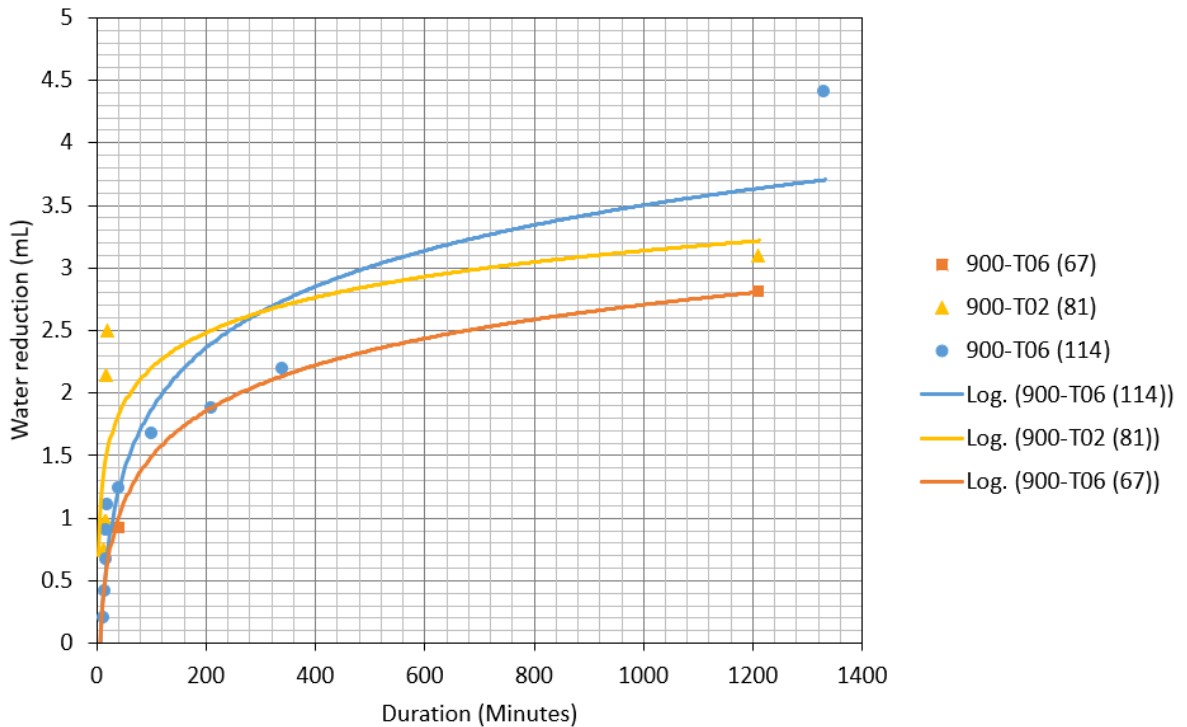


**Figure 36: Water Level Reduction for 20-hour Operation Test (T06).**

## 5.10 Summary

This chapter reports the testing results based on the ultimate and operating hydrostatic capacities and their failure modes. It was observed that the capacity decreased as the joint gap increased. During the test, the leakage could be visualized and monitored through the water level in the WSCC. Additional tests also showed that the test could be used for a larger diameter pipe, e.g. 1800 mm. The water level reduction charts could signify the severity of leakage during the tests. The gasket monitoring over 20 hours also revealed the behaviour of the gasket movement with respect to the joint gap.

## 5.11 References

Wong, L. and Nehdi, M.L. “Quantifying Resistance of Reinforced Concrete Pipe Joints to Water Infiltration”, ASCE Journal of Pipeline Systems - Engineering and Practice, Reston, Virginia, United States, 2020.

## CHAPTER 6

---

### 6 Joint Hydrostatic Performance Curves and Application

This chapter presents the real-world challenges in maintaining minimum RCP joint gaps during in-situ installation. Performance curves were developed using the data collected from the infiltration tests to provide quantified guidance to mitigate the risk of leakage due to the infiltration of groundwater.

#### 6.1 Hydrostatic Performance Implications

An ideal installation of RCP requires the contractor to minimize the joint gap during installation. The minimum joint gap, by design, is when the end face of the pipe is completely in contact with the adjacent pipe. In this position, the annular space created by the joint is minimized, implying that maximum compression of the rubber gasket can be achieved, and hence maximum sealing potential. Based on experimental testing completed thus far in this research, the conventional RCP and single offset gaskets can reach up to 600 kPa and 360 kPa for Gasket A in the aligned and offset positions, respectively. For Gasket B, the ultimate capacity can reach 650 kPa regardless of the alignment. CSA A257.2 reduced the target hydrostatic test pressure from 105 kPa under straight alignment to 35 kPa under offset alignment (67% reduction) to account for the potential influence of offset joints. In the infiltration test, the offset did influence the capacity, but not in a systematic manner. The joint gap seemed to be more influential on the sealing potential. Minimizing the joint gap also prevents the gasket from displacing and escaping from the annular space. **Figure 37 (a)** shows a typical gasket displacement captured by closed-circuit television (CCTV), which is comparable to the observation in the infiltration test of **Figure 37 (b)**.



**Figure 37: (a) Left: Displaced gasket captured by CCTV and (b) Right: observed in the infiltration test.**

## 6.2 Reality Challenges in Maintaining Minimum Joint Gap

The main reasons that RCP joint gaps cannot be minimized include site conditions, pipe alignment, gasket position, and manufacturing tolerances. Jointing the pipe is an important step in the installation process. FDOT (2019) specifies 16 mm (5/8”), 22 mm (7/8”) and 25 mm (1”) for 300 mm to 525 mm, 600 mm to 1650 mm, and 1800 mm or larger RCP with a minimum hydrostatic pressure resistance expectation of 35 kPa (5 psi) to be considered as a watertight joint. In Canada, CSA A257.1 requires a 13 mm deflection in the horizontal setup for RCP hydrostatic test to 90 kPa (CSA, 2019). This implies that the maximum permissible gap is 13 mm. In addition, the installation guide (OCPA, 2012) requires proper equipment and methods to create an acceptable RCP joint. The maximum sealing potential requires a resultant compression of the sealing material to be developed during the jointing process. Proper positioning of the gasket, as per its original design, implies proper development of such compression. Failure to follow the original design intent will result in inadequate jointing.

Also, the preparation of the bedding material, including levelling and compaction, is important to create conditions that mitigate potential differential settlements. For smaller diameter RCP with flared bells, a void must be created to house the larger bell section. This prevents a potential bridge effect that may cause longitudinal bending and joint rotation. Moreover, pipe alignment is one of the main causes of opened joints. Many contractors use joint gaps as their allowable deviations in installations without considering the potential implication to the hydrostatic performance. Inquiries



from contractors about how large a joint they can leave open are common. **Figure 38** shows a joint gap that was purposely created by inserting a piece of wood to maintain alignment of the pipe run. The offset of the joints is also common, but it is hard to determine because its main causes are the differential settlement of bedding materials, uneven backfill, surcharge loading from construction equipment, and possible live loads from traffic in shallow buried depths.

Furthermore, the permissible manufacturing tolerances can affect the joint quality, in addition to the construction alignment tolerances. **Figure 37(a)** and **(b)** show the lay length measurements of 2425 mm and 2445 mm from the inside of the pipe on the left and right sides of an installed pipe, respectively. The design lay length of this pipe is 2438 mm. The measurement reaches the maximum variation of lay length on the opposite side that is permitted by CSA A257.2. **Wong and Nehdi (2018)** synthesized the maximum variation permitted by several standards around the world. **CSA A257 (2014) and ASTM C76 (2016)** allow a 6 mm to 20 mm difference between opposite sides for various pipe sizes, while **AS/NZ 4058 (2007)** allows 2 to 10 mm for corresponding pipe sizes. This tolerance may be too large, considering the risk of infiltration. Nonetheless, the lack of understanding of the importance of joint gaps in relation to the hydrostatic performance and its risk implications cannot be overstated.

### 6.3 Performance Curve Development

**Figure 39, Figure 40, and Figure 41** illustrate the gasket performance against infiltration for 600 mm, 900 mm and 1200 mm RCP joints, respectively. Three groups of information for the data collected from the hydrostatic infiltration tests for 600 mm, 900 mm and 1200 mm diameter RCP were plotted against the joint gap. The ultimate pressure data points, their logarithmic trend lines, and the sealing potential based on the load-deformation performance for each gasket material were presented in the graphs. The ultimate pressure data were determined from each hydrostatic test setup. The sealing potential curves were derived based on the calculation described in the previous section. This figure is intended to compare the sealing potential derived from the gasket geometric calculation to the actual hydrostatic performance from the RCP joint infiltration test with respect to the various joint gaps.



**Figure 38: Joint gap on the (a) left, and (b) right side of the pipe created in the job site to account for the manufacturing tolerance to maintain sewer alignment.**

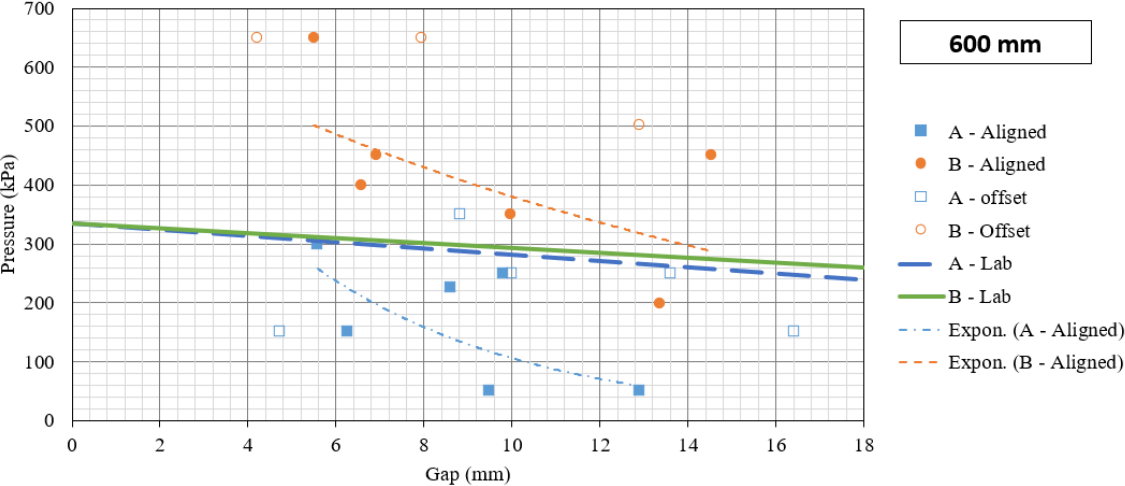


**Figure 39: 600 mm RCP infiltration Joint Test Performance Curves.**

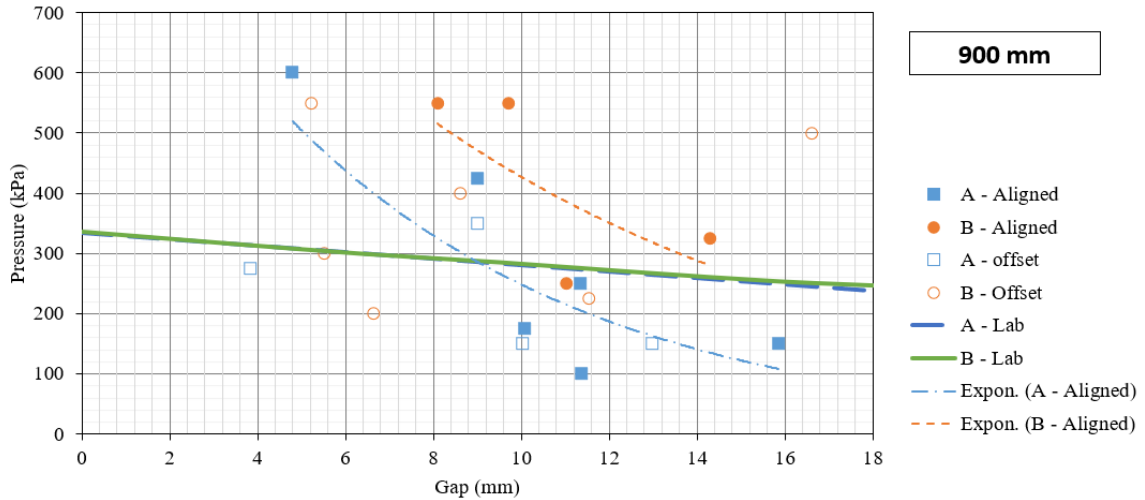


**Figure 40: 900 mm RCP infiltration Joint Test Performance Curves.**

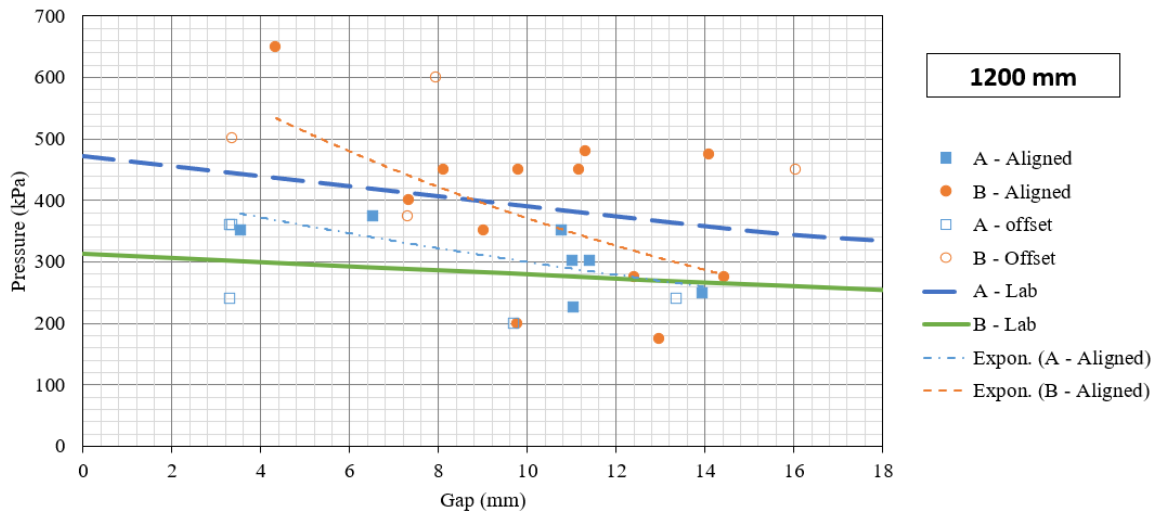


**Figure 41: 1200 mm RCP infiltration Joint Test Performance Curves.**

## 6.4 Test Results

**Figure 39** shows the joint performance versus infiltration for the 600 mm pipe specimens. The actual capacity indicated a downward trend for both gasket specimens. Gasket B generally had approximately twice the capacity of Gasket A. In the aligned condition, Gaskets A and B had 70% and 30% reduced sealing potential at a 12 mm gap in comparison to that at a 6 mm gap, respectively. Although results from the offset condition showed a similar downward trend, the gasket specimens seem to have been less affected by the offset orientation. Moreover,

according to CSA A257.2, the target for the hydrostatic test with a deflected joint, i.e. joint with a 13 mm opening, is 90 kPa. Based on the infiltration test results, Gasket A had a sealing capacity for infiltration below 90 kPa when the joint gap exceeded 11 mm; hence, it failed to meet this requirement.

**Figure 40** shows the joint performance against infiltration for the 900 mm pipe specimens. Results for Gasket A were more consistent comparing to Gasket B, following a downward logarithmic trendline. The sealing capacity for infiltration decreased by 230 kPa between the joint gap of 6 mm and 12 mm. Gasket B had larger fluctuation resulting from a larger variance of the influence of the ratio of stretched unit mass to annular space. For gasket A, the offset alignment seemed to affect the infiltration performance, while Gasket B was more substantially affected by the offset alignment.

**Figure 41** shows the joint performance versus infiltration for the 1200 mm pipe specimens. Gasket A had better consistency following a downward trend. An 80 kPa reduction in sealing potential for infiltration was observed between the joint gap of 6 mm and 12 mm. Gasket B exhibited a higher reduction of 160 kPa between a joint gap of 6 mm and 12 mm. In addition, a larger variance was observed for Gasket B, resulting from a larger variance of the influence ratio in comparison to Gasket A. The offset alignment influenced the results for Gasket A more than for Gasket B.

In conclusion, the infiltration performance of the gasket is in agreement with the prediction derived from the gasket geometry. However, the prediction of the sealing potential decreased less drastically with increasing joint gap than in the case of the hydrostatic performance in the infiltration test.

## 6.5 Prediction Using Gasket Load-deformation Tests

Laboratory predictions are obtained through a theoretical estimate based on the material load-deformation tests described in the earlier section of this Chapter. The curves show a somewhat linear reflection in its elastic response in the load-deformation behaviour. The sealing potentials from the load-deformation test are plotted in **Figure 39**, **Figure 40**, and **Figure 41** using solid lines for 600 mm, 900 mm and 1200 mm, respectively.

For 600 mm gasket specimens, predictions with zero gap were 335 kPa and 334 kPa, decreasing linearly to 267 kPa and 281 kPa, with a 13 mm gap for Gaskets A and B, respectively. This indicates that Gasket B had slightly higher sealing potential under laboratory conditions with a larger gap than Gasket A. In addition, increasing the joint gap from 6 mm to 12 mm decreased the sealing potential in laboratory tests by 34 kPa and 26 kPa for Gaskets A and B, respectively, which is substantially less than that in the hydrostatic infiltration experiments. This is because the rubber gasket sample does not experience a frictional force perpendicular to the applied load in the load performance test, whilst the pressure perpendicular to the joint face can be substantial in the infiltration test. For the 900 mm gasket samples, laboratory predictions were somewhat similar because the gasket profiles were identical to that of the 600 mm samples. With a slight difference in strength length, a similar reduction in sealing potential comparisons would be expected.

For the 1200 mm gasket samples, the average widths of the gasket were 21.9 mm and 20.1 mm, 4.4 mm and 3.0 mm larger than that in the 600 mm for Gaskets A and B, respectively. Larger base areas resulted in higher frictional resistance when subjected to similar infiltration force. Gasket B had less profile size than that of Gasket A, resulting in a lower sealing potential in the laboratory test given the same annular space. Compared to the infiltration test, the laboratory results seemed to overestimate the results for Gasket A and underestimate it for Gasket B.

In conclusion, as illustrated in **Figure 19**, the load-deformation test does not account for the slippage of the gasket, does neither consider the actual boundary (i.e. concrete and rubber), nor the load that is applied normally to the contact surface. The actual infiltration pressure was exerted on the gasket parallel to the boundary surface. The gasket tended to slip when the frictional resistance was exceeded. The actual sealing potential needs to consider the frictional resistance caused by the gasket movement. This also indicates that the hydrostatic performance curves for infiltration may not be linear.

## 6.6 Discussion on Uncertainty of Data

The general overview of the test data shows significant scatter and spread larger than what was expected despite the downward trends, e.g. **Figure 26**. The scatter may result from other

hidden or exogenous variables, which will be addressed in the machine learning modelling approach in Section 7. It may also be attributed to the non-quantifiable assumptions. The gasket sample was lubricated inside the tube section to allow self-equalization during the installation. However, it is not certain whether the gasket is completely equalized. It is also not certain that the lubrication was applied evenly covering the entire gasket. Moreover, during the jointing process, the top bell end of the pipe sample was lowered and inserted into the spigot end of the pipe by a forklift. It was assumed to be level, and the joint was evenly closed. It was, in fact, impossible to make it perfectly level. These may contribute to the spread of the test results. To obtain the actual infiltration performance data for the RCP joint, the results are a first attempt in this research to reach rational behavior. Despite the scatter and data spread, it provides a starting point for future research. The results can also provide a support to the future development of guidelines and acceptance criteria after conducting a wider scope of experiments that resolve the limitations of this study, the uncertainty of the assumptions, and more robust control of the experimental setup to reduce data scatter.

## 6.7 Application of Performance Curves

### 6.7.1 Process

The extent of pipe infiltration is usually site-specific. For new sewers, the quantifiable factors include the pipe material standards and methods, quality of workmanship (i.e. installation), ground conditions, and, more importantly, the height of the groundwater level and its seasonal variation (**Butler and Davies, 2004**). Part of the quantifiable measures to associate the quality of installation and expected performance against infiltration is to associate the RCP joint hydrostatic performance test for infiltration through the performance curves developed earlier. This should provide a practical tool to mitigate potential infiltration into new sewer pipes that could result from a specific site condition. Such an assessment could further provide installation guidance based on the selected gasket and pipe material to minimize leakage after installation. **Figure 42** presents an assessment flow chart to relate field conditions to testing results. This model consists of three components: inputs, analysis and outputs. The process takes the hydrostatic pressure from the high groundwater level compared to the hydrostatic performance curves for infiltration and the gasket load-deformation curves of the gasket

materials. An infiltration potential factor is introduced to relate the field condition and the experimental results. The maximum allowable joint gap can be derived for the hydrostatic performance curve from the infiltration test. The information can be used for quality control when jointing the RCP during installation. The assessment procedure should: (i) determine the maximum pressure head from the high groundwater condition; (ii) apply infiltration potential factor to account for the statistical variance of the gasket and pipe materials; and (iii) Obtain the maximum allowable joint gap from the hydrostatic performance curve.

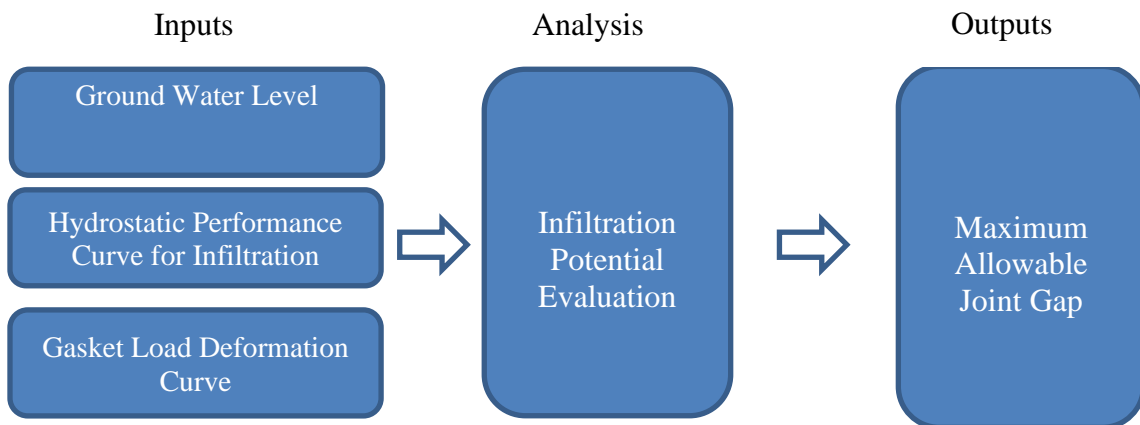


**Figure 42: Infiltration Potential Assessment Model.**

### 6.7.2 Infiltration Potential Factor

Similar pressure predictions with different reduction scale with respect to the joint gap based on material tests and infiltration tests were observed. This is due to the different loading models used in the tests. The pressure reduction was faster when increasing the joint gap than that predicted using material testing. This is because the gasket was forced to slip under the infiltration pressure pushing towards the inside joint face. The direction of movement is parallel to the face of the concrete. The frictional coefficient between rubber and wet concrete ranges between 0.45 and 0.75; and between 0.6 and 0.85 for dry concrete (**The Engineering Toolbox, 2004**). This also explains why the pressure reduction was faster when the joint gap increased. The contact face was wetter due to less pressure between concrete and rubber, resulting in lower pressure. The surface roughness may also contribute to the frictional resistance (**El-Sherbiny et al. 2012**).

A potential infiltration factor is recommended to be introduced to relate the findings from the test and the field expectations. For example, the Ontario Ministry of Transportation requires the pipe to withstand 10.5 m pressure head equivalent to 105 kPa (MTO, 2014). The performance from the gasket material tests reported herein ranged between 250 kPa to 350 kPa. It is suggested that a factor of 3:1 can be used related to the experimental results to the field expectation. The factor may further increase to account for the omission of the slippage between the bearing surface and the gasket sample in the material test.

In addition, long term performance factor should also be considered. In the 20-hour hydrostatic test for operation conditions, 80% of the ultimate capacity is used as the test target. Therefore, in interpreting the infiltration potential factor, an additional 20% should be reduced from the performance curves.

**Figure 43** exhibits the infiltration potential factor in a performance model of the RCP joint. The tested ultimate performance is represented by the upper curve, followed by a reduction trend reflecting the reduction potential in long-term performance due to the rubber relaxation and gasket movement. The final in-field capacity is illustrated by an offset curve accounting for the specification deficiency, manufacturing tolerances, construction tolerances and the design of the joint and gasket. The actual design requirements ought to be based on the maximum groundwater table obtained by a geotechnical investigation. The difference between the ultimate test capacity and the design requirement is considered to be the infiltration potential factor. As the long-term performance is progressively reduced, the difference between the ideal long-term factor of safety and the design requirement is considered to be the required factor of safety. However, the actual performance is lower than the design requirement, leading to infiltration potential.



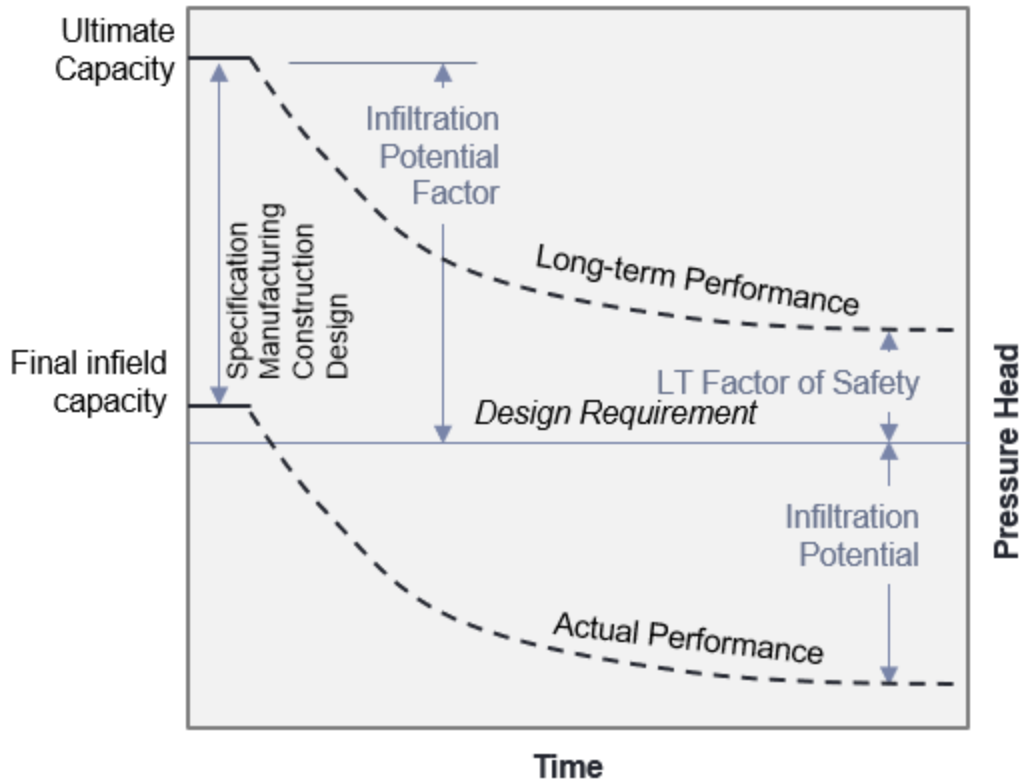


**Figure 43: Infiltration Potential Assessment Illustration.**

### 6.7.3 Illustrative Case Study

A sample pipe installation project located in West Gwillimbury in the Region of York, Ontario, Canada, included a 600 mm concrete sanitary sewer with an average buried depth of 12 to 13 m from the finished grade to the underside of the pipe. The 100-year high groundwater level was found at 235 m to 236 m above sea level. The stormwater pipe was designed to match its crown to the high groundwater level, whilst the 600 m sanitary trunk line was designed to be deeper at about 228 m. The sanitary sewer was submerged in the groundwater after installation and exposed to potential infiltration. **Figure 44** shows a simplified illustration of the profile view of the ground condition and pipe design. The high groundwater table located at 235 m to 236 m measured above sea level was expected to exert approximately 8.0 m (80 kPa) to 8.5 m (85 kPa) of hydrostatic pressure against the RCP. To apply a 3:1 infiltration potential factor, the 600 mm concrete pipe supplier needed to demonstrate that the joint can withstand infiltration pressure of 255 kPa under operating condition. Considering that 255 kPa was 80% of the ultimate capacity requirement, the maximum permissible joint gaps that can withstand

320 kPa (255 kPa divided by 0.8) of infiltration pressure based on the performance curves are 4 mm and 13 mm for Gaskets A and B, respectively.

Gasket B was recommended for use in this project partly because the testing results showed high variation for Gasket A, and partly because the 4-millimetre allowable joint gap is difficult to achieve in the field. In addition, the maximum allowable joint gap of 13 mm when using Gasket B can be controlled by the contractor during the installation. It is critical to validate the joint gap during the installation process and correct the gap if, for any reason, the maximum joint gap cannot be maintained. It would be much less costly to repair the joint during installation than afterwards.

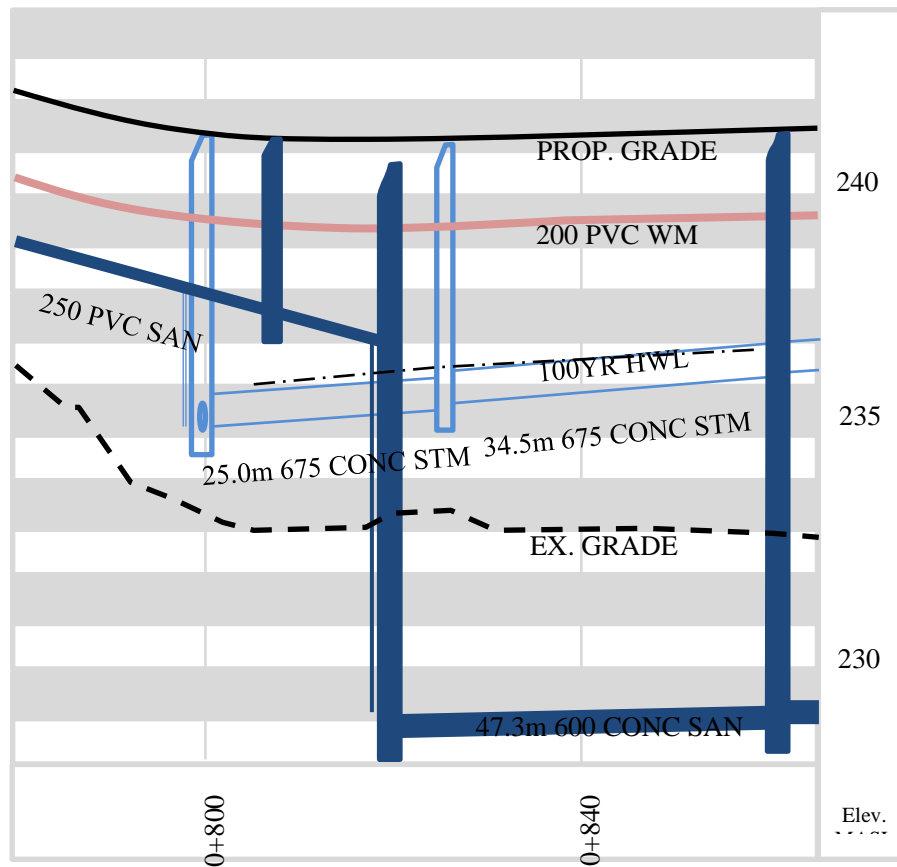


**Figure 44: Profile View of a Potential Infiltration Case.**

## 6.8 Summary

The actual challenges in maintaining minimum RCP joint gaps include construction conditions and manufacturing tolerances, indicating that the ideal joint is difficult to achieve. Performance curves developed based on the test results quantify the influence of the joint gap. The infiltration potential requires consideration of not only the joint itself but also the groundwater conditions. An illustrative case study was presented to assess the infiltration potential based on a suggested infiltration potential factor to mitigate the risk of infiltration using the performance curves developed.

## 6.9 References

- ASTM C76 “Standard Specification for Reinforced Concrete Culvert, Storm Drain and Sewer Pipe”, ASTM International: West Conshohocken, PA, USA, 2016, 11 p.
- AS/NZS 4058, “Precast Concrete Pipes (Pressure and Non-Pressure)”, Australian Standard: Environmental Health Directorate, East Perth, Australia, 2007, 65 p.
- CSA A257, “Standards for Concrete Pipe and Manhole Sections”, CSA Group, Mississauga, ON, Canada, 2019, 40 p.
- El-Sherbiny Y.M., Hasouna A. T. and Ali W. T. “Friction Coefficient of Rubber Sliding Against Flooring Materials”, ARPN Journal of engineering and Applied Sciences, Vol. 7, No. 1, January 2012: Islamabad, Pakistan, 2012
- Engineering Toolbox, “Friction and Friction Coefficients”, online available at [https://www.engineeringtoolbox.com/friction-coefficients-d\\_778.html](https://www.engineeringtoolbox.com/friction-coefficients-d_778.html), Assessed Feb 25, 2020, 2004.
- Ministry of Transportation Ontario. “MTO Gravity Pipe Design Guideline”; Ministry of Transportation Ontario: St. Catharines, ON, Canada, 2007, p 183.
- OCPA, “Concrete Pipe Installation Pocket Guide”, Ontario Concrete Pipe Association, Kitchener, ON, Canada, 2012.
- Wong, L. and Nehdi, M.L. “Critical Analysis of Precast Concrete Pipe Standards”, Infrastructures 2018, 3(3), 18; <https://doi.org/10.3390/infrastructures3030018>, 2018.

## CHAPTER 7

---

### 7 Hydrostatic Performance for Infiltration Prediction Using Machine Learning Techniques

Concrete Pipe, the most commonly used product in sewage systems, faces a challenge in dealing with inflow and infiltration (*InI*) since the quality of the pipe joint relies not just on the joint materials and design, but also on the installation quality. Existing testing methods generally do not proactively capture the infiltration risk. Thus, a novel, simple and robust hydrostatic test for RCP infiltration was developed and presented in the previous chapters. A comprehensive testing program using the new test has collected hundreds of data points on the infiltration performance of RCP joints using existing joint designs and sealing materials.

The experimental procedure and dataset were aimed to capture multiple influential parameters in the design of RCP joints. Due to the nonlinear relationship between such design parameters, conventional statistical models failed to provide a comprehensive and reliable predictive tool to propose design guidelines. Therefore, advanced modelling techniques are required to capture all the underlying effects of different parameters. Substantial parts of this Chapter have been submitted for publication to the ASCE Journal of *Pipeline Systems Engineering and Practice*.

#### 7.1 Recent AI Applications

The evolution of artificial intelligence (AI) algorithms and soft computing techniques allowed solving diverse, complex engineering problems (**Reich, 1997, Reich and Barai, 1999, Koch et al., 2015**). Accordingly, supervised learning methods, namely regression and classification, demonstrated the potential to predict the behaviour of various engineering materials and

systems. A significant number of research studies have deployed robust supervised algorithms to model different civil engineering problems. **Table 22** presents some studies regarding the application of machine learning (ML) algorithms in various civil engineering areas. Regression tools, which are widely used in civil engineering, can be effectively applied to predicting the mechanical properties of concrete. (Nehdi et al., 2001, Yaseen, et al., 2018).

**Table 22: Recent Applications of Machine Learning in Civil Engineering**

Topic	Method	Ref.
The failure mode of concrete bridge columns	KNN, ANN, Tree-based methods, etc.	Mangalathu, 2019
Self-compacting concrete	ANN	Nehdi et al., 2001
Lightweight foamed concrete	Extreme learning machine	Yaseen, et al., 2018
Failure of beam-column joints	KNN, ANN, Tree-based methods, etc.	Mangalathu, 2018
Pavement crack detection	Deep learning	Zhang et al., 2017
High-rise building structures	Hybrid machine learning model	Rafiei and Adeli, 2017
Crack classification in concrete	SURF, CNN	Kim et al., 2019
Streamflow forecasting	ANN	Zealand, 1999

Classification techniques can also be used to investigate the complex behaviour of civil engineering systems. Prediction of the failure mode of structures, as well as defect detection in civil engineering infrastructure using classification problems, have been extensively investigated. For instance, **Melhem and Cheng (2019)** used the K-nearest neighbours (KNN) algorithm to predict the remaining service life of bridge decks and reported that larger datasets could result in higher predictive accuracy. **Mangalathu and Jeon (2019)** explored the failure mode of bridge columns using various ML algorithms such as KNN, decision trees, random forests, quadratic discriminant analysis, and artificial neural network (ANN). They reported that ANN achieved 11% higher accuracy in predicting the failure mode compared to existing models in the literature. They predicted the failure mode of beam-column joints using a dataset containing 536 examples of experimental tests (**Mangalathu and Jeon, 2019**). Similar studies in the literature exhibit how developing predictive ML models can help engineers propose rational guidelines for the design of complicated infrastructures.

Therefore, the present study explores several ML techniques, including gradient boosting, random forest, extra trees coupled with data oversampling methods to develop intelligent models for prediction of hydrostatic pipe infiltration. The proposed models demonstrated high accuracy in the prediction of joint performance, considering the design parameters included in the experimental data collection process. It is anticipated that robust predictive models could allow developing design charts that aid municipalities in proactively averting sewage system infiltration problems at low cost, instead of the current costly reactive approach to this problem.

## 7.2 Machine Learning Literature Review

This section captures the state-of-the-art classification techniques used in model development. Among all major types of classifiers, tree-based ensembles, including Random Forest, Extra trees, and Gradient Boosting, achieved higher performance, and thus are outlined below. The sampling techniques for handling imbalanced data, such as the Synthetic Minority Over-sampling Technique (SMOTE) and Density-Based SMOTE, are also discussed in this section. K-nearest neighbors (KNN), which is also deployed in the process of generating synthetic data, is elaborated on herein.

### 7.2.1 Tree-based classifiers

Supervised learning methods have been widely implemented in various engineering fields in the form of regression and classification algorithms, as mentioned earlier. Many classification algorithms can be employed to predict either binary-class or multi-class outputs. Decision trees are one of the algorithms that have been employed for various classification problems in recent decades (**Mangalathu and Jeon, 2018, Mangalathu and Jeon, 2019**). The decision tree recursively splits the dataset into several smaller subsets. Each decision tree is composed of a root node that contains all the data, a group of internal nodes called splits for decision making in feature space, and a group of terminal nodes called leaves for the final decision (**Figure 45**). Using a decision tree classification algorithm, a dataset is classified by subdividing it in a sequential manner based on the decision criteria defined by the tree. Consequently, each observation in the dataset is assigned with a class label according to the corresponding leaf node (**Friedl and Brodley, 1997**). Furthermore, the capability of the decision tree algorithm

in modelling complex problems is improved by the emergence of tree-based ensemble methods (Quinlan, 2006, Breiman, 1996, Breiman et al., 1984, Liaw and Wiener, 2002). Boosting and bagging are the major ensemble methods used for classification and regression problems. Each ensemble method is composed of several single decision trees as multiple predictors that are aggregated to obtain the final output. More details on the bagging and boosting ensembles can be found in (Breiman, 1996, Breiman et al., 1984, Liaw and Wiener, 2002). Various well-known ensembled algorithms, such as random forest (RF), extra trees (ET), and gradient boosting (GB) have been utilized in different engineering problems. In this study, RF, ET, and GB classifiers are used to model the RCP joint performance for infiltration.

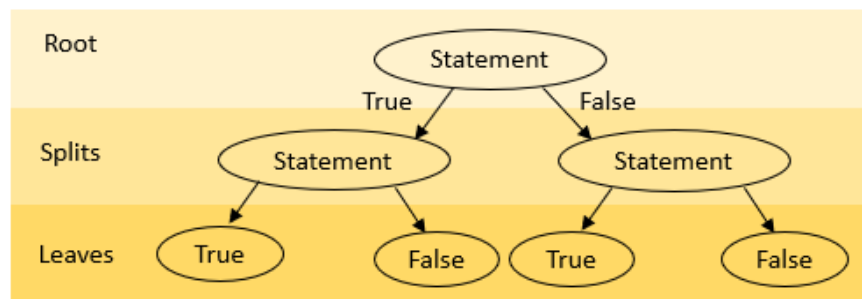


**Figure 45: Decision Tree Scheme.**

### 7.2.1.1 Random Forest Classifiers (RFC)

RFC is among the most promising and powerful ensemble models even for high-dimensional or skewed classification problems. Random forest is an ensemble of decision trees considered as a robust classifier having several weaker classifiers (Rodriguez-Galiano et al., 2012). In other words, RFC is a combination of several single decision tree classifiers with one vote to predict the class of each input observation. Accordingly, every single classifier is created considering a random vector that is independently driven from the input vector. Bootstrap aggregation, i.e. bagging, is employed to enhance the performance of the weak learners by means of generating a group of classifiers. Using RFC, the training of each estimator is performed using a training subset sampled from the original training set in a random manner. Consequently, each estimator assigns a vote to classify the input vector (Breiman, 1996, Breiman et al., 1984, Liaw and Wiener, 2002, Rodriguez-Galiano et al., 2012, Azar et al., 2014).

### 7.2.1.2 Extra Trees Classifier (ETC)

The extra trees algorithm is a tree-based ensemble model that has recently been used for many classification and regression problems. The algorithm was proposed by **Geurts *et al.* (2006)** as a modified version of the random forest algorithm in which any single decision tree is trained based on a randomly selected subset of the data (**Geurts, 2006, John et al., 2015**). In contrast to the random forest, the training subset for each decision tree in the extra trees algorithm is not selected using the tree bagging method, and thus, all the decision trees in the ensemble are trained using the entire training dataset. Moreover, ETC selects the best feature and its associated value in a random manner to split the node. Therefore, the extra tree algorithm has a more robust performance in terms of avoiding overfitting (**Ahmad et al., 2018, Geurts, 2006**). More details on the algorithm and its performance can be found in **Ahmad et al. (2018), Geurts (2006), and John et al. (2015)**.

### 7.2.1.3 Gradient Boosted Classifier (GBC)

Gradient boosting (GB) is a tree-based machine learning algorithm that has demonstrated high efficiency and accuracy in many prediction problems such as binary and multi-class classification (**Ke et al., 2017, Torres-Barran, 2019, Liu et al., 2017**). GB is a boosting ensemble method in which weak predictors are combined iteratively. The boosting iterations are optimized according to the gradient descent method to result in a robust predictor (**Torres-Barran, 2019, Mason, 2000**).

## 7.2.2 Oversampling

Imbalanced datasets are often inevitable in real-world problems. Consequently, imbalanced classification problems have been emphatically addressed by data scientists in recent years. From a technical point of view, an imbalanced classification problem is formed based on a binary or multiclass dataset in which the size (i.e. number of observations) of one of the classes is significantly lower compared to the others. Yet, the minority class in the imbalanced dataset represents the desirable concept to predict in nearly all cases. In this study, the observation of leakage in the conducted tests is considered a minority class, leading to the collection of an



imbalanced dataset. The crucial issue associated with such classification problems is the likely biased prediction performance of the learning algorithm toward the majority class.

One prevalent approach to overcome the imbalanced nature of biased datasets is to resample them in the preprocessing stage (**Cordon et al., 2018**). The resampling can be conducted using either under-sampling, which is the elimination of some majority class observations, or oversampling in which new instances of the minority class are appended to the training dataset using oversampling methods. Oversampling is preferred for rebalancing data considering that no relevant example in the dataset is eliminated. Moreover, the concept represented by the minority class is reinforced after oversampling such that the trained model would not misclassify the minority observations. There have been a great number of oversampling methods proposed to mitigate imbalanced datasets. The basics of two popular methods are briefly discussed herein.

#### 2.4.1 K-Nearest Neighbours (KNN)

KNN is a non-linear technique that has been widely used for binary and multi-class classification problems owing to its simplicity and efficiency (Melhem and Cheng 2019). The number of observations to be considered for decision making, *i.e. the number of neighbours* is the most influential parameter in the algorithm that needs to be tuned. Indeed, the number of neighbours,  $k$ , demonstrates the complexity of the decision boundary between the classes (Varmuza 2014). The optimal number of neighbours is greatly dependent on the dataset; however, a large value of  $k$  mitigates the noise effect while making the classification boundaries more complicated.

#### 7.2.2.1 Synthetic Minority Over-sampling Technique (SMOTE)

*SMOTE* was first proposed by **Chawla et al. (2002)** as a state-of-the-art oversampling technique to mitigate the imbalanced nature of real-world datasets in classification problems. The key idea of this method was to oversample the minority class by means of generative data examples called “synthetic” rather than using the replacement method. They created the synthetic examples over the manner of operating in “feature space” instead of in “data space,”

which is referred to as an application-specific manner. In this procedure, each minority class observation is taken into account, and the synthetic samples are introduced over the line segments considering either any or all the  $k$  minority class nearest neighbours (**Chawla et al. 2002**). The number of  $k$  nearest neighbours are selected in a random manner based on the amount of the required oversampling, i.e. *proportion* (**Chawla et al. 2002**). Therefore, the proportion of the required synthetic data and the number of nearest neighbours are key parameters in the performance of the SMOTE method. More details on this method can be found in (**Chawla et al. 2002**).

#### 7.2.2.2 Density-Based SMOTE (DBSMOTE)

Bunkhumpornpat *et al.* (**2012**) introduced DBSMOTE to improve the performance of the SMOTE method. Over-generalization harmfully influence the SMOTE method since it blindly generalizes the oversampling over the minority class while the majority class is not considered. This is more highlighted in overlapping regions (**Bunkhumpornpat et al., 2012**). Using DBSMOTE, the new data are synthesized within a distance of the center of the cluster called *eps* (**Bunkhumpornpat et al., 2012, Wong et al., 2016**). Therefore, synthetic samples do not fall into the majority class. **Bunkhumpornpat et al. (2012)** reported that the DBSMOTE algorithm had better performance results compared to the SMOTE method.

### 7.3 Model Development

#### 7.3.1 Data Preparation

The dataset used for the modelling purpose is an exclusive comprehensive design-wise data collected by the author of this thesis from a real novel test facility, as mentioned earlier. The testing program included nine input parameters: pipe size, gasket model, gasket length, gasket mass, pressure, pressure duration, joint gap, and setup alignment. In total, 1338 pressure data points were collected. Therefore, the dataset used for ML models has nine input features along with a binary-class output. **Table 23** summarizes the data parameters used in this analysis. The pipe size captures a discrete value of the nominal pipe diameter size in millimetre. The gasket models capture five unique profiles of single offset gaskets commonly used by the industry.

Gasket length is the unstretched length being measured before the test. Gasket mass is a unit mass in gram per metre. The pressure is recorded in kilopascal. Duration is measured in a minute during which the pressure was maintained. For the 20-hour operational pressure test, the duration is recorded as 1200 minutes. The water level was measured in millimetre with respect to a datum. The internal diameter of the water supply connecting cylinder is 100 mm; hence, each millimetre reduction in the cylinder corresponds to 7853 mm<sup>3</sup> or 7.853 mL reduction. The joint gap is measured in millimetre and is taken as maximum during each test, where it usually occurs at maximum applied pressure. The data containing pressure at zero kPa when time is zero was removed from the dataset. In addition, the gasket model is identified by separating into fields with a Boolean option of 0 and 1 to identify its model.

**Table 23: Data Parameters for ML**

Parameters	Input / Output	Type	Unit
Pipe Nominal Size	Input	Value	mm
Gasket Model	Input	Boolean	1 / 0
Gasket Length	Input	Value	mm
Gasket Mass	Input	Value	gram / metre
Pressure	Input	Value	kPa
Duration	Input	Value	Minute
Water level	Input	Value	mm
Joint Gap	Input	Value	mm
Setup	Input	Option	1 / 2
Leakage	Output	Boolean	Yes / No

### 7.3.2 Data Statistical Distribution

Based on the known behaviour of rubber used as a jointing sealant illustrated in **Figure 46**, a smaller joint gap minimizes the annular space; thus, it maximizes the sealing potential. Conversely, a larger joint gap maximizes the annular space; thus, minimizes the sealing potential. The testing program consisted of 123 successful tests that collected a total of 1338 data points. The pressure level at ultimate capacity and the corresponding operating capacity is plotted in **Figure 47**. Using conventional regression analysis, the distribution showed significantly large variation with a coefficient of determinations,  $R^2$ , equal to 0.072 and 0.081 from the linear (**Eq. 8**) and logarithmic regression (**Eq. 9**), respectively. The reason for using logarithmic regression is that when the rubber is under a completely confined condition, the sealing pressure is way beyond the testing range. This is due to the fact that the confined space

allows the rubber to develop viscoelastic behaviour where the same amount of deformation requires an incremental amount of applied pressure. The linear regression is also being used for comparison purposes.  $R^2$  is calculated by subtracting from a value of one the ratio between the sum of the square of regression error and the sum of the square of total error (**Eq. 10**). These coefficients indicate that two variables: pressure and joint gap, were poorly related and close to independence. The upper and lower 95% confidence level presented a gradual decline at a rate of 25 kPa and 10 kPa per millimetre joint gap increase. The linear and logarithmic trendlines, and the 95% upper and lower confidence levels are plotted in **Figure 47**.

$$\text{Eq. 8} \quad y = mx + b$$

$$\text{Eq. 9} \quad y = m \ln(x) + b$$

where  $y$  – output value,  $x$  – input value,  $m$  – slope,  $b$  – constant

$$\text{Eq. 10} \quad R^2 = 1 - \frac{\sum(y_i - \hat{y})^2}{\sum(y_i - \bar{y})^2}$$

where  $R^2$  – the coefficient of determination,  $y_i$  – output value,  $\hat{y} = f(x_i)$  fitted output value,  $\bar{y} = \frac{\sum y_i}{n}$  – mean output value

The coefficients of determination for linear and logarithmic regression were very small, indicating that the joint pressure capacity and joint gap do not have a clear relationship. By grouping and categorizing the data based on data parameters, the coefficients of determination were substantially increased. In the case of the dataset with various joint gaps under offset alignment for Gasket Model T07, the coefficient of determinations was higher = 0.77, indicating that the hydrostatic performance of the gasket profile under that setup and duration was predictable.

**Table 24** summarizes the coefficients of determination for linear and logarithmic regression analysis. The order of variables introduced is based on the parameters known to be most impactful on the outcome. **Figure 48** plots the coefficients against the number of variables, which shows an increase in predictability with an increase in the number of variables. In conclusion, traditional regression models were unable to predict the performance boundary due to multi-variables that influence the output. Machine learning could yield a better method of analysis by utilizing all the data, including both success and failure conditions. The classification models were thus more suitable to determine the performance boundary.

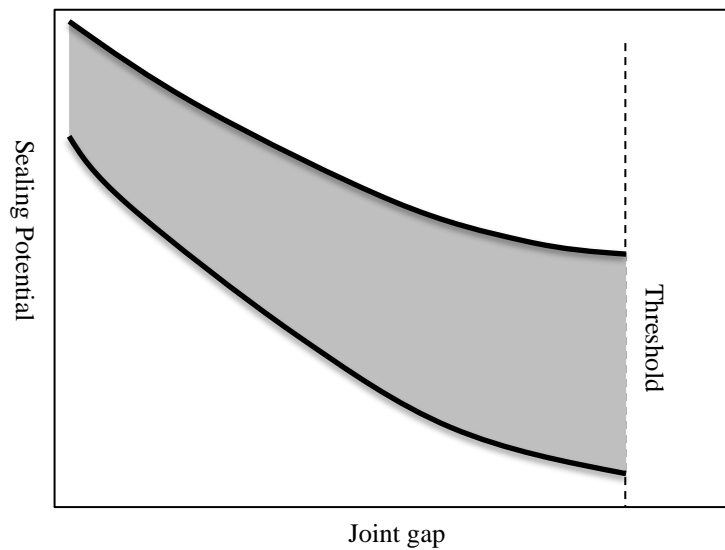


**Figure 46: Behaviour of Rubber used as RCP Joint Sealant.**

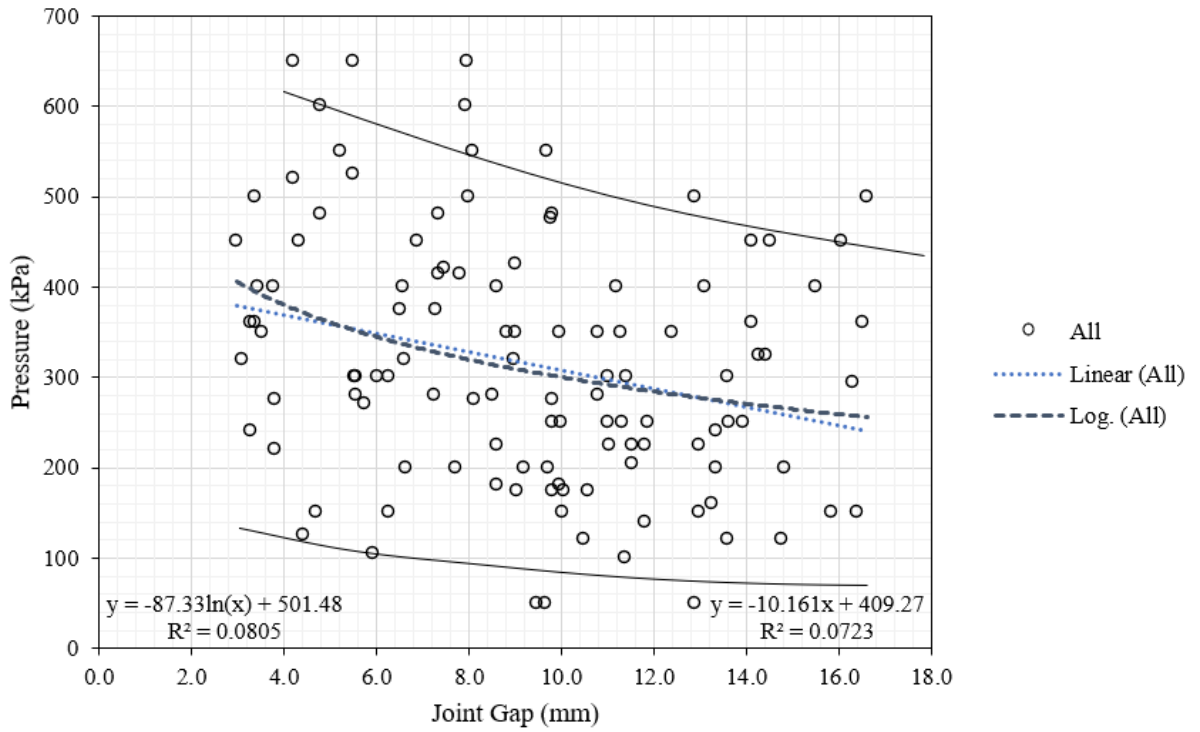


**Figure 47: Statistical Distribution and Trends of RCP Infiltration Test Results.**

**Table 24: The Summary of Coefficient of Determination from the Regression Analysis**

No. of Variables	Variables	Number of Data Point	Linear Regression	Logarithmic Regression
1	Joint Gap	113	0.0723	0.0805
2	Joint Gap, Aligned	67	0.107	0.118
	Joint Gap, Offset	46	0.041	
3	Joint Gap, Aligned, Ultimate	41	0.148	0.156
	Joint Gap, Aligned, Operating	26	0.092	
	Joint Gap, Offset, Ultimate	26	0.055	
	Joint Gap, Offset, Operating	20	0.071	
4	Joint Gap, Aligned, Ultimate, T06	10	0.367	0.402
	Joint Gap, Aligned, Ultimate, T07	7	0.482	
	Joint Gap, Aligned, Ultimate, T02	12	0.339	
	Joint Gap, Aligned, Ultimate, T03	12	0.037	
	Joint Gap, Aligned, Operating, T06	6	0.298	
	Joint Gap, Aligned, Operating, T07	5	0.585	
	Joint Gap, Aligned, Operating, T02	10	0.376	
	Joint Gap, Aligned, Operating, T03	4	0.630	
	Joint Gap, Offset, Ultimate, T06	9	0.006	
	Joint Gap, Offset, Ultimate, T07	4	0.612	
	Joint Gap, Offset, Ultimate, T02	8	0.084	
	Joint Gap, Offset, Ultimate, T03	4	0.032	
	Joint Gap, Offset, Operating, T06	6	0.028	
	Joint Gap, Offset, Operating, T07	5	0.421	
	Joint Gap, Offset, Operating, T02	8	0.143	

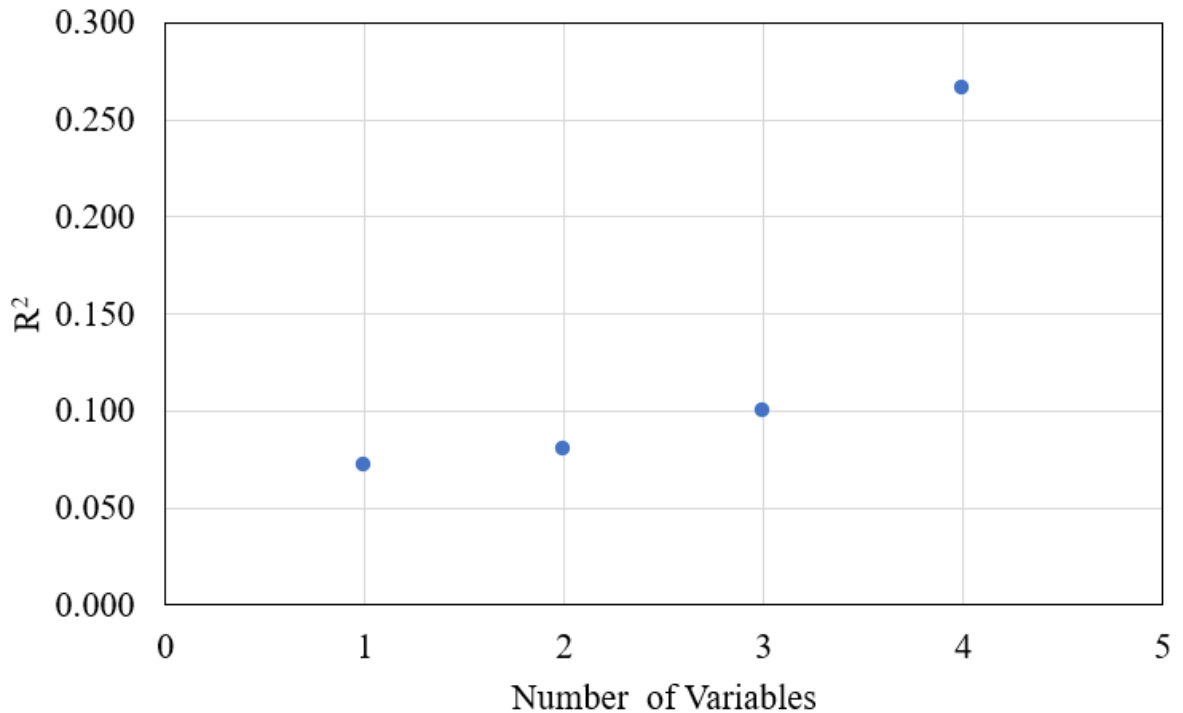


**Figure 48: Regression Analysis.**

### 7.3.3 Machine Learning Model

A classification model framework (**Figure 49**) was developed to predict leakage of the pipe setup using the dataset explained earlier. For this purpose, three different ML algorithms were initially applied to the imbalanced original dataset, including random forest classifiers (RFC), extra trees classifier (ETC), and gradient boosting classifier (GBC). Each model was tuned to acquire the best performance while avoiding potential overfitting. 80% of the dataset was used for model training, known as original training data; and 20% was used for model testing, known as original testing data. The performance of each model on the original testing data was evaluated using well-known classification metrics introduced below. `RandomizedSearchCV` from `scikit-learn` in Python, along with 5-Fold cross-validation, were implemented to tune the most influential hyperparameters of the aforementioned algorithms (**Pedregosa et al., 2011**). Subsequently, oversampling methods were implemented to mitigate the biased trend in the dataset and avert overfitting in the classifiers.

Among the tuned models, the best model achieved using the original testing data was selected for the oversampling step. Due to the imbalanced number of classes in the dataset, two oversampling methods: SMOTE and DBSMOTE, were applied to the training dataset to avoid misclassification of the minority class. The oversampled datasets are called SMOTE data and DBSMOTE data, respectively. These data were randomly split into 80% for training and 20% for testing, known as SMOTE training and testing data, as well as DBSMOTE training and testing data, respectively. For this purpose, the `smote-variants` package in Python was implemented. Kovács (2019) developed the `smote-variants` package using 85 different minority oversampling methods proposed in the literature. In this study, SMOTE and DBSMOTE were utilized, as explained earlier. Furthermore, to prevent the biased performance of the model toward any classes after oversampling, the parameters of each method were tuned so as to maintain the most desirable accuracy of prediction using the original testing data. The prediction accuracy of the models after implementing each oversampling algorithm on the original testing data was evaluated using different classification metrics further explained below.



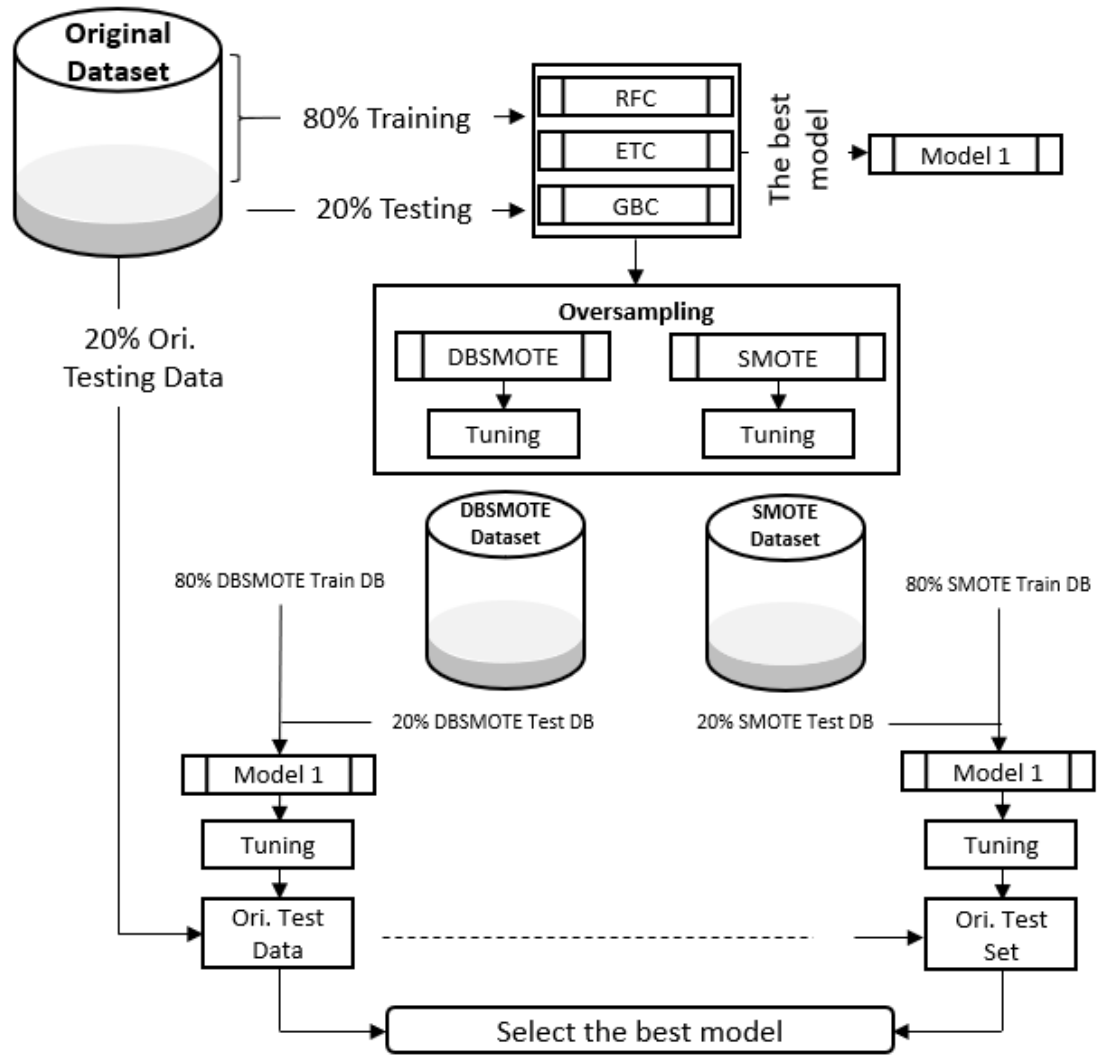


**Figure 49: Classification ML Model Framework for RCP Joint Performance Data.**

### 7.3.4 Classification Performance

The evaluation of classification algorithms is a crucial stage in the development of predictive models using different classifiers. The purpose of an ML classifier model is to learn using training data so that it can predict the class label for new unseen data, called testing data (Tharwat, 2018). A confusion matrix is a preliminary metric to evaluate the predictive performance of a predictive classifier. In a binary classification model, assume  $P$  for positive class and  $N$  for negative class. The confusion matrix presents the four possible outputs after the prediction, as shown in **Figure 50**. The blue cells in the matrix indicate correct predictions for both classes, *i.e.* *True Positive and True Negative*, while the red cells represent false

predictions. If the output of the observation is positive, and it is predicted as positive (correctly classified observation), it is considered as a *true positive (TP)*. If it is misclassified as negative, it is counted as *false negative (FN)*. By the same token, if the example is negative and correctly predicted as negative, it is *true negative (TN)*; if it is negative and misclassified as positive, it is regarded as *false positive (FP)*. The confusion matrix is the basis for the calculation of many classification metrics (**Tharwat, 2018**). Accuracy, precision, and recall are among the most widely used measures to assess the performance of classification models. These three metrics can be calculated using the following equations (**Tharwat, 2018, Sokolova et al., 2006**):

<b>Actual Class</b>	No Leak (-)	Leak (+)
	No Leak (-)	Leak (+)
No Leak (-)	<b>TN – True Negative</b> <i>Correctly predicted no leak</i>	<b>FP – False Positive</b> <i>Predicted leak But it did not leak</i>
Leak (+)	<b>FN – False Negative</b> <i>Predicted no leak, but it leaked</i>	<b>TP – True Positive</b> <i>Correctly predicted leak</i>
	<b>No Leak (-)</b>	<b>Leak (+)</b>
	<b>Predicted Class</b>	

**Figure 50: Confusion Matrix.**

**Eq. 11:** 
$$Accuracy = \frac{TP+TN}{TP+TN+FP+FN}$$

**Eq. 12:** 
$$Precision = \frac{TP}{TP+FP}$$

**Eq. 13:** 
$$Recall = \frac{TP}{TP+FN}$$

According to Tharwat (2018), all of the aforementioned metrics can be used to evaluate the performance of imbalanced classification problems. However, some other measures have proven to be beneficial in assessing classifiers.  $F_1$  – score is a metric that demonstrates the harmonic mean of precision and recall (**Tharwat, 2018, Sokolova et. al., 2006**).  $F_1$  – score can be calculated using **Eq. 14**. The score can vary from zero to one, with one indicating the supreme performance.

$$\text{Eq. 14} \quad F_1 = 2 \times \frac{\text{Precision} \times \text{Recall}}{\text{Precision} + \text{Recall}} = \frac{TP}{TP + 0.5FN + 0.5FP}$$

Two other important metrics for evaluating classification models are sensitivity metrics, i.e. true-positive rate (*TPR*) and false-positive rate (*FPR*). *TPR* indicates the ratio of the positive samples that are classified correctly to the total number of positive examples. Similarly, *FPR* denotes the ratio of negative examples classified incorrectly to the total negative observations (Tharwat, 2018). Accordingly, they can be calculated using Eq. 15 and Eq. 16.

$$\text{Eq. 15} \quad TPR = \frac{TP}{TP + FN}$$

$$\text{Eq. 16} \quad FPR = \frac{FP}{FP + TN}$$

*TPR* and *FPR* are generally used to create a useful graphical metric called receiver operating characteristic (*ROC*) curve (Figure 51). This graph plots the *TPR* (y-axis) versus *FPR* (x-axis) by changing the prediction thresholds in the feature spaces. It correspondingly has four important points. Point 1 (0,0) in the lower-left corner of the curve shows that there is no positive classification in the classifier, while all negative examples are predicted correctly. In other words, both *TPR* and *FPR* are zero at point 1. Similarly, Point 2 (0,1) in the top left corner of the graph indicates the best performance of the classifier, where all positive and negative observations are classified correctly. Point 3 (1, 0) in the bottom right corner indicates the worst performance of the classifier, where all positive and negative observations are classified incorrectly. Lastly, Point 4 (1,1) in the top right corner indicates that there is no negative classification in the classifier, while all positive examples are predicted correctly. Using the *ROC* curve, any classifier that lies within the upper left space of the graph has a better performance compared to those located at the lower right domain of the graph (Tharwat, 2018). A very important metric to quantify the *ROC* curve for a better understanding of the classifiers' performance is the area under the *ROC* curve, known as *AUC*. This score is always between 0 and 1, while the ideal performance occurs at *AUC*=1. Figure 51 illustrates a schematic *ROC* curve along with its important points. Curve *B* has a higher *AUC* than Curve *A*, thus has better performance. More details on the evaluation criteria for classification algorithms can be found in (Tharwat, 2018). `YellowBrick` package in python was employed to plot the results reported herein (Bengfort, 2019).

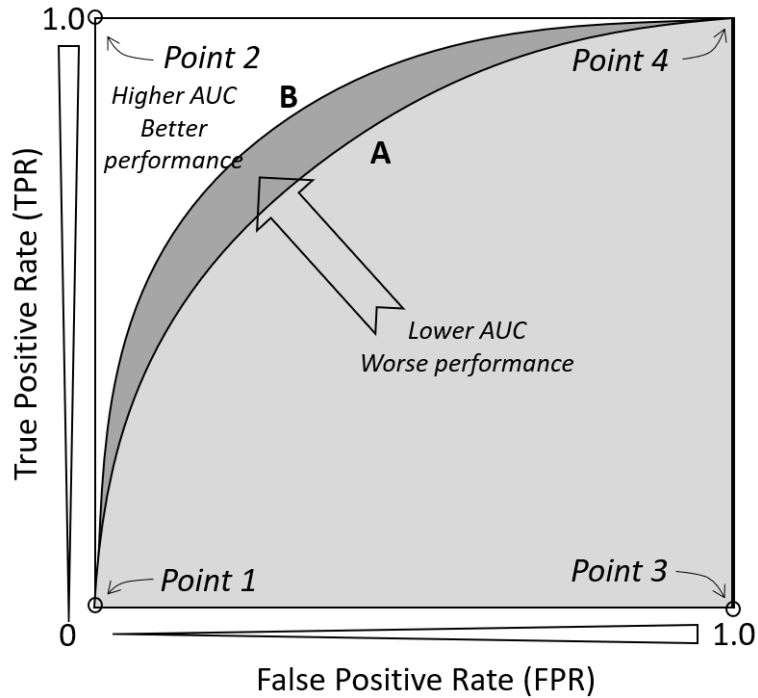


**Figure 51: Scheme ROC Curve.**

## 7.4 Results and Discussions

### 7.4.1 General

The prediction performance of different classification models explained earlier was first evaluated. The best classification algorithm was distinguished using the original dataset. Subsequently, the oversampling techniques were applied to the original training dataset based on the framework presented in **Figure 49**, and the performance of the best classification model was measured to achieve the best model for further studies using the original testing data.

### 7.4.2 Performance of Tree-based Models Before Oversampling

To evaluate the predictive performance of the three tree-based ensemble models, different classification metrics discussed earlier were used to assess the performance of each model applied to the original dataset. **Figure 52** (a), (b) and (c) show the classification reports for the *RFC*, *ETC*, and *GBC* models, respectively, using original training data without resampling,

including precision, recall and *FI-score* for both classes of “Leakage” and “No Leakage.” These classifiers reported excellent performance in learning the “No leakage” cases. In the case of ETC, the false positive was zero, indicating that no error was made in predicting the “No leakage” cases, leading to 100% precision. However, the recall shows the lowest value among all classifiers, indicating that the ability to detect “Leakage” was only 42.9%. It is important to accurately detect leakage, therefore among the classifiers, GBC performed the best and was thus used for further development.

In evaluating the classifiers using the original testing data, as shown in **Figure 53** (a), (b), and (c) for RFC, ETC, and GBC respectively, all models demonstrated robust performance in predicting the “No Leakage” class, whilst they had a poor performance in predicting the “Leakage” class. This can also be visualized in **Figure 54**. This performance was due to the imbalanced nature of the dataset. Indeed, the original dataset was biased towards the “No Leakage” class, and thus, the models were overfitted in predicting the “No Leakage” class. This trend is better distinguishable in confusion matrices of the models. As mentioned earlier, 20% of the dataset, i.e. 146 instances, was allocated for testing, which was called original testing data. Among these, only ten observations were labelled with the “Leakage” class. According to the confusion matrices, the *RFC* and *ETC* models predicted only 3 and 1 examples correctly, respectively, while *GBC* predicted 5 data observations correctly. Therefore, the models were not capable of predicting the leakage of the pipelines accurately. However, the *GBC* model exhibited better performance compared to the *RFC* and *ETC* models. It should be noted that the confusion matrix is more rationale for evaluating the performance of classifiers due to the imbalanced dataset. Moreover, the results reported in **Figure 53** (a), (b), and (c) are from tuned models. Tuning was carried out using the `RandomizedSearchCV` package with 5-fold cross-validation, as mentioned earlier. The *AUC* was monitored as the evaluation metric. **Table 25** presents the best values for each model after tuning.

(a) RFC

L	0.900	0.551	0.684
NL	0.960	0.994	0.977
	P	R	F

True Class	NL	529	3
	L	22	27
		NL	L

*Predicted Class*

(b) ETC

L	1.000	0.429	0.600
NL	0.950	1.000	0.974
	P	R	F

True Class	NL	532	0
	L	28	21
		NL	L

*Predicted Class*

(c) GBC

L	0.789	0.612	0.690
NL	0.965	0.985	0.975
	P	R	F

True Class	NL	524	8
	L	19	30
		NL	L

*Predicted Class*

(d) GBC-SMOTE

L	0.940	0.832	0.883
NL	0.957	0.986	0.971
	P	R	F

True Class	NL	422	6
	L	19	94
		NL	L

*Predicted Class*

(e) GBC-DBSMOTE

L	0.994	0.956	0.974
NL	0.967	0.995	0.981
	P	R	F

True Class	NL	433	2
	L	15	323
		NL	L

*Predicted Class*

**Figure 52: Classification Report and Confusion Matrix from: (a), (b) and (c) Original Training Data; (d) SMOTE Training Data; and (e) DBSMOTE Training Data**

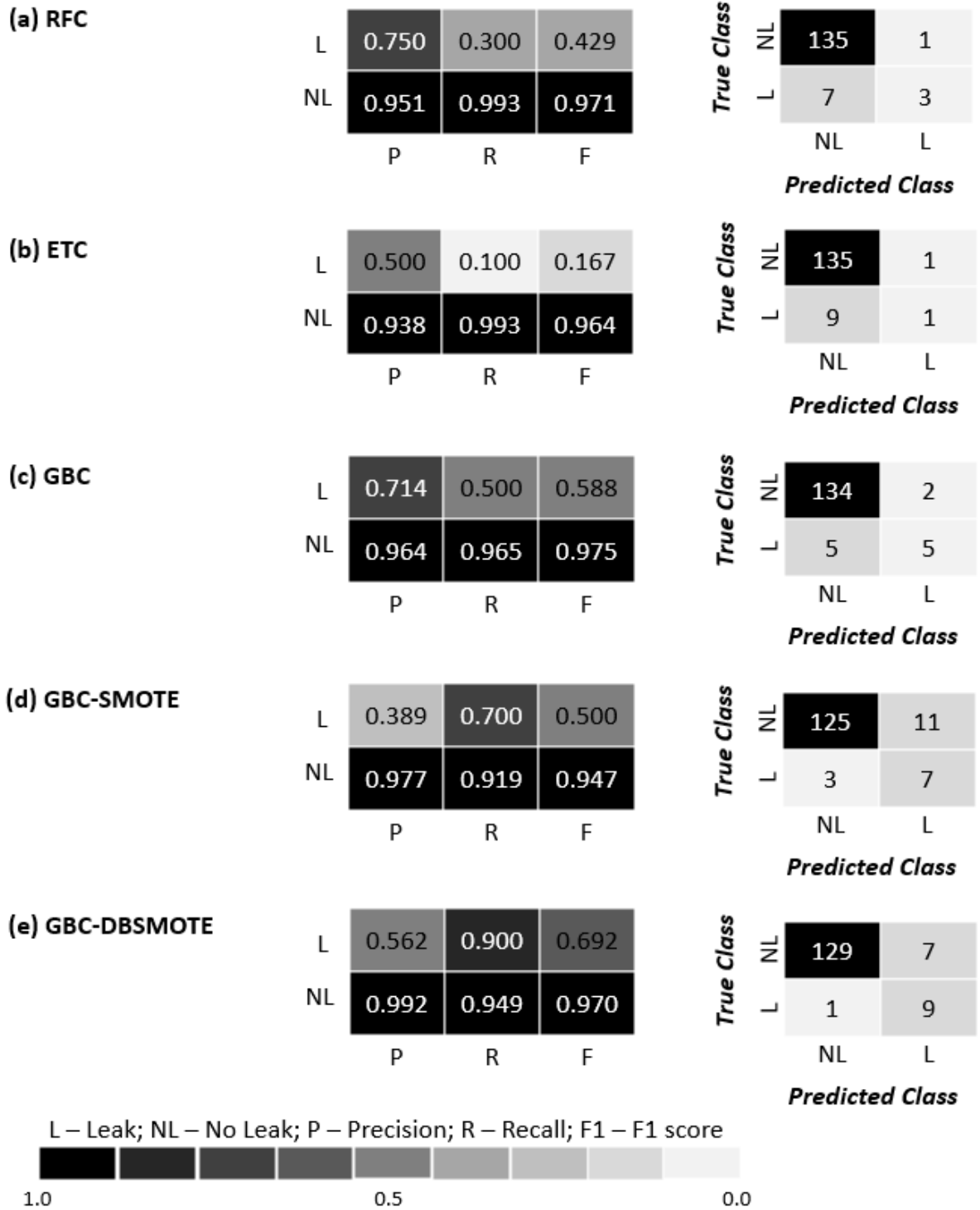
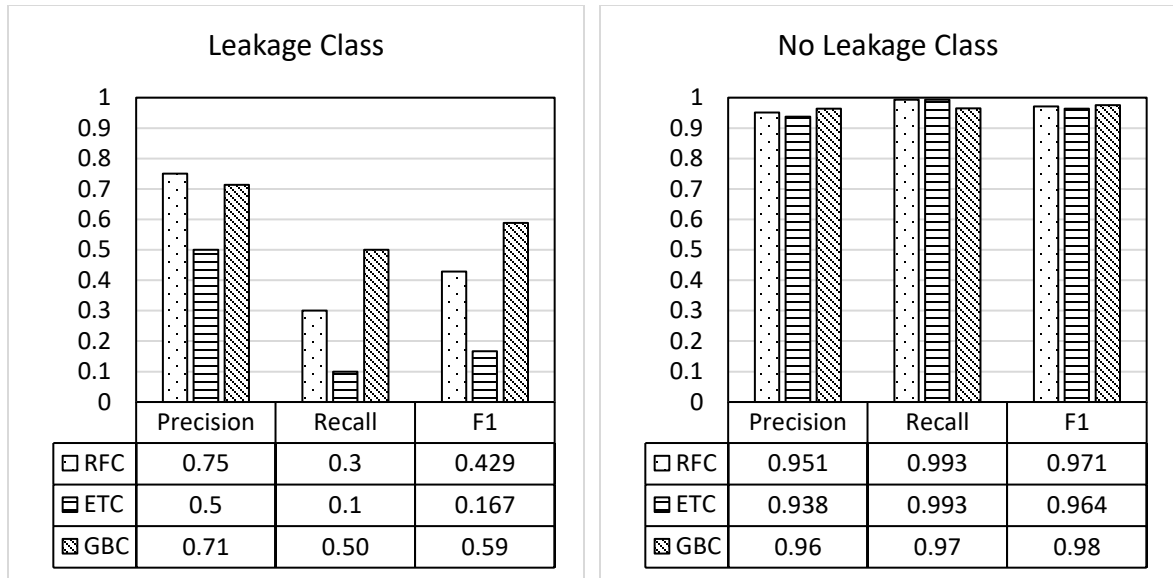


Figure 53: Classification Report and Confusion Matrix from the Original Testing Data



**Figure 54: Performance Comparison Among Tree-based Classifiers on Testing Data**

**Table 25: Hyperparameters for Tuning ML Learning Models**

Model	RFC	ETC	GBC
n_estimator	100	100	245
learning_rate			0.35
max_depth	6	8	1
min_samples_split	9	10	27
min_samples_leaf	1	1	19
subsample			0.37
max_features	8	9	9

### 7.4.3 Oversampling Methods

To overcome the imbalanced feature of the dataset, oversampling techniques were employed to generate synthetic data points belonging to the minority class, i.e. “Leakage.” For this purpose, the *SMOTE* and *DBSMOTE* oversampling methods were applied to mitigate the biased distribution of the data. **Figure 55** shows a comparison of the synthetic data created for the minority class between *SMOTE* and *DBSMOTE*. The percentage of the minority class was increased from 8.4% to 21% and 45% of total data using the *SMOTE* and *DBSMOTE* approaches, respectively. *GBC* found earlier to have better prediction accuracy was used for modelling using the oversampled training dataset. Purposefully, the parameters of each



oversampling method were tuned to acquire the highest performance in terms of accuracy and *AUC*. Furthermore, the *GBC* model was tuned again using the oversampled training dataset. Hence the results presented here are extracted from the tuned hybrid models to ensure the best predictive performance.

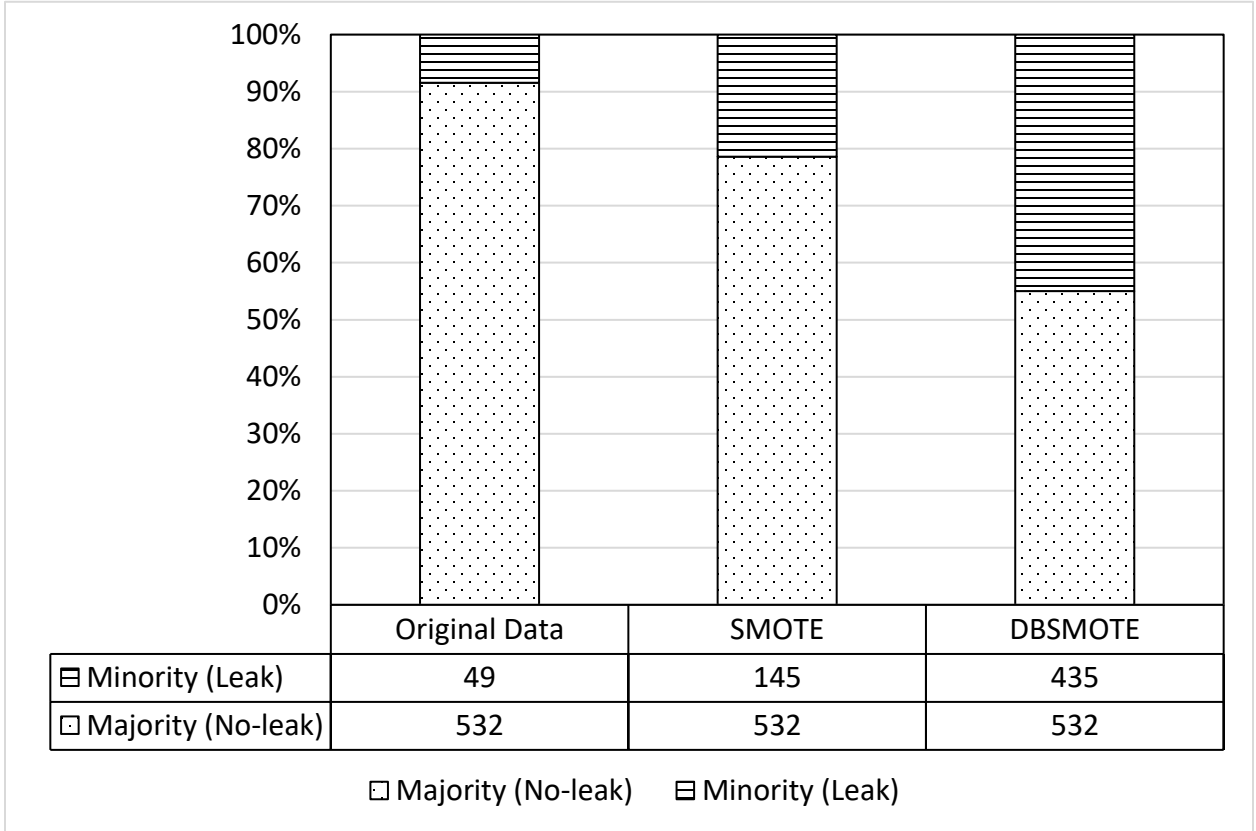


**Figure 55: Comparison of data counts between oversampling techniques**

#### 7.4.4 SMOTE

The predictive performance of the *GBC* model after oversampling was highly dependent on the parameters of the *SMOTE*, including `n_neighbors` and `proportion`. The high values of `proportion` resulted in many synthetic data points in the new dataset. Therefore, an excessive tendency towards the “Leakage” class could have emerged. Moreover, the high number of neighbours considered for generating new data points led to poor representation of the minority class. Accordingly, several models having different parameters were executed to achieve the best performance considering the classification metrics explained earlier.

**Figure 56** indicates the variation of accuracy and *AUC* of the *GBC-SMOTE* model with respect to the `n_neighbors` for both original testing data and the *SMOTE* testing dataset. The optimum values for `n_neighbors` and `proportion` for *SMOTE* were 7 and 0.2, respectively, as per a trial-and-error approach. It should be noted that the *AUC* score based on 5-fold cross-validation was monitored for obtaining the best values of the *SMOTE* parameters. **Figure 53 (d) (left)** displays the classification report of the *GBC-SMOTE* model for the original testing dataset. Accordingly, the precision for the “Leakage” class was reduced compared to the *GBC* model before oversampling, whilst the recall score was increased significantly. Regarding the definitions of the precision and recall explained earlier, the obtained trend demonstrated that the *GBC-SMOTE* was less overfitted towards the “No Leakage” class due to lower values of *TP*, *FN*, and *FP*, as shown in the confusion matrix (**Figure 53 (d) (right)**).

The original testing data used for the preparation of classification reports and confusion matrices of *GBC-SMOTE* and *GBC* models were equal. It can be observed in **Figure 53(c) and (d)** that the number of “Leakage” observations in the original testing data predicted correctly was increased from 5 to 7 in the *GBC-SMOTE* model compared to the *GBC*. This illustrates the less biased performance of the *GBC-SMOTE* model in predicting the “Leakage” class. Meanwhile, the accuracy of the model in predicting the “No Leakage” class was slightly decreased in the *GBC-SMOTE* model, as evidenced in classification reports and confusion matrices. Therefore, the *GBC-SMOTE* model was less overfitted and provided more reliable predictions. It is worth mentioning that the confusion matrix was the best metric for evaluating the predictive performance of each model since the original dataset was highly biased towards the majority class, and thus, models were extremely prone to overfitting.

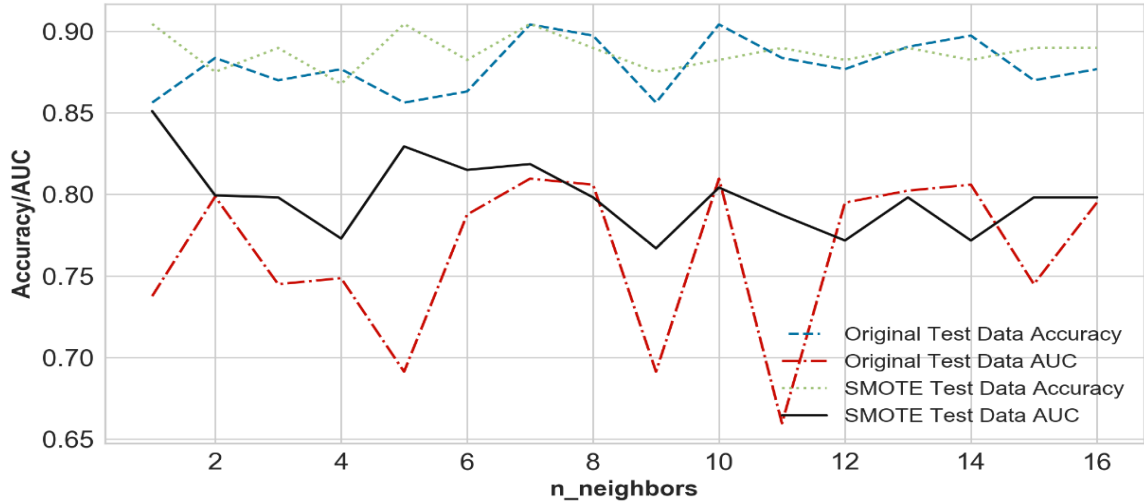


**Figure 56: Accuracy and AUC Comparison between Original Testing Data and Oversampled Data using SMOTE.**

#### 7.4.5 DBSMOTE

*DBSMOTE* is an improved version of the *SMOTE* method. Similar to *SMOTE*, the tuning of the *DBSMOTE* parameters has a noticeable effect on the predictive performance of the classification model. This method is available in the `smote-variants` package of Python and has tunable parameters, including `proportion`, `eps`, and `min_samples`. `eps` (maximum distance between two samples in the neighbourhood of each other) and `min_samples` (number of samples in the neighbourhood of the core point). After several trials, the optimum values for `proportion`, `eps`, and `min_samples` were found to be 0.8, 0.1, and 3, respectively. **Figure 57** and **Figure 58** display changes of the *AUC* and accuracy of the *GBC-DBSMOTE* model with respect to `eps` and `min_samples`, respectively. With the increase in the values of `eps` and `min_samples`, both accuracy and *AUC* of the model considering the original testing data decreased. Meanwhile, the *AUC* and accuracy of the model increased for the case of the *DBSMOTE* testing dataset. Such performance demonstrates that high values of these two parameters could lead to model overfitting towards the synthetic data. However, owing to the density-based generation of synthetic data in the most suitable places, it is possible to generate a higher proportion of data representing the minority class.

The classification report of the *GBC-DBSMOTE* model over the original testing data is indicated in **Figure 53 (e) (left)**. Accordingly, the *GBC-DBSMOTE* model had superior

prediction performance compared to that of *GBC* and *GBC-SMOTE* considering precision, recall, and *F1-score* metrics. Moreover, among 136 and 10 “No Leakage” and “Leakage” observations in the original testing data, 129 and 9 were predicted correctly by the *GBC-DBSMOTE* model, respectively, as shown in the confusion matrix (**Figure 53 (e) (right)**). Therefore, the *GBC-DBSMOTE* model achieved less biased predictions using the original testing dataset. As mentioned earlier, the developed models were tuned again after oversampling, and **Table 26** presents the tuned hyperparameters of the *GBC-SMOTE* and *GBC-DBSMOTE* models using the oversampled training dataset.

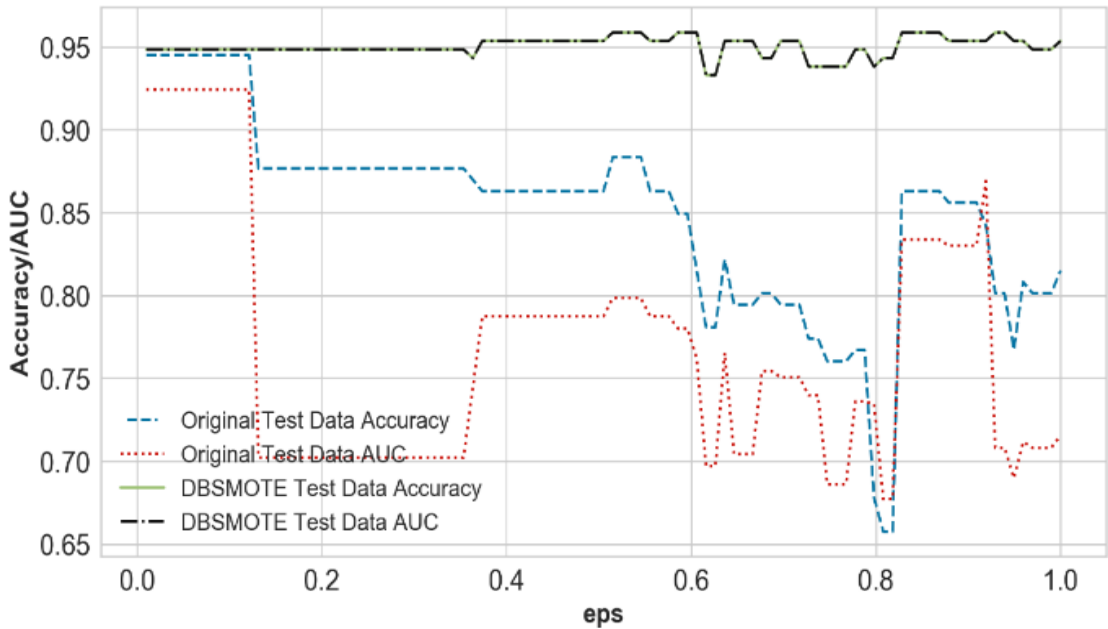


**Figure 57: Accuracy Measurements Against eps Using DBSMOTE.**

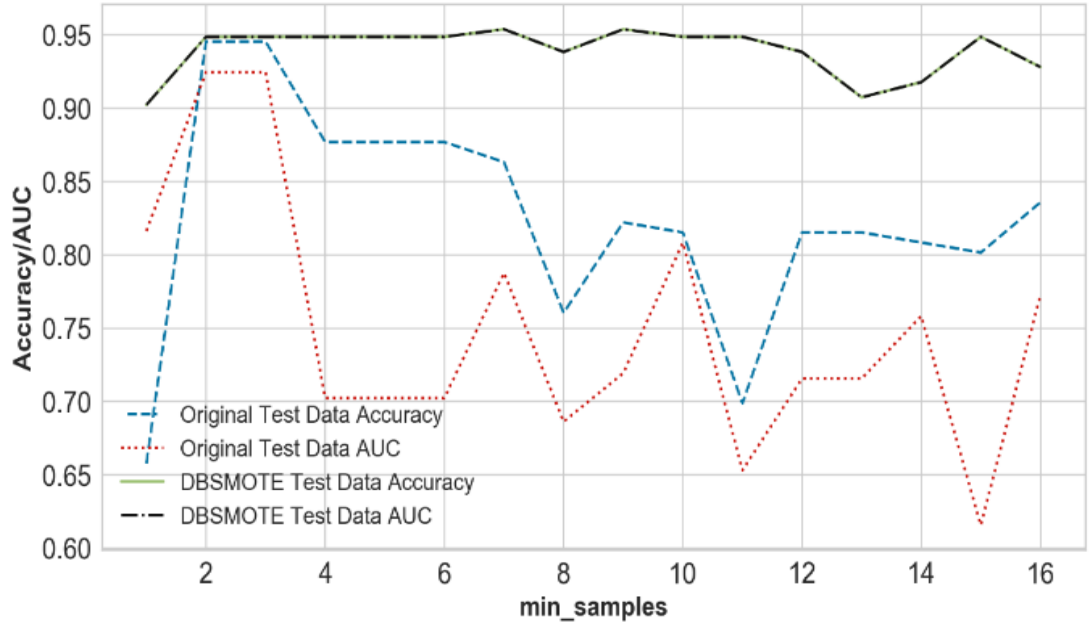


**Figure 58: Accuracy Measurements Against min\_samples Using DBSMOTE.**

**Table 26: Hyperparameters for Tuning SMOTE and DBSMOTE Models**

Model	GBC-SMOTE	GBC-DBSMOTE
n_estimator	190	190
learning_rate	0.21	0.215
max_depth	1	1
min_samples_split	2	2
min_samples_leaf	1	10
subsample	0.68	0.74

#### 7.4.6 Comparison between different models

**Figure 59** shows the precision, recall, and *F1-score* comparison for the minority class along with the accuracy and AUC using gradient boosting classifiers trained by the original, SMOTE and DBSMOTE training data. Precision is not a good measure of imbalanced data because it is affected by the incorrectly predicted negative class, i.e. majority class. Recall, on the other hand, reflects the reality of the positive class because it only considers the positive class, i.e. minority class. Among these three models, GBC-DBSMOTE had a recall value of 0.9, and AUC had 0.92 and was the best performer in handling the leakage class.

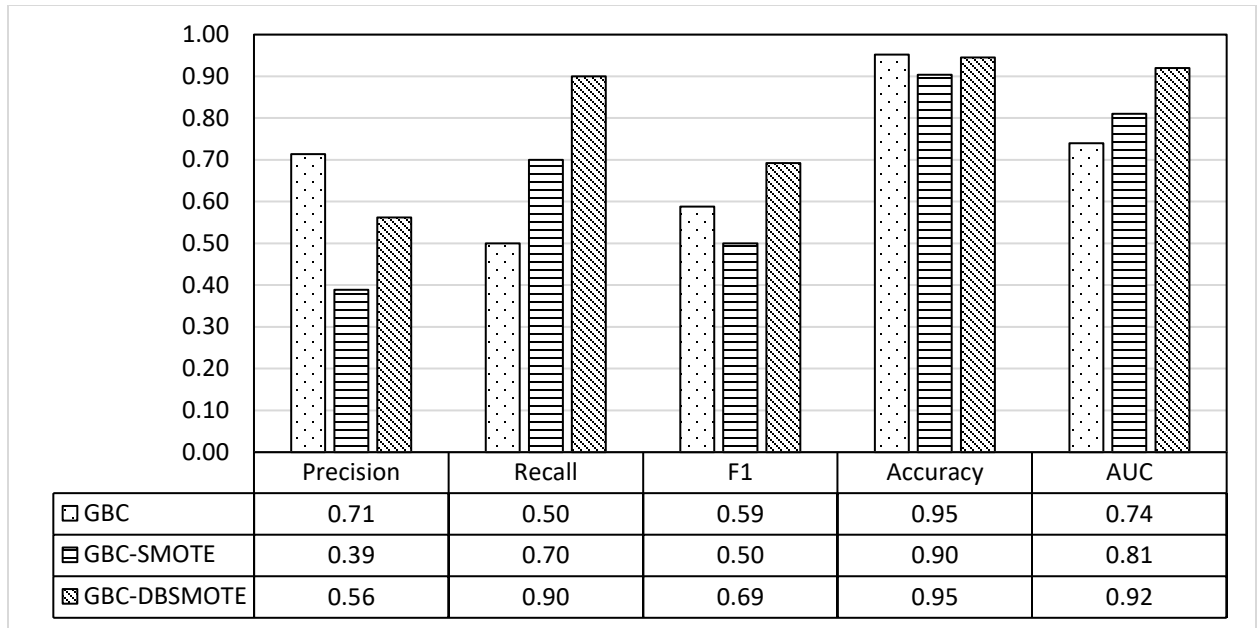


**Figure 59: Comparison of performance using gradient boosting classifiers trained by the original, SMOTE and DBSMOTE training data.**

To have a rational comparison between the predictive performance of the *GBC*, *GBC-SMOTE*, and *GBC-DBSMOTE* models considering various splits of the original dataset, the performance of each model was assessed using three different seeds of data split. **Table 27** presents the confusion matrix, accuracy, and *AUC* of each seed (i.e. data split) for all models developed herein. *GBC-DBSMOTE* demonstrated better performance in predicting the class of observations in the original testing data compared to *GBC* and *GBC-DBSMOTE*. Accordingly, the *GBC-DBSMOTE* was less overfitted towards any class of the dataset, whereas *GBC* was extremely overfitted towards the majority class, and *GBC-SMOTE* was slightly biased towards the synthetic minority class. It is noted that the accuracy of the models after oversampling is slightly lower compared to the *GBC* model, which indicates that it was overfitted. Thus, accuracy alone is not adequate to assess the predictive performance of the model. Nonetheless, the *AUC* of the models after oversampling was significantly improved in all cases of data split. Moreover, the superior performance of *GBC-DBSMOTE* was evident from the confusion matrices so that a high portion of the testing data examples were predicted correctly in all split cases.

**Table 27: The Confusion Matrix, Accuracy, And AUC using Various Splits of the Original Dataset**

Model	Case 1			Case 2			Case 3					
	Confusion matrix		Accuracy	AUC	Confusion matrix		Accuracy	AUC	Confusion matrix		Accuracy	AUC
GBC	134	2	95.21	0.74	135	5	92.47	0.65	132	1	93.15	0.65
	5	5			6	3			9	4		
GBC-SMOTE	125	11	90.41	0.81	118	19	85.62	0.82	81	52	63.7	0.77
	3	7			2	7			1	12		
GBC-DBSMOTE	129	7	94.52	0.92	125	12	90.41	0.85	122	11	90.41	0.84
	1	9			2	7			3	10		

### 7.4.7 Feature Importance

**Figure 60** exhibits the feature importance based on DBSMOTE. The feature importance evaluation is a technique to examine how useful the input features are impacting the output. The feature importance score plays an important role in providing insight on what to further investigate, feature selection and providing the basis for dimensional reduction. In the case of this research, joint gap, applied pressure, and gasket length are the three most impactful features, followed by pipe size and gasket mass. The water level and duration exhibit a lower impact on the output.

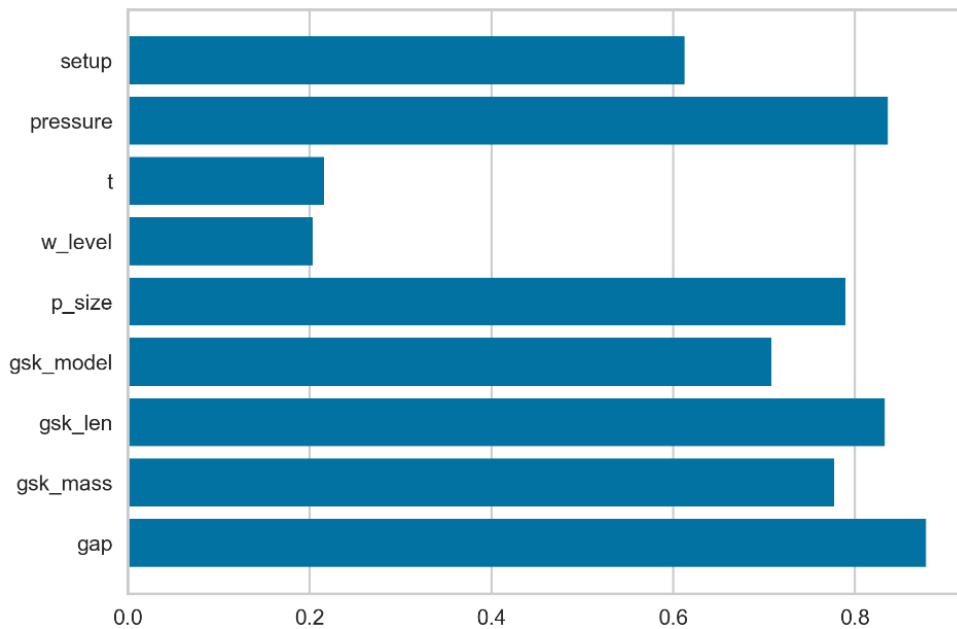


**Figure 60: Feature Importance Using DBSMOTE**

#### 7.4.8 Design Approach: Recommendations for Future Work

The exclusive and comprehensive data collected from the novel experimental procedure developed in this thesis captures the influential parameters in the design of RCP joints. The nonlinear relationship between different attributes of the data resulted in poor performance of conventional statistical methods for predicting the performance of various RCP joint configurations. Nevertheless, the proposed intelligent data-driven GBC-DBSMOTE model achieved high accuracy in predicting the failure of RCP joints. The model distinguished the most influential parameters in the design of joints in great agreement with experimental findings. As observed in real-world practice, the proposed intelligent model recognized the “pressure” and “joint gap” as the attributes having higher feature importance. This predictive tool is aimed to serve as a new guideline for designing durable RCP joints under *InI* condition. Using the hybrid model developed in this study, comprehensive design charts respecting various configurations, i.e. pipe size, gasket type, joint gap, etc., can be proposed. Moreover, design failure thresholds for different RCP configurations could be identified in future work. *InI* performance-based optimization of RCP joint configurations using the ML framework introduced here is a vital design step to be pursued in future work.

### 7.5 Summary

This chapter demonstrates the successful application of machine learning to model hydrostatic infiltration in reinforced concrete pipe joints where conventional regression analysis techniques have failed to produce reliable predictions given the complex inter-relationships of a multitude of input parameters. An exclusive experimental dataset was collected from a comprehensive test procedure containing 9 design-wise input features. Tree-based supervised machine learning techniques: *RFC*, *ETC* and *GBC* were deployed in this study. Considering that the experimental dataset was extremely imbalanced, two oversampling techniques, *SMOTE* and *DBSMOTE*, were adopted to mitigate the biased performance of classifiers. Accordingly, the conclusions below can be drawn from this study:



1. Among the different classifiers considered, *GBC* had the best predictive performance according to several classification metrics, including accuracy, recall, *F1-score*, and *AUC*.
2. After being turned, all the basic classifiers indicated overfitted performance towards the majority class in the dataset, i.e. “No Leakage,” due to the imbalanced dataset
3. The oversampling techniques mitigated the bias in the dataset and thus, improved the prediction performance.
4. *DBSMOTE* demonstrated better predictive performance compared to *SMOTE* according to various classification metrics, such as confusion matrix and *AUC*.
5. The tuning of the oversampling algorithms resulted in considerable improvement in their predictive performance.
6. Using *DBSMOTE*, more synthetic data could be appended to the dataset for training, i.e. higher values of proportion, without overfitting the dataset towards synthetic data compared to *SMOTE*.
7. The *GBC-DBSMOTE* hybrid model provided the most promising and reliable results over different splits of the original datasets compared to *GBC* and *GBC-SMOTE*.
8. The proposed hybrid model proved to be a reliable predictive tool for providing design guidelines for different pipe joint configurations.

In conclusion, this ML model framework developed in this Chapter could provide a foundation for developing design RCP joint hydrostatic performance charts against infiltration for various models of sealing gaskets, duration and level of pressure, pipe size and other influential input parameters, which should be pursued in further study.

## 7.6 References

- Ahmad, M. W., Reynolds, J., Rezgui, Y. “Predictive modelling for solar thermal energy systems: A comparison of support vector regression, random forest, extra trees and regression tree”, *Journal of Cleaner Production* Vol. 203, 2018, pp. 810-821.
- Azar, A. T., Elshazly, H. I., Hassanien, A. E., Elkorany, A. M. “A random forest classifier for lymph diseases”, *Computer Methods and Programs in Biomedicine*, Vol. 113, 2014, pp. 465-473.

- Bengfort, B., Billbro, R. “Yellowbrick: Visualizing the Scikit-Learn Model Selection Process”, *The Journal of Open Source Software*, Vol. 4, 2019, pp. 1075
- Breiman, L., “Bagging Predictors”, *Machine Learning*, Vol. 24, 1996, pp. 123-140.
- Breiman, L., Friedman, J. H., Olshen, R. A., Stone, C. J. ”Classification and Regression Trees”, Chapman & Hall/CRC, New York, NY, United State, 1984.
- Bunkhumpornpat, C., Sinapiromsaran, K., Lursinsap, C. “DBSMOTE: Density-Based Synthetic Minority Over-sampling Technique”, *Applied Intelligence*, Vol. 36, 2012, pp. 664-684.
- Cordon, I., Garcia, S., Fernandez, A., Herrera, F., “Imbalance: Oversampling algorithms for imbalanced classification in R”, *Knowledge-Based Systems*, Vol. 161, 2018, pp. 329-341.
- Chawla, N. V., Bowyer, K. W., Hall, L. O., Kegelmeyer, W. P., “Journal of Artificial Intelligence Research, Vol. 16 pp. 321-357, 2002.
- Friedl, M. A., Brodley, C. E., “Decision Tree Classification of Land Cover from Remotely Sensed Data”, Elsevier Science Inc., New York, NY, United State, 1997.
- Geurts, P., Ernst, D., Wehenkel, L., “Extremely randomized trees, *Machine Learning*, Vol. 63, 2006, pp. 3-42.
- John, V., Lui, Z., Guo, C., Mita, S., Kidono, K. “Real-time Lane Estimation Using Deep Features and Extra Trees Regression”, *Pacific-Rim Symposium 2015*, Auckland, New Zealand, November 25-27, 2015, pp. 721 – 733.
- Ke, G., Meng, Q., Finley, T., Wang, T., Chen, W., Ma, W., Te, Q., Liu, T. “LightGBM: A Highly Efficient Gradient Boosting Decision Tree”, *31<sup>st</sup> Conference on Neural Information Processing Systems*, Long Beach, CA, United State, 2017.
- Kim, H., Ahn, E., Shin, M., Sim, S. H. “Crack and Noncrack Classification from Concrete Surface Images Using Machine Learning”, *Structural Health Monitoring*, Vol. 18, Issue 3, 2019, pp 725-738.
- Koch, C., Georgieva, K., Kasireddy, V., Akinci, B., Fieguth, Paul., “A review on computer vision based defect detection and condition assessment of concrete and asphalt civil infrastructure”, *Advanced Engineering Informatics*, Vol. 29, 2015, pp. 196-210.
- Kovacs, G. “Somte-variants: A python implementation of 85 minority oversampling techniques”, *Neurocomputing*, Vol. 366, 2019, pp. 352-354.
- Liaw A., Wiener, M. “Classification and Regression by randomForest”, *R News*, Vol. 2/3, 2002, pp. 18-22.
- Liu, Y., Gu, Y., Nguyen, J. C., Li, H., Zhang, J., Gao, Y., Huang, Y., “Symptom severity classification with gradient tree boosting”, *Journal of Biomedical Informatics*, Vol. 75, 2017, pp. S105-S111.

- Mangalathu, S., Jeon, J. S. “Classification of failure mode and prediction of shear strength for reinforced concrete beam-column joints using machine learning techniques”, *Engineering Structures*, Vol. 160, 2018, pp. 85-94.
- Mangalathu, S., Jeon, J. S. “Machine Learning-Based Failure Mode Recognition of Circular Reinforced Concrete Bridge Columns: Comparative Study”, *American Society of Civil Engineering – Journal of Structural Engineering*, Reston, Virginia, United States, 2019.
- Mason, L., Baxter, J., Bartlett, P., Frean, M. “Boosting algorithms as gradient descent”, *Advances in Neural Information Processing Systems*, 12 512–518. MIT Press, Cambridge, MA. 2000, pp. 512- 518.
- Melhem, H. G., Cheng, Y. “Prediction of Remaining Service Life of Bridge Decks Using Machine Learning”, *American Society of Civil Engineering – Journal of Computing in Civil Engineering*, Reston, Virginia, United States, 2019.
- Nehdi, M., Chabib, H. E., Naggar, M. H. “Predicting Performance of Self-Compacting Concrete Mixtures Using Artificial Neural Networks”, *ACI Materials Journal*, September – October 2001 Issue, 2001, pp. 394 – 401.
- Pedregosa, F., Varoquaux, G., Gramfort, A., Michel, V., Thirion, B., Grisel, O., Blondel, M., Prettenhofer, P., Weiss, R., Dubourg, V., Vanderplas, J., Passos, A., Cournapeau, D., Brucher, M., Perrot, M., Duchesnay, E. “Scikit-learn: Machine Learning in Python”, *Journal of Machine Learning Research*, Vol. 12, 2011, pp. 2825-2830.
- Quinlan, J. R., “Bagging, Boosting, and C4.5”, University of Sydney, Australia, 2006.
- Rafiei, M. H., Adeli, H. “A novel machine learning-based algorithm to detect damage in high-rise building structures”, *Structural Design of Tall and Special Buildings*, Vol. 26, Issue 18, e1400, 2017.
- Reich, Y., “Machine Learning Techniques for Civil Engineering Problems”, *Microcomputers in Civil Engineering*, Vol. 12, Malden, MA, United States, 1997, pp. 295 – 310.
- Reich, Y., Barai, S. V. “Evaluating machine learning models for engineering problems”, *Artificial Intelligence in Engineering*, Vol. 13, 1999, pp. 257-272.
- Rodriguez-Galiano, V. F., Ghimire, B., Rogan, J., Chica-Olmo, M., Rigol-Sanchez, J. P. “An assessment of the effectiveness of a random forest classifier for land-cover classification, *ISPRS Journal of Photogrammetry and Remote Sensing*, Vol. 67, 2012, pp. 63-104.
- Sattar, A.M.A., Ertuğrul, Ö., Gharabaghi, B. *et al.* Extreme learning machine model for water network management. *Neural Comput & Applic* **31**, 2019, pp. 157–169.
- Sokolova, M., Japkowicz, N., Szpakowicz, S. “Beyond Accuracy, F-Score and ROC: A Family of Discriminant Measures for Performance Evaluation”, *LNAI Vol. 4304*, 2006, pp. 1015-1021.

- Tharwat, A. "Classification assessment methods", *Applied Computing and Informatics*, 2018, (In press).
- Torres-Barran, A., Alonso, A., Dorronsoro, J. R. "Regression tree ensembles for wind energy and solar radiation prediction", *Neurocomputing*, Vol. 326–327, 2019, pp. 151-160.
- Varmuza, K., Filzmoser, P., Hilchenbach, M., Kruger, H., Silen, J. "KNN classification – evaluated by repeated double cross validation: Recognition of minerals relevant for comet dust", *Chemometrics and Intelligent Laboratory Systems*, Vol. 138, 2014, pp. 67-71.
- Wong, S. C., Gatt, A., Stamatescu, V., McDonnell, M. D., "Understanding data augmentation for classification: when to wrap?", 2016 International Conference on Digital Image Computing: Techniques and Applications (DICTA), Institute of Electrical and Electronic Engineers, Gold Coast, QLD, Australia, 2016.
- Yaseen, Z. M., Deo, R. C., Hilal, A., Abd, A. M., Bueno, L. C., Salcedo-Sanz, S., Nehdi, M. L., "Predicting compressive strength of lightweight foamed concrete using extreme learning machine model", *Advances in Engineering Software*, Vol. 115, 2018, pp. 112-125.
- Zealand, C. M., Burn, D. H., Simonovic, S. P., "Short term streamflow forecasting using artificial neural networks", *Journal of Hydrology*, Vol. 214, 1999, pp. 32-48.
- Zhang, A., Wang, C. P., Li, B., Yang, E., Dai, X., Peng, Y., Fei, Y., Liu, Y., Li, J. Q., Chen, C., "Automated Pixel-level Pavement Crack Detection on 3D Asphalt Surfaces Using a Deep-Learning Network", *Computer-aided Civil and Infrastructure Engineering*, Vol. 32, 2017, pp. 805-819.

## CHAPTER 8

---

### 8 Summary, Conclusions and Recommendations

Sanitary sewage networks are key infrastructure assets in today's civilization. Undesirable inflow and infiltration (*InI*) into piped drinking and/or sewage flows mixed with flows from the natural environment can cause a huge financial burden to municipalities. *InI* is among the top challenges for municipalities and results primarily from stormwater percolating into the ground and finding its way into sanitary sewer systems. This tremendously escalates the operating costs of water treatment facilities. RCP, the most commonly used product in sewage systems, faces a challenge in dealing with *InI* since the quality of the pipe joint relies not just on the joint materials and design, but also on the installation quality.

Chapter 2 reviewed the deficiencies of existing standards in many places around the world, which generally do not proactively capture the infiltration risks. The state-of-the-art practice of manufacturers for testing the water tightness of reinforced concrete pipe does not provide useful results regarding performance under in-situ groundwater pressures. The true performance requirements for RCP joints are to resist the external hydrostatic pressures resulting from high groundwater tables. Combined with previous research efforts, the situation demands a simple method to evaluate the capacity of the RCP joint performance for infiltration.

Accordingly, a novel testing method was introduced in Chapter 3 to allow RCP manufacturers to conduct an in-factory test in a safe and efficient way. The testing apparatus, setup, and procedures were described in detail. A comprehensive testing program, presented in Chapter 4, using the new test, has collected hundreds of data points on the infiltration performance of RCP joints using existing joint designs and gasket materials.

Chapter 5 provided a comprehensive analysis of the testing data and reviewed the influence factors. Performance charts for those gaskets were developed in Chapter 6 from these data points. An illustrative case was used to connect the experimental data to a real-life case where a high groundwater table above the obvert of the pipe posed an infiltration potential. A safety factor can be derived from the performance chart providing quantified guidance in permissible joint gaps in the construction quality.

Furthermore, the novel experimental dataset is influenced by multiple nonlinear factors. Thus, several advanced machine learning (ML) techniques were used to create a rational predictive model. Those techniques, presented in Chapter 7, consist of Gradient Boosting with DBSMOTE, addressed the imbalanced data challenges and provided the best accuracy model.

## 8.1 Conclusions

Based on the research work reported in this thesis, the main emanating conclusions can be categorized into three parts: existing standards and literature, experimental developments, and ML modelling techniques as follows.

### 8.1.1 Existing Standards and Literature

Standard provisions for precast concrete pipe around the world regarding RCP hydrostatic performance evaluation do not provide a true evaluation of the joint performance against infiltration. There has been little effort to critically analyze the international experience gained in this field, to compare performance criteria, and to derive the best international practice guidelines. This effort has exposed various knowledge deficiencies along with deviations between the standards and the end-user expectations in terms of infiltration. There is a clear need for improvement to bridge the gap between true hydrostatic performance requirements and current testing procedures.

## 8.1.2 Experimental Development

This study developed a simple and safe method to examine the capacity of RCP joints for infiltration. Over 100 tests were conducted, and the test procedure was successfully repeated. The proposed test methodology is concluded to be able to provide consistent and reliable measurements, controls and outputs. Eight additional special tests were conducted with gasket and pipe samples beyond the ones selected for the research program. The results demonstrated that the procedure is able to accommodate a larger variation of the samples. These include precise pressure measurements, joint gap monitoring, and capture of water consumption values in the system during the test. Based on the experimental observations and findings, the following conclusions can be drawn:

1. Current pipe joint designs and gaskets used by industry can withstand significantly higher pressure than the commonly accepted pressure rating of 105 kPa (13 psi) as per CSA A257. With tighter and restrained joint gaps, experiments demonstrated the possibility of achieving 480 to 680 kPa against infiltration. The results of the current study indicated that, with better control of the joint gap during pipe installation, the joint would not be the weakest link of a drainage network.
2. Traditional pipe hydrostatic performance tests generally rely on visual inspection for leakage. In the current proposed test, a more rational approach is used where WSCC measures the volumetric water loss during the test. During testing, leakage was first detected by observing an increase in the water reduction rate. This eliminates guesswork and helps the operator focus on the quantitative aspects of the test.
3. The test results provided a relationship between the pressure and movement of the gasket. This revealed that the current design of the pipe joint is driven by providing better performance under existing standards. Such designs can be perceived as a reverse of what is actually needed to withstand the infiltration of groundwater. It also reflects a misunderstanding of the end-user expectations and incorrect assumption that the pipe joint design and gasket would perform equally regarding both exfiltration and infiltration.
4. The hydrostatic capacity of the RCP joint is predominantly influenced by the joint gap. In conventional hydrostatic testing, **CSA A257, ASTM C443, ASTM C1628, and BS**

**EN 1916** require the joint to remain watertight with a 13-mm deflection on one side. There is no maximum acceptable joint gap defined in these specifications. Accordingly, engineers expect similar performance under a 13-mm joint gap in the field. **ACPA (2009)** states that the manufacturer shall define the maximum allowable joint gap. However, there is no research in the open literature that relates actual hydrostatic performance to the joint gap. Hence, the results obtained in this research provide a trend showing that the capacity of the pipe joint to withstand infiltration pressure decreases as the joint gap increases.

5. Based on the findings, the maximum allowable joint gap should be a variable based on the type of the gasket, applied pressure, and the joint type. However, 13 mm can be an acceptance criterion for a target pressure defined in the specifications given that the pipe producers can demonstrate it using the infiltration test.
6. The ultimate infiltration pressure is a function of the influence ratio,  $I_g$ , the ratio of the mass of the gasket, to the effective annular space. The higher the influence ratio, the higher the infiltration pressure capacity the gasket can achieve.
7. High variations in the pressure-joint gap curve likely result from other factors such as the mechanical properties of the rubber gasket. Further studies on these factors are recommended.
8. The ultimate infiltration pressure is not sensitive to the pipe size given the same gasket profile and joint profile. However, larger size of the pipe will require different joint height and thickness for providing shear transfer, thus the gasket profile design varies based on the size of the pipe. The ultimate infiltration pressure may be affected with different gasket and joint profile.
9. The proposed 20-hour test provides evidence of the essential steps for evaluating the operating pressure when the pipe is placed in service. Gasket movement tends to stabilize in a longer duration compared to the conventional 10-minute test. The larger the joint gap, the more severe is the movement.
10. The new test method introduced in the current study demonstrated operational advantages, including a much higher level of safety compared to conventional pressure tests such as **ASTM C361 and AWWA C302** since only a limited amount of water is needed in the test. The minimum water volume required also shortens the filling time compared to conventional pressure tests.



11. In the new test, unlike existing exfiltration tests, failure does not pose safety hazards to the operator nor to anyone near the testing area. Moreover, the height of the pipe allows the operator to easily access the inside of the pipe for visual examination. Water level monitoring in the WSCC can be used to quantify the leak, unlike current tests that rely on qualitative assessment.
12. The hydrostatic behaviour of the RCP joint serves a critical function in drainage networks. By providing a method to evaluate the ability of the joint to withstand infiltration, the present study opens many possibilities for innovation and improvement to add value to RCP advantages, including strength, durability, sustainability, and resiliency.
13. The preliminary results benchmarked the hydrostatic performance of existing RCP joints and gasket designs. Hence, the proposed testing method can allow a better understanding of the relationship between joint hydrostatic performance and joint gap, with the potential to develop enhanced RCP installation guidelines. This would empower contractors to mitigate infiltration risks and make sounder decisions based on actual field conditions.
14. The discovery of the time-dependent gasket movement in the annular space can lead to improvements in existing single offset joints. In the subsequent phase of this research, additional parameters, including joint gap, joint offset, and various gasket and pipe materials, will be considered to make a more reliable evaluation.
15. The eight additional tests conducted beyond the original scope evaluated 675 mm, 750 mm and 1800 mm RCP, wedged profile gasket, and lined pipes. The test method was found suitable to cover a wide variety of different pipe joints, pipe types, and gasket types.
16. The spacer ring and lateral hydraulic jack added to the originally developed test method can reasonably simulate field conditions and installation quality. The hydrostatic performance under various joint gaps and joint offsets can be quantified using this method.
17. The study effectively relates the material behaviour of RCP joint and field conditions, such that an assessment factor can be suggested for a rational engineering decision process.

18. There are some differences in the sealing potential predictions between material tests and infiltration tests. The material tests do not reflect the real sealing potential scale; indeed, comparison tests indicated that their results might be biased. The pressure reduction was faster in the infiltration test with an increased joint gap than that in the material testing. This is due to the different loading schemes in those tests.
19. The gasket height influences the hydrostatic performance. It affects the infiltration test more than it does for the material load test. The effect was more severe when the joint gap increased.
20. The infiltration performance of the gasket agrees with the prediction derived from the gasket geometry. However, the prediction of the sealing potential decreased less drastically with increasing joint gap than in the case of the hydrostatic performance in the infiltration test.

### 8.1.3 Machine Learning Modeling

The following conclusions can be drawn from ML modelling using the experimental data:

1. ML models can be used to provide reasonable predictions of RCP infiltration.
2. Among the different ML classifiers considered, *GBC* had the best predictive performance according to several classification metrics, including accuracy, recall, *F1-score*, and *AUC*.
3. The modelling procedure requires tuning of the model to avoid overfitting performance towards majority class in the dataset, i.e. “No Leakage,” due to the imbalanced dataset
4. The oversampling techniques used mitigated the bias in the dataset and thus, improved the prediction performance. *DBSMOTE* demonstrated better predictive performance compared to *SMOTE* according to various classification metrics, such as confusion matrix and *AUC*.
5. The tuning of the oversampling algorithms resulted in considerable improvement in their predictive performance. Using *DBSMOTE*, more synthetic data could be appended to the dataset for training, i.e. higher values of proportion, without overfitting the dataset towards synthetic data compared to *SMOTE*.

6. The *GBC-DBSMOTE* hybrid model provided the most promising and reliable results over different splits of the original datasets compared to *GBC* and *GBC-SMOTE*.

## 8.2 Recommendations

This research has emphasized the critical analysis of existing standards, including the necessity to review and update concrete pipe standards in order to capture modern developments in concrete technology and to bridge the performance evaluation gap in the context of joint performance for infiltration. The testing method proved to be simple, robust, and repeatable for measuring the infiltration capacity of RCP joints. One observation related to the uncertainty may require further investigation where under higher level of applied infiltration pressure, the result seemed to have larger spread with respect to the joint gap. In addition, further, increase of the joint gap beyond the threshold will allow the data to reveal the complete performance spectrum. One of the limitations at the beginning of the research was to select the parameters that influence the output. With assistance from machine learning, the feature importance was revealed providing insight into those parameters that may require further investigation. The actual material properties being tested, such as rubber hardness to the infiltration test, may be considered. These allow the acceptance criteria for routine quality control tests to be established. Lastly, the testing method can also be used in RCP joint and gasket profile development for better sealing potential.

Further study is recommended to evaluate the factors that influence the long-term performance, i.e. 20 hours or longer, such as gasket relaxation and movement under sustained infiltration pressures. A joint effort between the gasket and precast RCP manufacturers to develop performance curves for their products and combinations thereof is needed. These curves can then be used to evaluate the risks associated with actual field conditions.

The improvement of secondary gaskets can increase the efficiency of the test. The effect of the secondary gasket type, properties and profile were not detailed and investigated. In some tests, it caused certain challenges in holding the pressure. The use of external steel bands to create the space for pressurization could be an option. More advanced instrumentation, such as water levels and joint gap measurements, as well as linking to an applied pressure using datalogger, can be an option to increase accuracy.

The machine learning model framework developed in this Chapter could provide a foundation for developing design RCP joint hydrostatic performance charts against infiltration. These could include various models of sealing gaskets, duration and level of pressures, pipe sizes and other influential input parameters, which should be pursued in further study.

### 8.3 References

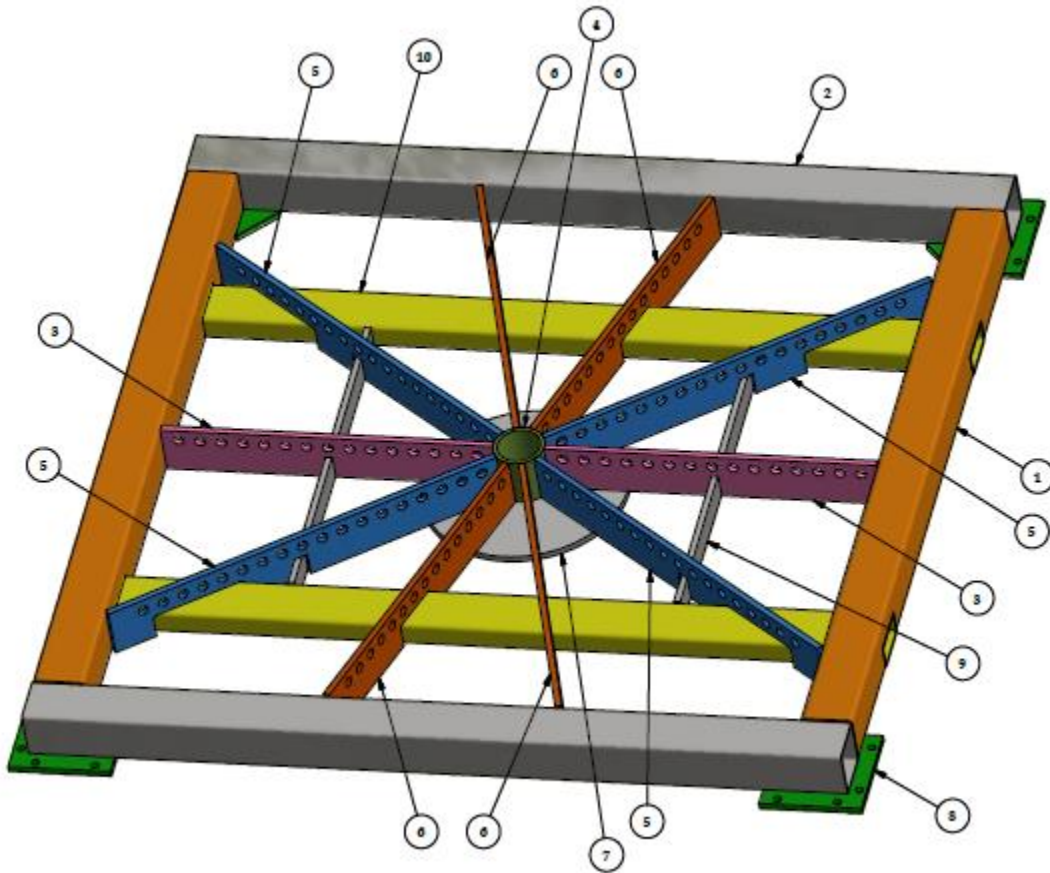
- American Concrete Pipe Association “Concrete Pipe Joints Your Best Choice”, ePipe. Resource #e-07-124 08/09, 2009.
- ASTM C361M-14, “Standard Specification for Reinforced Concrete Low-Head Pressure Pipe”, ASTM International, West Conshohocken, PA, USA, 26 p.
- ASTM C443-12, “Standard Specification for Joints for Concrete Pipe and Manholes, Using Rubber Gasket” ASTM International, West Conshohocken, PA, USA, 2012, 3 p.
- ASTM C1628-17 “Standard Specification for Joints for Concrete Gravity Flow Sewer Pipe, Using Rubber Gaskets”, ASTM International, West Conshohocken, PA, USA, 2017, 7 p.
- AWWA C302, “Reinforced Concrete Pressure Pipe, Non-cylinder Type, American Water Works Association, Denver, CO, USA, 2016, 40 p.
- BS EN 1916:2002, “Concrete Pipes and Fittings, Unreinforced, Steel Fibre and Reinforced”, British Standards Institution (BSI), London, UK, 2002, 94 p.
- CSA A257, “Standards for Concrete Pipe and Manhole Sections”, CSA Group, Mississauga, ON, Canada, 2019, 40 p.

## Bibliography

**Lui Sammy Wong** was the VP of Engineering and Quality at Con Cast Pipe. He holds a Master of Engineering Science in civil engineering from the University of Western Ontario. Sammy is a professional engineer and designated consulting engineer in Ontario, Canada, interested in the precast infrastructure design, manufacturing, quality and installation. Projects that he was involved with as a technical director include bridge elements for Hwy 407 East Extension, precast tunnels sections for Eglinton Crosstown LRT Kennedy Station and Mount Dennis Station, precast bridge elements for several bridge replacement projects along the Richmond Hill GO train line and Stouffville GO train line, and many other large span culverts and bridges for MTO, etc. With more than 15 years of experience in the precast industry, he is currently taking an active role in several technical committees such as the Ontario Concrete Pipe Association, Canadian Concrete Pipe and Precast Association, *CSA A257 Standards of Concrete Pipe and Manhole Sections*, Canadian Precast and Prestressed Concrete Institute (CPCI), and Quality Assurance Council at Canadian Precast Concrete Quality Assurance (CPCQA) Certification Program. He also volunteers in *CSA S6 Canadian Highway Bridge Design Code – Section 7 Buried Structure* sub-committee since 2016. With his passion in the concrete pipe industry, Sammy enrolled in the Ph.D. program at Western University, London, Ontario, to develop better testing and evaluation methodologies over the reinforced concrete pipe application.

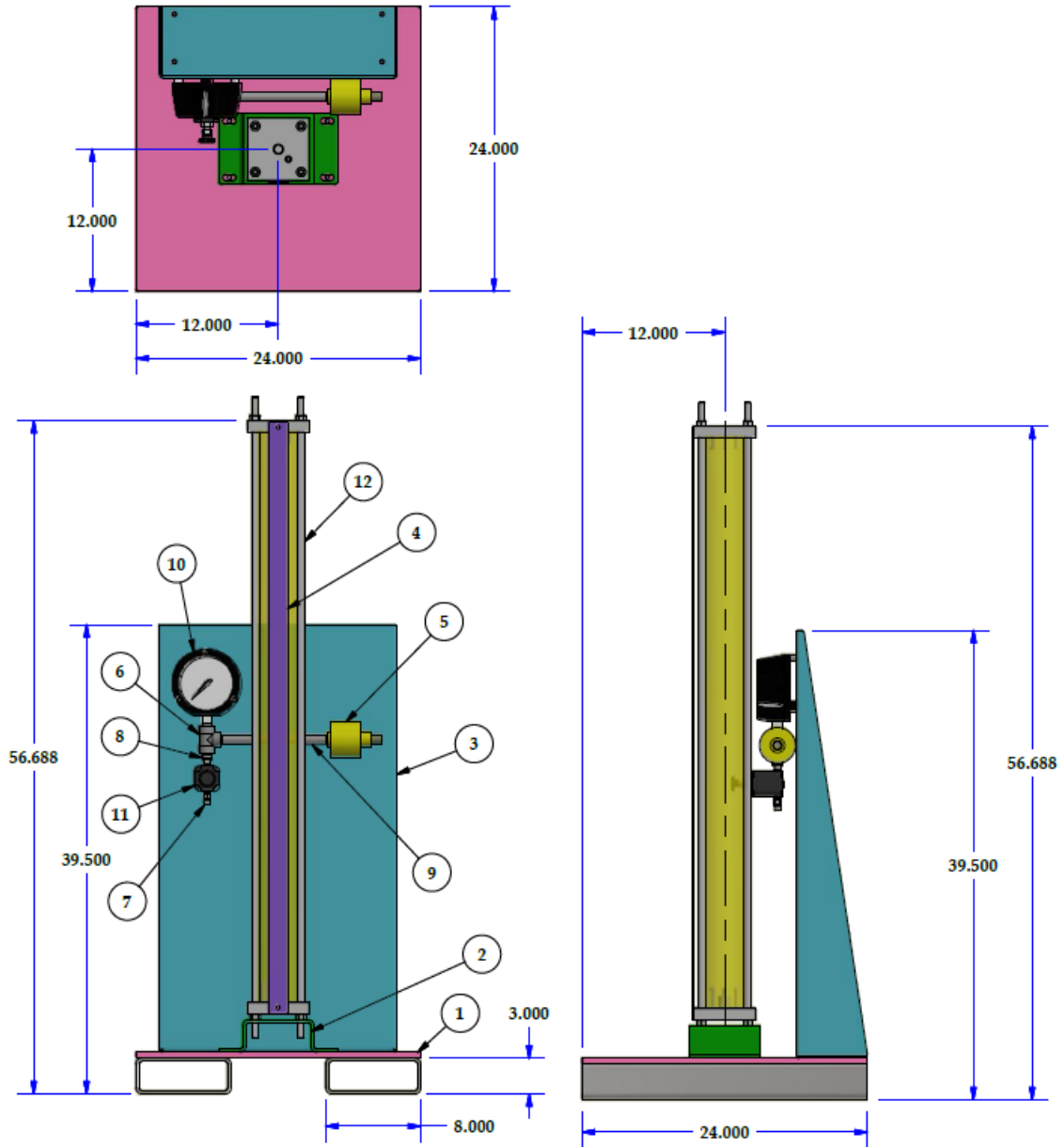
## Appendix A – Design of the Testing Apparatus

## Base Frame Assembly



Parts List				
ITEM	ITEM QTY	PART NUMBER	DESCRIPTION	QTY
1	2	10047398	6 x 6 x 1/4 HSS TUBE	168.000 in
2	2	10047399	6 x 6 x 1/4 HSS TUBE	192.000 in
3	2	10047400	STRAP DOWN RIB - 1	2
4	1	10047401	6" O.D. x 1/2" WALL TUBE	1
5	4	10047402	STRAP DOWN RIB - 2	4
6	4	10047403	STRAP DOWN RIB - 3	4
7	1	10047405	CENTER FOOT	1
8	4	10047406	CORNER FOOT	4
9	2	AISC - 3x3/4 - 42	Flat Bar Steel	84.000 in
10	2	AISC HSS - 6 x 3 x 1/4 - 96	Rectangular tube	192.000 in

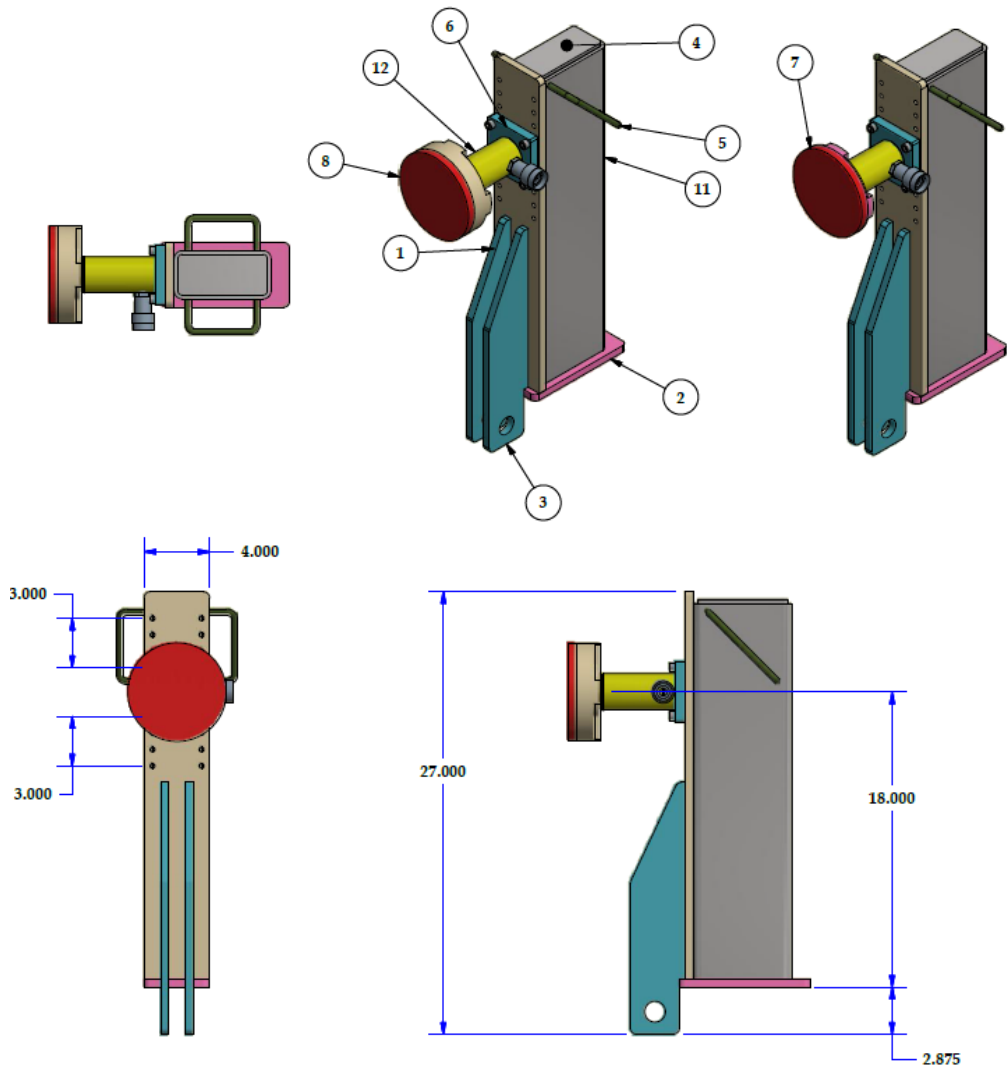
## Pressure System and Stand Assembly



Parts List				
ITEM	ITEM QTY	PART NUMBER	DESCRIPTION	QTY
1	1	10048033	PRESSURE SYSTEM STAND FRAME ASSEMBLY	1
2	1	10048035	PRESSURE SYSTEM STAND FRAME - TANK MOUNT	1
3	1	10048037	PRESSURE SYSTEM STAND FRAME - AIR PANEL	1
4	1	10049264	PRESSURE SYSTEM STAND SCALE MOUNT	1
5	1	65.625	SLIDE VALVE, 2 POSITION, 3-WAY	1
6	1	ASME B16.11 Tee Threaded - Class 2000 1/2	Forged Threaded Tee - Class 2000	1
7	1	DIN EN 10242 Hexagon Nipple N8 1/4	Nipple	1
8	1	ISO 49 Reducing Hexagon Nipple N8 1/2 x 1/4	Malleable cast iron fittings - Reducing Hexagon Nipple N8	1
9	1	JIS B 2302 Long Nipple 1/2 x 250	Nipple	1
10	1	PRESSURE GAUGE		1
11	1	R820-03F	PRECISION REGULATOR	1
12	1	SAO-4 X 48-WTB=2	STEP AP203	1

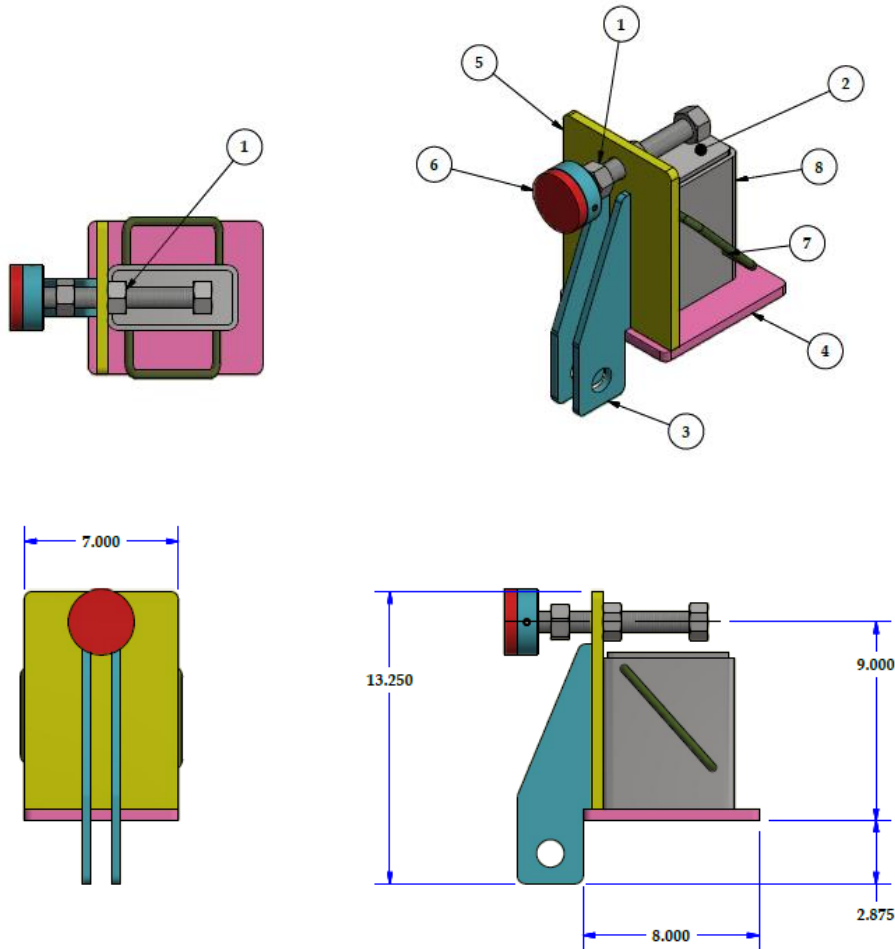


## Jacking Post Assembly



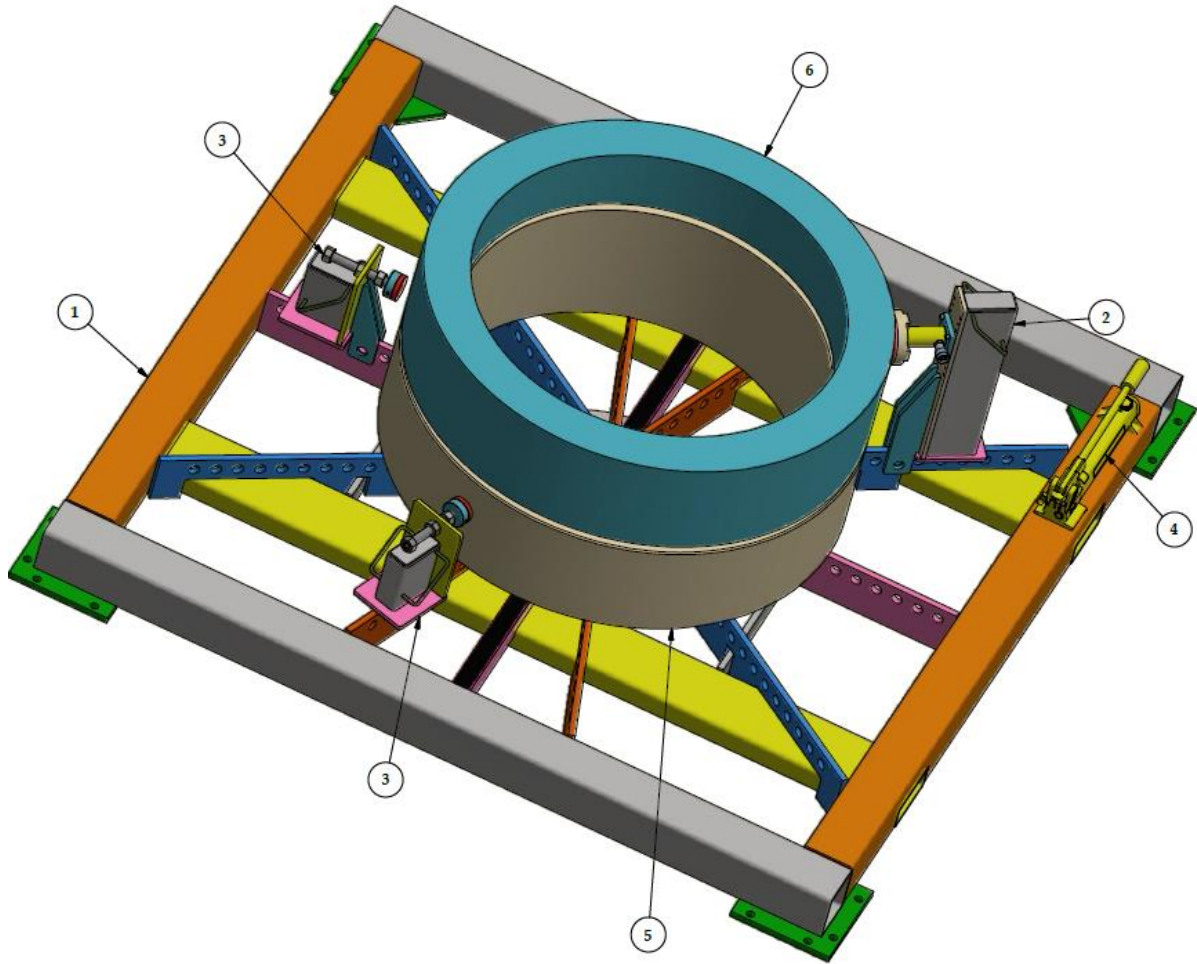
Parts List				
ITEM	ITEM QTY	PART NUMBER	DESCRIPTION	QTY
1	1	10053931	JACKING POST - BACK PLATE	1
2	1	10053932	JACKING POST - BASE PLATE	1
3	2	10053933	JACKING POST - MOUNTING GUSSET	2
4	1	10053945	JACKING POST - TUBE END CAP	1
5	2	10053989	POST HANDLE	2
6	1	10054142	JACKING POST - ENERPAC MOUNT	1
7	1	10054186	ENERPAC JACK ROD END ASSEMBLY	1
8	1	10054640	ENERPAC JACK LONGER ROD END ASSEMBLY	1
9	4	3/8-16 UNC - 1	Socket Head Cap Screw	4
10	2	5/16-18 UNC - 0.75	Socket Head Cap Screw	2
11	1	HSS - 6 x 3 x 1/4 - 22.875	RECTANGULAR HSS TUBE	22.875 in
12	1	RC-102	ENERPAC JACK - 10 TON	1

## Back-stop Post Assembly



Parts List				
ITEM	ITEM QTY	PART NUMBER	DESCRIPTION	QTY
1	2	1 - 8	Hex Nuts (Inch Series)	2
2	1	10053966	BACK-STOP POST - TUBE END CAP	1
3	2	10053967	BACK-STOP POST - MOUNTING GUSSET	2
4	1	10053968	BACK-STOP POST - BASE PLATE	1
5	1	10053969	BACK-STOP POST - BACK PLATE	1
6	1	10053971	BACK-STOP POST - ADJUSTABLE STOP ASSEMBLY	1
7	2	10053989	POST HANDLE	2
8	1	HSS - 6 x 3 x 1/4 - 6.875	RECTANGULAR HSS TUBE	6.875 in

## Complete Setup Assembly



Parts List				
ITEM	ITEM QTY	PART NUMBER	DESCRIPTION	QTY
1	1	10047397	OVERALL ASSEMBLY	1
2	1	10053928	JACKING POST ASSEMBLY	1
3	2	10053970	BACK-STOP POST ASSEMBLY	2
4	1	P-392	ENERPAC P-Series, Hydraulic Lightweight Hand Pumps	1
5	1	10054341	SPIGOT PIPE SECTION 1067mm I.D. x 1333mm O.D.	1
6	1	10054342	BELL PIPE SECTION 1067mm I.D. x 1333mm O.D.	1
7	1	10054638	BELL PIPE SECTION 1142 mm O.D.	1
8	1	10054639	SPIGOT PIPE SECTION 1142 mm O.D.	1

## Appendix B – Testing Results

The content of Appendix B can be found in Supplemental Content.

## Appendix C – Machine Learning Source Code and Output

The content of Appendix C can be found in Supplemental Content.

# Curriculum Vitae

- Name:** Lui (Sammy) Wong
- Post-secondary Education and Degrees:** University of Western Ontario  
London, Ontario, Canada  
1997-2001 B.E.Sc.
- The University of Western Ontario  
London, Ontario, Canada  
2001-2002 M.E.Sc.
- The University of Western Ontario  
London, Ontario, Canada  
2017-2020 Ph.D.
- Honours and Awards:** The Milos Novak Memorial Award 2002
- Winner of the Peter S. Higgins Structural Analysis Competition 2001
- Awarded Certificate of Merit for the Final Year Project 2001
- Related Work Experience** Precast Concrete Engineer 2006 - 2020
- Publications:**
- Wong, L.S. (2020). *Are Reinforced Concrete Pipe Joint Infiltration Proof?*, Environmental Science & Engineering Magazine, June/July 2020 Issue, pp. 30-33.
- Wong, L.S., Marani, A. and Nehdi, M.L. (2020, Submitted). *Hybrid Tree-Based Ensemble-Oversampling Prediction of RCP Joint Performance for Infiltration*, ASCE Journal of Pipeline Systems - Engineering and Practice, Reston, Virginia, United States.
- Younis, A., Ramadan, A., Wong, L.S., Nehdi, M. L. (2020 submitted). *Modified Three-Edge Bearing Test for Reinforced-Concrete Pipe Eliminating Crack-Width Criteria*, Structures.
- Younis, A., Shehata, A., Ramadan, A., Wong, L.S., Nehdi, M. L. (2020 submitted). *Numerical Modeling of Reinforced-Concrete Pipe with Single, Double and Triple Cage Reinforcement*, Engineering Structures.
- Ramadan, A., Younis, A., Wong, L.S., Nehdi, M. L. (2020). *Investigation of Structural Behavior of Precast Concrete Pipe with Single Elliptical Steel Cage Reinforcement*, Engineering Structures.

- Ramadan, A., Shehata, A., Younis, A., Wong, L.S., Nehdi, M. L. (2020 submitted). *Modeling Structural Behavior of Precast Concrete Pipe with Single Elliptical Steel Cage Reinforcement*, Structures.
- Wong, L.S. and Nehdi, M.L. (2020). *Predicting Hydrostatic Infiltration in Reinforced Concrete Sewer Pipes Considering Joint Gap and Joint Offset*, ASCE Journal of Pipeline Systems - Engineering and Practice, Reston, Virginia, United States.
- Wong, L.S. and Nehdi, M.L. (2020). *Quantifying Resistance of Reinforced Concrete Pipe Joints to Water Infiltration*, ASCE Journal of Pipeline Systems - Engineering and Practice, Reston, Virginia, United States.
- Wong, L.S., Cameron, J., Nehdi, M.L. (2019). *Study of Precast Concrete Cracking Due To Moist Curing*, CSCE June 12-15, 2019, Montreal.
- Ramadan, A., Younis, A., Wong, L.S., Nehdi, M.L. (2019). *Reinforced Concrete Pipe Design With Single Elliptical Cage Reinforcement*, CSCE June 12-15, 2019, Montreal.
- Wong, L.S. (2019). *Precast Concrete Tunnel Segments - Go Beyond The Limit!*, Concrete Pipe Journal, Spring Issue 2019
- Wong, L.S. (2019). *Self-compacting Bedding*, Concrete Pipe Journal, Spring Issue 2019
- Wong, L.S., Nehdi, M.L. (2018). *New Test Method For Reinforced Concrete Pipe Joint Hydrostatic Infiltration*, CSCE June 13 – June 16, 2018, Fredericton
- Vuk, F., Campbell, P., Wong, L.S., (2018). *Hidden Valley Road Bridge Replacement*, Concrete Pipe Journal, 2018 Spring Issue
- Wong, L.S., Nehdi, M.L. (2018). *Critical Analysis of International Precast Concrete Pipe Standards*, Infrastructures
- Wong, L.S. (2016). *Full Scale Manufacturing of Steel Fibre Reinforced Concrete Pipe*, CSCE Conference, Jun 1-3, 2016, London Ontario Canada.
- Wong, L.S., Allouche, E.N., Dhar., A.S., Baumert., M., Moore, I.D. (2006). *Long-term Monitoring of SIDD Type VI Installation*, Canadian Geotechnical Journal, pp. 394-408.
- Wong, L.S. and Allouche, E. N. (2002). *SimSEWER – Interactive Educational Simulation Software for Buried Infrastructure Management*, Pipeline Engineering and Construction International Conference 2003, American Society of Civil Engineering
- Wong, L.S., Allouche, E.N. and Moore, I.D. (2002). *Long-Term Monitoring And Analysis of Full Scale Concrete Pipe Test Beds*, ASCE Pipelines 2002, August 4-7, Cleveland, OH, USA.

Allouche, E.N., Wong, L. S. and Baumert, M.E. (2001). *Full Scale Testing of Concrete Pipe Bedding Design*, 2001 International conference on underground infrastructure, June 10-13, Waterloo, Ontario, Canada, pp. 117-124.